Numerical Modelling of Flood Forces due to Storm Surges

高潮氾濫時の流体力評価の数値モデル

2023/06

Justin Joseph Panlilio VALDEZ

ヴァルデス　ジャスティン　ジョセフ　パンリリオ

Numerical Modelling of Flood Forces due to Storm Surges

高潮氾濫時の流体力評価の数値モデル

2023/06

Waseda University Graduate School of Creative Science and Engineering

Department of Civil and Environmental Engineering, Research on Coastal Engineering and Management

Justin Joseph Panlilio VALDEZ
ヴァルデス　ジャスティン　ジョセフ　パンリリオ

ACKNOWLEDGEMENTS

And ultimately, I would like to thank the Lord for giving me an opportunity to study and complete my research in Japan. His grace strengthened me through the ups and downs of my PhD research. This study was conducted and accomplished for the greater glory of God. Ad Majorem Dei Gloriam.

Maraming salamat po.

ABSTRACT

Typhoon Haiyan in 2013 was one of the most powerful storms to have affected the Philippines, devastating in its path a wide portion of Leyte and Samar, and causing extensive damage to structures in Tacloban City. To understand the likely impacts that would be exerted by a storm surge on a structure deemed important (such as a school) the authors used a coupled model that hindcasted the flooding that took place during Haiyan. This coupled model included the use of the Weather Research and Forecasting (WRF) Model (with Bogussing scheme) to simulate the atmospheric conditions during the passage of Haiyan, the Finite Volume Coastal Ocean Model (FVCOM) to simulate the storm surge and obtain the boundary conditions for the wind and flood (hydrostatic, hydrodynamic, and breaking wave), and the Structural Analysis and Designing Program (STAAD.Pro) to calculate the corresponding axial, shear, and bending moment envelopes based on the storm surge simulation. A 4-floor public school building in Tacloban was modeled and the effects that the storm surge would have on a corner column were analyzed. Based on the results, the axial, shear, and moment at the corner column significantly increased when considering flood loads, indicating the importance of including such loads in the design of essential structures.

To demonstrate its versatility, the weather-surge-structure model was then used simulate two more tropical cyclone cases: the 2021 Typhoon Rai in the Philippines and the 2022 Cyclone Batsirai in Mauritius. Typhoon Rai hit the central Philippines and reportedly brought storm surges in Cebu and Bohol. The model was able to verify that storm surges occurred in the area as well as high waves. A small two-storey house structure was then hypothetically placed in Pangapasan, a small island off the coast of Tubigon, Bohol to evaluate the storm surge driving

forces. The structural analysis showed the ground floor column was also a critical member as it experienced the maximum axial, shear, and moment values due to the typhoon.

To further show the flexibility of the models, the numerical methodology was extended to a different region. For the Cyclone Batsirai case, the main objective was to identify potential storm surges and high wave attack due to the cyclone in Mauritius. The simulation was able to show a small surge generated by the passage of Cyclone Batsirai off the coast of Port Louis, the capital of Mauritius. With improvements in the numerical set-up, the methodology in this dissertation would serve as one of the references for capacity building in Mauritius for modelling of cyclones and surges. Overall, the numerical methodology in this dissertation could evaluate the driving forces generated during a storm surge event on which can be used for analyzing the loads experienced by a structure and identify critical members for building back better, particularly in the Philippines.

TABLE OF CONTENTS

CHAPTER 1: INTRODUCTION

1.1 Background of the Study

The Philippines is an archipelago country situated on the Northwest Pacific (NWP) Basin, which is the most active ocean basin in terms of tropical cyclone formation (Lapidez et al. 2015). The Japan Meteorological Agency (JMA) and the Philippine Atmospheric, Geophysical, and Astronomical Services Administration (PAGASA) both monitor any tropical disturbances such as formation of typhoons in the NWP basin, with the latter focused on the Philippine Area of Responsibility (PAR). Around 20 typhoons enter the PAR annually with around 9 making landfall in the country, mostly in the Luzon and Visayas regions (Hernandez et al. 2015; Lapidez et al. 2015). From the Philippines' Presidential Decree No. 1149, the PAGASA is the agency mandated to "provide protection against natural calamities and utilize scientific knowledge as an effective instrument to insure [sic] the safety, well-being and economic security of all the people, and for the promotion of national progress" of the country (Malacañang Records Office 1977). One of the main tasks of PAGASA is to warn the citizens of impending danger from typhoons by giving public storm signal numbers to the areas that will be affected.

The location of the Philippines is unfortunate in terms of the pathways of typhoons, which can cause massive damage to structures due to severe winds and storm surges. Perhaps the most significant Philippine storm surge event in recent history was from Typhoon Haiyan in 2013, which brought surges of around 5-6 meters at Tacloban City in Leyte based on numerous field surveys and research conducted (Chock et al. 2013; Mori et al. 2014; Shibayama et al. 2014; Tajima et al. 2014; Hernandez et al. 2015; Mas et al. 2015; Esteban et al. 2016; Mikami et al. 2016; Takagi et al. 2017). Field survey and satellite imagery showed that a higher number of structures located along the coast of Tacloban were heavily

1

damaged, compared to inland areas where the inundation was much lower (IRIDes 2014; Mas et al. 2015; Mikami et al. 2016).

In December 2021 Typhoon Rai, with local name Odette, hit the Visayas region of the Philippines. Rai was the 15th typhoon to come to the PAR that year. It had a minimum sea level pressure (MSLP) of 915 hectopascals (hPa) and a maximum sustained wind speed of 54.02 m/s and was classified as a violent typhoon by the Japan Meteorological Agency. Rai caused massive damage to infrastructure and housing, with more than 1.1. million houses destroyed in the Central Visayas region (NDRRMC 2022). Rai passed through the vulnerable islands of Bohol and Cebu, where high storm surge heights could be expected from strong typhoons (Lapidez et al., 2015). A field survey documented some visible damage and watermarks, recording surge levels of up to 2.54 m and 4.24 m in Cebu and Bohol, respectively (Esteban et al 2022).

The similar threat of typhoons to the Philippines can also be observed in other countries such as Mauritius. The small island country of Mauritius lies east of Madagascar in the Indian Ocean and is exposed to the dangers of cyclones. In early 2022, Cyclone Batsirai, with Category 4 strength on the Saffir-Simpson scale, heavily affected Mauritius, the nearby Réuinion island, and Madagascar. A Class IV cyclone warning, the highest level, was issued by the Mauritius Meteorological Services. Mauritius was basically shut down during the cyclone, with people advised to remain in homes or evacuation shelters while all transport services were suspended. High waves were reported in the eastern coastal town of Mahébourg, damaging the waterfront.

Since many buildings, including public schools, were destroyed in the Philippines by the storm surge generated by Typhoon Haiyan and Typhoon Rai, it is important to adequately design such structures and improve the long-term resilience of the populations they serve. In Panalaron Central School, the original one-storey building was badly damaged, based on imagery (MapAction 2013), and ten people died during the surge (Roughneen 2014). The Department of Works and Highways (DPWH) and the Department of Education (DepEd) modified their standard classroom school building plans based on the updated 2015 National Structural Code of the Philippines (2015 NSCP) by the Association of Structural Engineers of the Philippines (ASEP 2016) to consider the lessons learnt due to Typhoon Haiyan, such as including a section for design flood loads. However, when designing buildings in the Philippines (such as the DPWH-DepEd standard public-school building), only dead, live, wind, and earthquake loads are usually considered. Thus, it is unclear how the new inclusion of flood loads would impact the design of such buildings, especially for the case of a storm surge event generating high momentum waves (such as what took place during the Typhoon Haiyan event). Field survey and satellite imagery showed that a higher number of structures located along the coast of Tacloban were heavily damaged, compared to inland areas where the inundation was much lower (IRIDes 2014; Mas et al. 2015; Mikami et al. 2016).

1.2 Statement of the Problem

The accurate estimation of both the wind and flood loads generated by a strong typhoon is necessary to understand the impact that each load can have on a structure, and numerical simulations can be helpful for this. Since the driving forces of a storm surge event are wind and flood loads, there is a need to consider their combined effects on structures. In Li et al. (2012), the structural and non-structural losses to residential buildings resulting from wind,

surge, and combined wind and surge forcing due to hurricanes were estimated using probabilistic methods. Jia and Sasani (2021) presented a copula-based joint probability model to develop wind speed and flood elevation hazard curves which can be used to evaluate simultaneous threats due to these two hazards. However, although it would be valuable to investigate the effects of flood and wind loads on a structure by reproducing a historical storm surge event through numerical simulations, such an integrated weather-surge-structure numerical methodology has not yet been formulated.

1.3 Objectives of the Study

The primary aim of the present study is to clarify the importance of considering flood loads when designing structures against significant storm surge events, compared with other design loads such as wind loads, by using numerical simulations. To do so, a numerical methodology that integrates weather, storm surge and structural simulations was developed. Namely, the wind and flood forces that were generated by three tropical cyclone cases (Typhoon Haiyan and Typhoon Rai in the Philippines, and Cyclone Batsirai in Mauritius) were simulated as accurately as possible through the application of WRF and FVCOM models (improving upon the methodology of Nakamura et al. 2016). Using the simulated forces, a structural analysis of the axial, shear, and bending moment applied on a structural member of a typical 4-floor public school building, which was selected as a target structure in the present study, was also conducted with Structural Analysis and Designing Program or STAAD.Pro (Bentley Systems 2012). STAAD.Pro is commercially available software that can perform finite element analysis and design on a model structure. Three storm surge loading cases were performed: at the start of inundation, and at the time of maximum wind speed, and at maximum inundation. Additionally, the results were compared with another

4

case, at the time of maximum wind but ignoring flooding, to highlight the importance of considering flood forces during a storm surge event in structural analysis.

The other two tropical cyclone cases, Rai and Batsirai, also have specific objectives aside from numerical modelling of storm surges and evaluation of flood forces. For the case of Typhoon Rai, the methodology aims to verify the possibility of storm surge and high waves at a selected coastal town and islands and compare with field survey results (Esteban et al. 2022). For the case of Cyclone Batsirai, the main objective was to identify potential storm surges and high wave attack due to the cyclone in Mauritius. The methodology in this dissertation would serve as one of the references for capacity building in Mauritius for modelling of cyclones and surges. All the results from the model are limited to the tropical cyclone cases that were studied. However, it can be said that the coupled WRF-FVCOM-STAAD.Pro model has the potential to be applied to other tropical cyclone cases in different coastal areas if sufficient data is available for input.

CHAPTER 2: REVIEW OF RELATED LITERATURE

2.1 Tropical Cyclones and Storm Surges

A tropical cyclone is an intense weather disturbance formed in warm ocean basins characterized by strong winds rotating on a low-pressure area (LPA) and can bring heavy rainfall. As the warm air from the ocean rises then sinks as it cools from above, a low pressure is formed, and the movement of air generates winds. Due to the Coriolis effect, the direction of winds is deflected and causing it to rotate (counterclockwise in the northern hemisphere and clockwise in the southern hemisphere) around the LPA. When the sustained winds reach a certain significant maximum speed, it is classified into a typhoon (Pacific Ocean), hurricane (Atlantic Ocean), or cyclone (Indian Ocean) depending on where it originated.

A typhoon has the potential to induce a storm surge over a coastal area. The storm tide is the combination of the storm surge and the astronomical tide, and wind-driven waves can also be produced on top of it. A storm surge is a temporary abnormal rise in the water level as a response to high wind-induced surface shear stress and low-pressure fields, then the water is pushed inland. The height of the storm surge is further amplified depending on several factors such as the typhoon size, track, forward speed, and the local topography. Storm surges cause massive destruction to structures and severe flooding in coastal communities such as Kobe City in Japan from the 2018 Typhoon Jebi (Takabatake et al. 2018).

2.2 Typhoon Haiyan (2013)

Typhoon Haiyan (**Figure 1**) was one of the strongest typhoons to make landfall in Philippines in recorded history. Haiyan started as a low-pressure area near Micronesia on

2 November 2013 and was classified as a tropical depression a day later. On 04 November 2013, the weather disturbance was categorized as a tropical storm by the Japan Meteorological Agency (JMA) and the Joint Typhoon Warning Center (JTWC) and was given the name Haiyan. Haiyan then became the 25th typhoon to enter PAR that year and was given the local name of "Yolanda" by PAGASA. On 07 November 2013 12:00 Haiyan reached its lowest central pressure at 895 hPa and had a ten-minute sustained wind speed of 230 km/h. Storm signal no. 4 warnings (the highest level) were then given to the Samar and Leyte provinces. Haiyan made its first landfall at the municipality of Guiuan, Eastern Samar on 08 November 2013, 04:40 local time (UTC +9). It then passed over San Pedro Bay and made its second landfall over the municipality Tolosa, Leyte two hours later. The typhoon left the country in the afternoon of 09 November 2013 and continued to move over the West Philippine Sea towards Vietnam, leaving more than 6,000 people dead, more than 28,000 people injured, more than a thousand people missing, and around 39 billion pesos in damages (NDRRMC 2014). Two days later, then President Benigno Aquino III declared a 'State of National Calamity' to speed up the relief and rehabilitation efforts in the affected areas (Santos 2014).
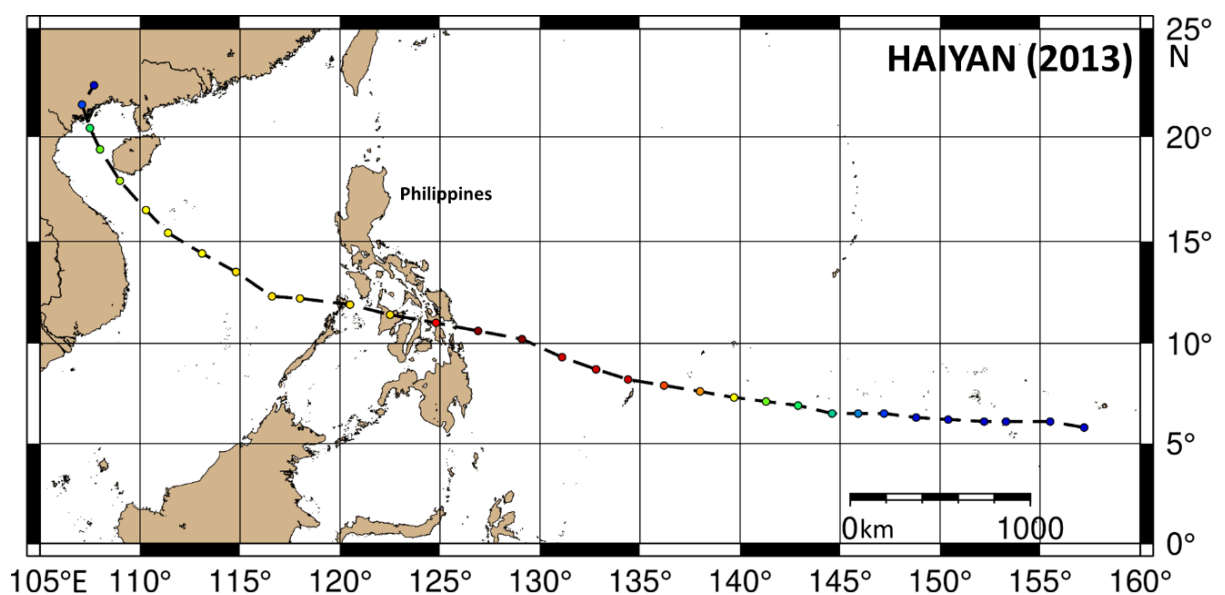
Figure 1. Observed Track of Typhoon Haiyan.

2.2.1 Storm Surges in Eastern Visayas

Due to the intensity and track of Haiyan, and the shallow bathymetry of the bay, the typhoon event was able to push a significant amount of water from the south towards Tacloban and nearby towns. Numerous research groups have visited the devasted areas to conduct post-damage field surveys and interviews (Mori et al. 2014; Shibayama et al. 2014; Tajima et al. 2014; Hernandez et al. 2015; Mas et al. 2015; Esteban et al. 2016; Mikami et al. 2016; Takagi et al. 2017). Also, the Japan Society of Civil Engineers (JSCE) and the Philippine Institute of Civil Engineers (PICE) conducted a joint field survey along the coastal areas of Leyte, Samar, and Eastern Samar from 12 December to 16 December 2013 (Tajima et al. 2014). The team measured inundation and run-up heights from visible water marks and from accounts given by local witnesses. Significant inundation was observed along the San Pedro Bay and at the east coast of Samar Island. Massive clean-up, demolition, and reconstruction were already ongoing at the time of this survey.

2.2.1.1 Samar

The Samar Island was the first province hit by Typhoon Haiyan as it made landfall in Guiuan. At the eastern coastline (where Guiuan is located), storm surge heights were measured to be from 4.9-6.6 meters. The western part of Samar, which is surrounded by San Pedro Bay, also received significant storm surges (around 5.0 meters in the municipality of Marabut).

2.2.1.2 Leyte

Several coastal towns in Leyte Province were heavily affected by Typhoon Haiyan as it passed over San Pedro Bay. Along the Leyte coast, storm surge heights of around 5.8 meters at northern town of Cabalawan and around 3.3 meters at Dulag in the south were

recorded (Tajima et al. 2014). Perhaps the most devasted city due to the storm surge was Tacloban, the capital city of Leyte, where heights of around 6-7 meters were recorded (Shibayama et al. 2014; Tajima et al. 2014). One area that was also severely damaged by Haiyan was Palo, a 3rd class municipality consisting of 33 barangays, located south of Tacloban City. Based on the weather reports, the eye of Haiyan passed near Palo, thus the municipality most likely experienced the maximum circulating winds. The coastal area of Palo was hit with an estimated storm surge height of 1.7 meters and inundation distance of 960 meters from the shore (Joint Research Centre 2013). The typhoon left 1,089 casualties in the municipality of Palo alone (NDRRMC 2014) and destroyed many structures (**Figure 2**). A case study was conducted to investigate the difference damage patterns due to severe winds and storm surges in Palo (Valdez 2014).

Figure 2. Damaged house in Palo, Leyte.

2.2.2 Revisions to the National Structural Code

Haiyan was estimated to have a maximum one-minute sustained wind speed of 315 kph, thus the typhoon "brought 7500-year winds to the affected areas" (Aquino et al. 2014). The

provisions in the 6th Edition of the National Structural Code of the Philippines (NSCP) accounts for no damage up to 700-year winds. Around 1 million houses were damaged, and the total cost of infrastructure amounted to 18 billion pesos (NDRRMC 2014). To consider the lessons learnt due to Typhoon Haiyan, the Association of Structural Engineers of the Philippines made some revisions to the NSCP in 2015 such as increasing the design wind speed and including a section for design flood loads (ASEP 2016).

2.2.2.1 Standard Public School Building

The latest 2015 NSCP became the reference for the structural design of the standard school buildings by the Department of Public Works and Highways (DPWH) and the Department of Education (DepEd). However, when designing buildings in the Philippines (such as the DPWH-DepEd standard public-school building), only dead, live, wind, and earthquake loads are usually considered. In Panalaron Central School at Tacloban, the original one-storey building was badly damaged, based on imagery (MapAction 2013), and ten people died during the surge (Roughneen 2014). Since many buildings, including public schools used as evacuation centers, were destroyed by Haiyan, it is important to check the effect of storm surge forces.

2.3 Typhoon Rai (2021)

In December 2021, Typhoon Rai (locally known in the Philippines as Typhoon Odette) was the 15th tropical cyclone to enter the Philippine Area of Responsibility (PAR) that year. It had an observed minimum central pressure of 915 hPa and a maximum sustained wind speed of 54.02 m/s and was classified as a violent typhoon by the Japan Meteorological Agency (JMA). Typhoon Rai struck the Visayas region, which was also impacted in 2013 by the strongest typhoon (Haiyan) in the recorded history of the Philippines. Typhoon Rai

passed through the vulnerable islands of Bohol and Cebu, where high storm surge heights could be expected from strong typhoons (Lapidez et al., 2015). Storm signal warning No. 4 (highest level) was given to the provinces of Surigao, Leyte, Samar, and Bohol as Rai approached the country. Rai made landfall at Surigao del Norte on 16 December 2021 05:30 UTC and passed through the central Philippines region (**Figure 3**). The Philippine government declared a state of calamity afterwards over the most heavily affected areas like Cebu and Bohol. The NDRRMC reported that more than two million houses were damaged, amounting to around Php 62.6 million in total cost. Damages to agriculture and infrastructure reached Php 17.7 billion and Php 29.3 billion, respectively. A total of 139 ports across the country had to suspend operations, with some boats reported to be aground (NDRRMC 2022).
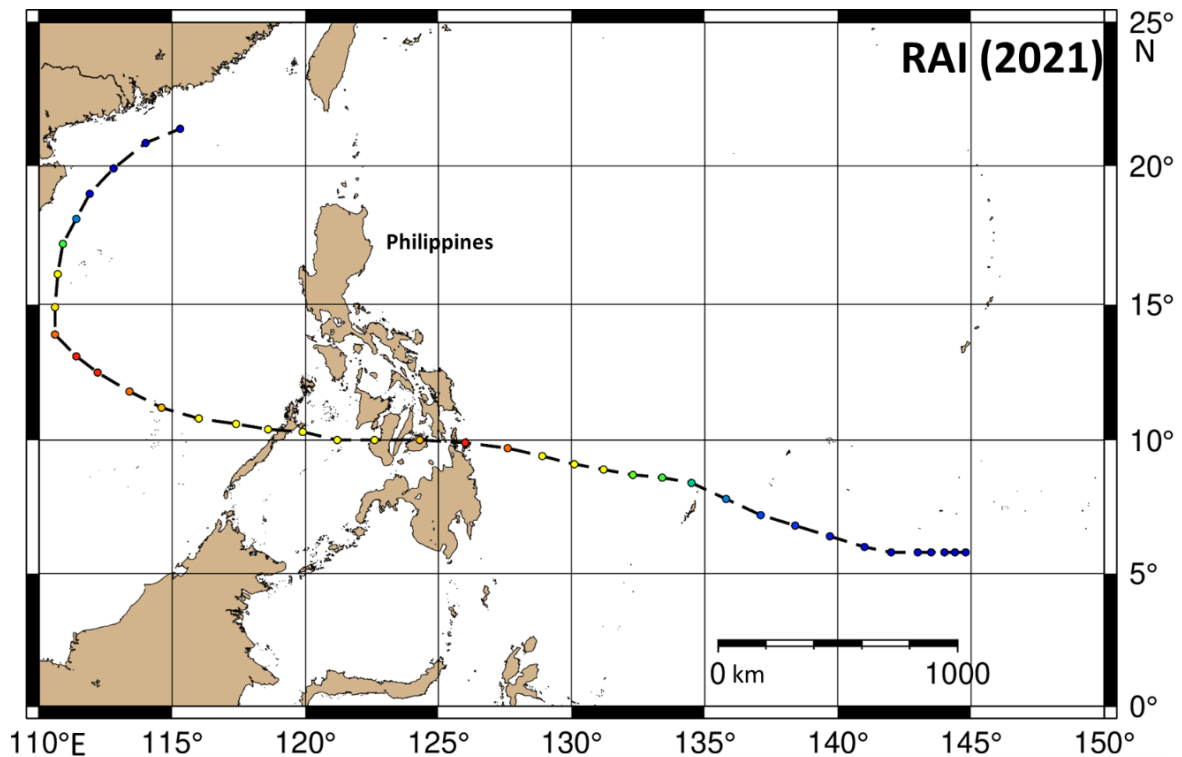
Figure 3. Observed Track of Typhoon Rai.

2.3.1 Storm Surges in Central Visayas

Reports of flooding and storm surges in coastal towns of Cebu and Bohol came afterwards the passage of Rai. Although it was difficult to travel to the Philippines at that time due to travel restrictions brought forth by the pandemic, the research team led by Professor Miguel Esteban of Waseda University (Esteban et al. 2022) was able to conduct a field survey in the region, particularly Cebu and Bohol, to verify the possibility of storm surges. The team conducted interviews, watermark measurements, and bathymetry survey around select coastal areas in these two provinces. The maximum storm surge height observed in Cebu and Bohol were 2.54 m and 4.24 m, respectively (Esteban et al. 2022).

When Typhoon Rai hit the Philippines, the country was still under travel restrictions due to the coronavirus (COVID-19) pandemic. Thus, it was difficult to conduct field surveys at that time. Even so, the research team led by Esteban et al. (2023) was able to visit Cebu and Bohol and record watermark levels around two months after the passage of Typhoon Rai. To aid in rapidly map and assess the extent of damage brought by the typhoon, satellite imagery using Sentinel-1 synthetic aperture radar (SAR) was performed (Bolanio et al. 2022; Meneses and Blanco 2022). However, no numerical calculations have been done to quantify and validate the occurrence of storm surges and high waves in the area.

2.3.1.1 Tubigon and Small Islands

One particular interest was the coastal town of Tubigon in Bohol (**Figure 4**) and the nearby small islands of Pangapasan, Ubay, Batasan, and Bilangbilangan. These islands, surrounded by coral reefs, experienced land subsidence (around 1 m) due to a magnitude 7.2 earthquake in 2013 and are now regularly flooded even during normal spring tides (Jamero et al. 2018; Esteban et al. 2019). The residents have been continuously adapting to

the rise in sea level using various methods such as piling corals as foundation for their houses.
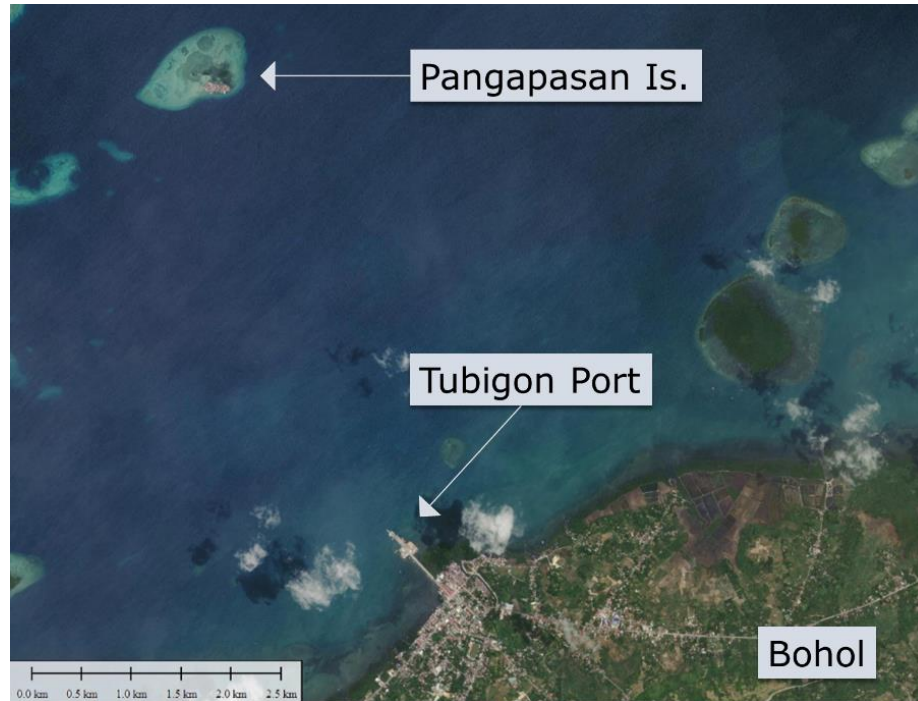
Figure 4. Location of Tubigon, Bohol and nearby Pangapasan Island.

Based on the field survey results, the measured storm surge around these islands ranged from 2.00 m at Batasan to 2.45 m at Pangapasan (Esteban et al. 2022). Several structures on the islands were damaged, possibly due to the surge and severe waves (**Figure 5**). A relatively high storm surge level of 4.24 m was measured at a house in Tubigon Port. It was noted in the field survey that a barge slammed at the nearby houses in the port where this measurement was taken. To further investigate the occurrence of storm surge in the area, another study based on numerical modelling (which is part of this dissertation) was conducted (Valdez et al. 2022).

Figure 5. Damaged structures at the coast of Pangapasan Island.

2.4 Cyclone Batsirai (2022) in Mauritius

Batsirai was the first intense cyclone and second weather disturbance to form at the Indian Ocean basin in 2022 after tropical storm Ana. It was categorized as a tropical storm on 27 January 2022 UTC and continued to rapidly intensify as it travelled over the warm waters of the Indian Ocean. Batsirai made landfall in Madagascar around 05 February 2022 12:00 URC and storm surge alert levels of up to 0.9 meters were raised (GDACS 2022). Although Madagascar was the main country devastated by Batsirai, Mauritius was still under threat of severe winds and waves as the cyclone passed at its north (**Figure 6**).
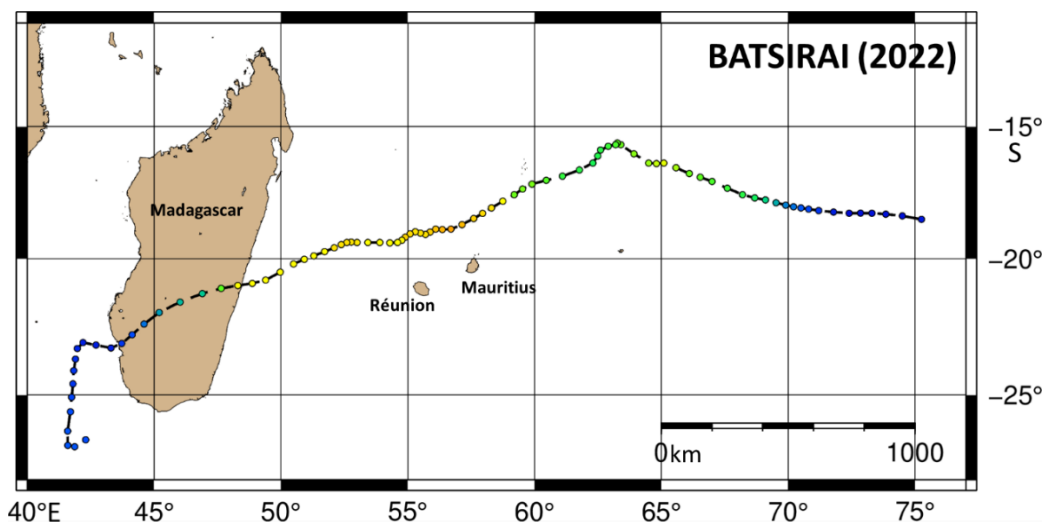
Figure 6. Observed Track of Cyclone Batsirai.

2.4.1 Storm Surge Prone Areas in Mauritius

The World Bank Group, in collaboration with the Global Facility for Disaster Reduction and Recovery (GFDRR), conducted a disaster risk profile assessment for the country of Mauritius under the Southwest Indian Ocean Risk Assessment and Financing Initiative or SWIO RAFI (World Bank Group 2016). From its analysis, around $91 million in direct losses occur annually from tropical cyclone hazards such as strong winds, flooding, and storm surge. At Rodrigues Island, a 100-year cyclone event could result in storm surges of up to 2 meters. In mainland Mauritius, the northwest (where the capital city of Port Louis is located) and southeastern parts of the island were determined to be storm surge prone areas.

In September 2022, a team of researchers from several universities in Japan led by Professor Tomoya Shibayama of Waseda University met with some local experts in the University of Mauritius at Port Louis. From the meetings and seminars, it was acknowledged that there is a need to conduct capacity building in Mauritius such as numerical modelling of cyclones and storm surges to further prepare the nation in the future. Some key locations which the research team conducted field surveys were Belle Mare in the north, Flic en Flac in the west, and Rivière des Galets in the southern part of Mauritius (**Figure 7**). These locations experience coastal erosion and high wave attack.

Figure 7. Wave breaking at Rivière des Galets, Mauritius.

2.5 Typhoon and Storm Surge Simulations

The Weather Research and Forecasting (WRF) model (Skamarock et al. 2008) is a popular numerical weather prediction model developed by the National Center for Atmospheric Research (NCAR) that can be used to simulate tropical cyclones. Nakamura et al. (2016) conducted research on Haiyan using the WRF model by employing the tropical cyclone (TC) bogussing scheme by Hsiao et al. (2010), focusing on how such an event could be intensified in the future by climate change. A symmetric typhoon model was used by Kim (2015) to estimate the storm surges generated by Haiyan in the Leyte Gulf. Islam, Srivastava, and Dai (2015) conducted a sensitivity analysis of the WRF physics parametrization on the simulation of Haiyan cloud properties, though there was a significant overestimation in the ice water path. Li, Song, and Li (2018) conducted high-resolution simulations of Haiyan using the WRF model to perform a sensitivity analysis of the tropical cyclone to different cumulus parametrizations. Takagi et al. (2017) developed a typhoon model based on the Myers formula to analyze the unusual characteristics of the event. However, these previous hindcast simulations of Haiyan have shown relatively high discrepancies in minimum sea level pressure (MSLP), maximum wind speed, and track

between simulated and observed results, all of which are important parameters to then simulate the resulting storm surges.

The Finite Volume Coastal Ocean Model (FVCOM) is a three-dimensional, unstructured grid model (Chen, Liu, and Beardsley 2003) that has been applied to simulate storm surges (Ge et al. 2014, Yoon et al. 2014, Nakamura et al. 2016, Wang et al. 2017a). Coupled WRF-FVCOM models have been used by several researchers to reproduce typhoon and storm surges under different scenarios. Ohira et al. (2012) developed a meteorology-wave-storm surge-tide coupled model to investigate the effects of climate change on coastal damage at Tokyo Bay. Tasnim et al. (2014) performed storm surge simulations over the Bay of Bengal using WRF and FVCOM. A case study on the extratropical cyclone Gudrun under climate change effects was studied by Mäll, Suursaar, and Nakamura (2017) using a coupled model. The vulnerability of the coastal areas of South Korea was investigated by Yoon (2018), who looked at how climate change could affect Typhoon Maemi. Nakamura, Mäll, and Shibayama (2019) used a nested FVCOM domain set-up to assess flood impact damage due to an extratropical cyclone at Nemuro, Japan. The effect of shelf bathymetry on the storm surges at the Gulf of Thailand-Sunda Shelf was investigated Tomkratoke and Sirisup (2020) using a parametric wind model and FVCOM. Other models that can be used to perform storm surge simulations include the coupled JMA Storm Surge Model and FLO-2D (Dasallas and Lee 2019), and the Delft3D Flow fluid dynamics model (Takagi et al. 2016).

CHAPTER 3: METHODOLOGY

3.1 Weather-Surge-Structure Numerical Modelling

The coupled weather-surge-structure model is illustrated in the figure below (**Figure 8**) and is explained in the succeeding sections. Parts of the model descriptions are also directly taken from the related master's thesis in Valdez (2019).
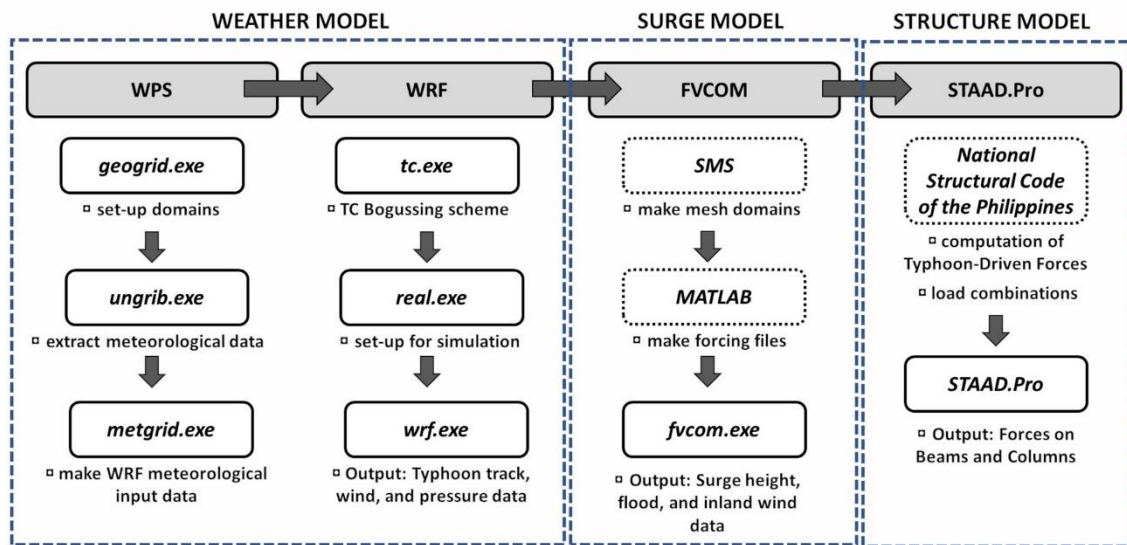
Figure 8. Numerical Models used in this study.

3.1.1   Weather Model: WRF

3.1.1.1 Overview and Governing Equations

The WRF is a fully compressible and nonhydrostatic model that can run idealized and real-time numerical weather prediction simulations, as well as options for data assimilation (Skamarock et al. 2008; Wang et al. 2017b). The governing equations are computed using the Runge-Kutta 2nd and 3rd order time integration schemes on a terrain-following hydrostatic pressure vertical coordinate and Arakawa C-grid staggering mesh. The WRF modelling system is composed of several components as shown in Figure 11. For real-data simulations, the important programs are the WRF Preprocessing System (WPS), the Real-

data Initialization Program (real.exe), and the WRF Numerical Integration Program (wrf.exe). When compiled serially, the WRF model can perform a simple Tropical Cyclone (TC) Bogussing scheme using the tc.exe program. The ARW Solver uses the governing equations defined in the NCAR Technical Note (Skamarock et al. 2008). The terrain following hydrostatic-pressure vertical coordinate η used in the ARW equations are expressed as:

$$\eta = \frac{(p_h - p_{ht})}{\mu}$$

$$\mu = p_{hs} - p_{ht} \tag{1}$$

where p_h is the hydrostatic pressure component; p_{ht} is the pressure value at the top boundary; and p_{hs} is the pressure value at the surface boundary. Given the geopotential variable $\phi = gz$, pressure variable p, and the inverse density variable $\alpha = 1/\rho$, the flux-form Euler equations are expressed as:

$$\partial_t U + (\nabla \cdot \mathbf{V}u) - \partial_x(p\phi_n) + \partial_\eta(p\phi_x) = F_U$$

$$\partial_t V + (\nabla \cdot \mathbf{V}v) - \partial_y(p\phi_n) + \partial_\eta(p\phi_y) = F_V$$

$$\partial_t W + (\nabla \cdot \mathbf{V}w) - g(\partial_\eta p - \mu) = F_W$$

$$\partial_t \Theta + (\nabla \cdot \mathbf{V}\theta) = F_\Theta$$

$$\partial_t \mu + (\nabla \cdot \mathbf{V}) = 0$$

$$\partial_t \phi + \mu^{-1}[(\nabla \cdot \mathbf{V}\phi) - gW] = 0 \tag{2}$$

The diagnostic relation for the inverse density and the equation of state are defined as:

$$\partial_\eta \phi = -\alpha\mu$$

$$p = p_o(R_d\theta/p_o\alpha)^\gamma \tag{3}$$

where $\gamma = c_p/c_v = 1.4$ is the ratio of the dry air heat capacities; R_d is the dry air gas constant; p_o is a refence pressure; and F_U, F_V, F_U, and F_Θ are the forcing terms. Given the mass of the dry air μ_d, the hydrostatic pressure of the dry atmosphere $p_{dh,}$, and the hydrostatic pressure at the top of the dry atmosphere p_{dht}, the vertical coordinate with respect to the dry air mass can be expressed as:

$$\eta = (p_{dh} - p_{dht})/\mu_d \tag{4}$$

Using the following coupled variables:

$$\mathbf{V} = \mu_d \mathbf{v}$$
$$\Omega = \mu_d \dot\eta$$
$$\Theta = \mu_d \theta \tag{5}$$

the moist Euler equations can be formulated as follows:

$$\partial_t U + (\nabla \cdot \mathbf{V}u) + \mu_d \alpha \partial_x p + (\alpha/\alpha_d)\partial_\eta p \partial_x \emptyset = F_U$$
$$\partial_t V + (\nabla \cdot \mathbf{V}v) + \mu_d \alpha \partial_y p + (\alpha/\alpha_d)\partial_\eta p \partial_y \emptyset = F_V$$
$$\partial_t W + (\nabla \cdot \mathbf{V}w) - g[(\alpha/\alpha_d)\partial_\eta p - \mu_d] = F_W$$
$$\partial_t \Theta + (\nabla \cdot \mathbf{V}\theta) = F_\Theta$$
$$\partial_t \mu_d + (\nabla \cdot \mathbf{V}) = 0$$
$$\partial_t \emptyset + \mu_d^{-1}[(\nabla \cdot \mathbf{V}\emptyset) - gW] = 0$$
$$\partial_t Q_m + (\nabla \cdot \mathbf{V}q_m) = F_{Q_m} \tag{6}$$

where $\alpha_d = 1/\rho_d$ is the inverse density of the dry air; α is the inverse density considering the full parcel density $\alpha = \alpha_d(1 + q_v + q_c + q_r + q_i + ...)^{-1}$. The q_* variables are the mixing

ratios for water vapor, cloud, rain, ice, etc. The diagnostic equations for the dry inverse density and the full pressure are

$$\partial_\eta \emptyset = -\alpha_d \mu_d$$

$$p = p_o (R_d \theta_m / p_o \alpha_d)^\gamma \tag{7}$$

where $\theta_m = \theta(1 + (R_v/R_d)q_v) \approx \theta(1 + 1.61q_v)$; $Q_m = \mu_d q_m$; and $q_m = q_v, q_c, q_i, \dots$.

3.1.1.2 WRF Preprocessing System (WPS)

The WRF Preprocessing System (WPS) prepares the input for real-data simulations from the given static geographical data and gridded meteorological data (**Figure 9**). This is performed by using three programs, namely *geogrid.exe*, *ungrib.exe*, and *metgrid.exe*. All the parameters to be used are defined in a *namelist.wps* file.

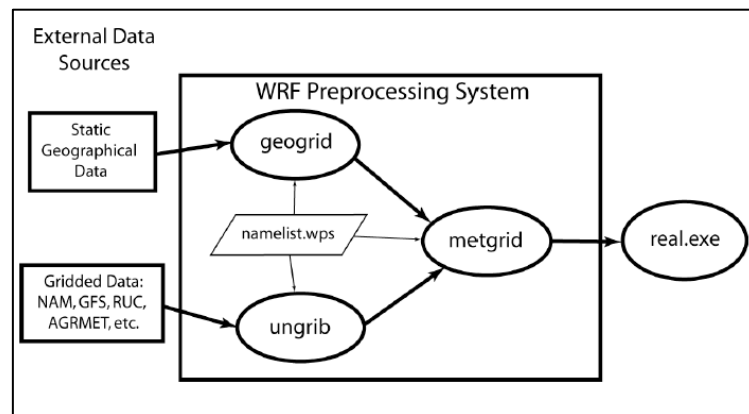**Figure 9**. WRF Preprocessing System (WPS).

The model coarse domain (and finer nested domains, if any) are created using the geogrid program. The size and location of the domains, as well as the map projection, are defined in the *namelist.wps*. The geographical data used was from the United States Geological Survey (USGS) dataset. The default land use information is obtained from the MODIS IGBP 21-category data.

The *ungrib.exe* program extracts the needed fields from the input time varying meteorological GRIB data. A variable table (Vtable), depending on the global or regional model used, is linked to the program to define which meteorological data fields will be used. After running *ungrib.exe*, the data is written in a simpler intermediate format.

The simulation domain files (from the *geogrid.exe* program) and intermediate-format meteorological files (from the *ungrib.exe* program) are then horizontally interpolated using the *metgrid.exe* program to create the meteorological input data (in netCDF format) needed for the real-time simulation. *Metgrid.exe* is also capable of combining meteorological and land-surface fields from multiple model sources.

3.1.1.3 WRF *real.exe* and *wrf.exe*

The WRF model provides several microphysics, cumulus parametrizations, surface physics, planetary boundary layer physics, and atmospheric radiation physics for different suitable applications. The desired physics options, as well as the simulation period and time step, are listed in the *namelist.input* file. To perform the numerical integration calculations using the selected parameters, the *real.exe* program for initialization and then the *wrf.exe* program are run. When successful, the simulation results are compiled in *wrfout* files for postprocessing such as plotting the tropical cyclone wind field and track.

3.1.1.4 Tropical Cyclone Bogussing (*tc.exe*)

To improve the boundary conditions in the simulation, the TC Bogussing scheme was utilized in the TC program of WRF. First, the existing tropical cyclone was removed by locating the point of maximum vorticity near the observed best track coordinates. A bogus

tropical cyclone was then added with a Rankine vortex-based wind profile centered at the desired location (Hsiao et al. 2010):

$$v = A(z)F(r)$$

$$F(r) = \begin{cases} \frac{v_m}{r_m}r; & r \leq r_m \\ \frac{v_m}{r_m{}^\alpha}r^\alpha; & r > r_m \end{cases} \tag{8}$$

where v is the wind speed, v_m is the maximum wind speed observed, r_m is radius of maximum wind, and α is a constant with a value of -0.75. $A(z)$ represents the scale factor or the maximum azimuthal mean wind, accounting for amplitude and height dependence. In the present study, $A(z) = 0.90$ was used, following the value used for $r_m = 50$ km on a 15 km domain grid size in Nakamura et al. 2016.

3.1.2   Surge Model: FVCOM

The FVCOM is an unstructured-grid, three-dimensional primitive equation free-surface coastal ocean model capable of simulating pressure- and wind-driven surges (Chen et al. 2011). The model uses the finite-volume approach, utilizing the geometric flexibility of finite-element methods and the computational efficiency of finite difference methods. This method is suitable in the simulation of mass, momentum, salt, and heat conservation in complex irregular coastal and estuarine areas. For the cases of Typhoon Rai and Cyclone Batsirai, the FVCOM-SWAVE or the FVCOM coupled with the Simulating WAIn this study, FVCOM and FVCOM-SWAVE version 4.1 were used.

The governing momentum, continuity, temperature, salinity, and density equations without snow and ice are:

$$\frac{\partial u}{\partial t} + u\frac{\partial u}{\partial x} + v\frac{\partial u}{\partial y} + w\frac{\partial u}{\partial z} - fv = -\frac{1}{\rho_o}\frac{\partial(p_H+p_a)}{\partial x} - \frac{1}{\rho_o}\frac{\partial q}{\partial x} + \frac{\partial}{\partial z}\left(K_m\frac{\partial u}{\partial z}\right) + F_u$$

$$\frac{\partial v}{\partial t} + u\frac{\partial v}{\partial x} + v\frac{\partial v}{\partial y} + w\frac{\partial v}{\partial z} - fu = -\frac{1}{\rho_o}\frac{\partial(p_H+p_a)}{\partial y} - \frac{1}{\rho_o}\frac{\partial q}{\partial y} + \frac{\partial}{\partial z}\left(K_m\frac{\partial v}{\partial z}\right) + F_v$$

$$\frac{\partial w}{\partial t} + u\frac{\partial w}{\partial x} + v\frac{\partial w}{\partial y} + w\frac{\partial w}{\partial z} = -\frac{1}{\rho_o}\frac{\partial q}{\partial z} + \frac{\partial}{\partial z}\left(K_m\frac{\partial w}{\partial z}\right) + F_w$$

$$\frac{\partial u}{\partial x} + \frac{\partial v}{\partial y} + \frac{\partial w}{\partial z} = 0$$

$$\frac{\partial T}{\partial t} + u\frac{\partial T}{\partial x} + v\frac{\partial T}{\partial y} + w\frac{\partial T}{\partial z} = \frac{\partial}{\partial z}\left(K_h\frac{\partial T}{\partial z}\right) + F_T$$

$$\frac{\partial S}{\partial t} + u\frac{\partial S}{\partial x} + v\frac{\partial S}{\partial y} + w\frac{\partial S}{\partial z} = \frac{\partial}{\partial z}\left(K_h\frac{\partial S}{\partial z}\right) + F_S$$

$$\rho = \rho(T,S,p) \qquad (9)$$

where x, y, and z are the east, north, and vertical axes in the Cartesian coordinate system; u, v, and w are the directional velocity components; T is the temperature; S is the salinity; ρ is the density; p_a is the sea surface air pressure; p_H is the hydrostatic pressure; q is the non-hydrostatic pressure; f is the Coriolis parameter; g is the gravitational acceleration; K_m is the vertical eddy viscosity coefficient; and K_h is the thermal vertical eddy diffusion coefficient. At the right-hand side of the equations, F_u, F_v, F_T, and F_S are the horizontal momentum, thermal, and salt diffusion terms, respectively.

The Mellor and Yamada level 2.5 (MY-2.5) turbulent closure model equations are shown below:

$$\frac{\partial q^2}{\partial t} + u\frac{\partial q^2}{\partial x} + v\frac{\partial q^2}{\partial y} + w\frac{\partial q^2}{\partial z} = 2(P_s + P_b - \varepsilon) + \frac{\partial}{\partial z}\left(K_q\frac{\partial q^2}{\partial z}\right) + F_q$$

$$\frac{\partial q^2 l}{\partial t} + u\frac{\partial q^2 l}{\partial x} + v\frac{\partial q^2 l}{\partial y} + w\frac{\partial q^2 l}{\partial z} = lE_1\left(P_s + P_b - \frac{\widetilde{W}}{E_1}\varepsilon\right) + \frac{\partial}{\partial z}\left(K_q\frac{\partial q^2 l}{\partial z}\right) + F_l \quad (10)$$

where q^2 is the turbulent kinetic energy; l is the turbulent macroscale; K_q is the vertical eddy diffusion coefficient; F_q and F_l are the horizontal diffusion of the turbulent kinetic

energy and macroscale; P_s and P_b are the shear and buoyancy production terms; ε is the turbulent kinetic energy dissipation rate; and W is a wall proximity function.

The unstructured triangular mesh domains were generated using the Surface Water Modelling System (SMS) version 12 software. The forcing files that incorporate the wind, air pressure, and open boundary condition data from the WRF output files to the mesh system were programmed in MATLAB. The wind drag coefficient C_D was computed based on the momentum transfer equations used in Nakamura et al. (2016), who combined the equations from Honda and Mitsuyasu (1980) and Yokota et al. (2011):

$$C_D = \begin{cases} 0.00128(1 - 0.01890v) & v \le 8.0 \; m/s \\ 0.000581(1 + 0.1078v) & 8.0 \; m/s \; < v \le 30 \; m/s \\ 0.00246 & v > 30 \; m/s \end{cases} \qquad (11)$$

where v is the wind speed (m/s).

3.1.3   Structure Model: STAAD.Pro

STAAD.Pro can easily convert a physical into an analytical model (Bentley Systems 2012). The program utilizes the Finite Element Method (FEM) and other complex methods in its static and dynamic analyses, depending on the required situation. The linear algebraic element stiffness equations can be written in the form:

$$\{P\}=[K]\{d\} \qquad (12)$$

where {P} is the element force vector, [K] is the element stiffness matrix, and {d} is the element displacement vector. In this study, the STAAD.Pro Connect Edition version 22 was used.

3.2 Numerical Condition Set-up

The coupled weather-surge-structure model is applied to the three tropical cyclone cases of Typhoon Haiyan, Typhoon Rai, and Cyclone Batsirai.

3.2.1 Typhoon Haiyan

3.2.1.1 WRF Set-up

A parent domain (d01) with a grid size of 9 km by 9 km covering the track of Typhoon Haiyan from its early formation in the Pacific Ocean until its departure from the Visayas region was set-up. A smaller 3 km by 3 km nested domain (d02) that covers the San Pedro Bay and the Leyte and Samar islands was prepared for a finer resolution of the pressure and wind fields. Two-way nesting was imposed for this set-up, with the Mercator map projection being used for both domains (**Figure 10**).
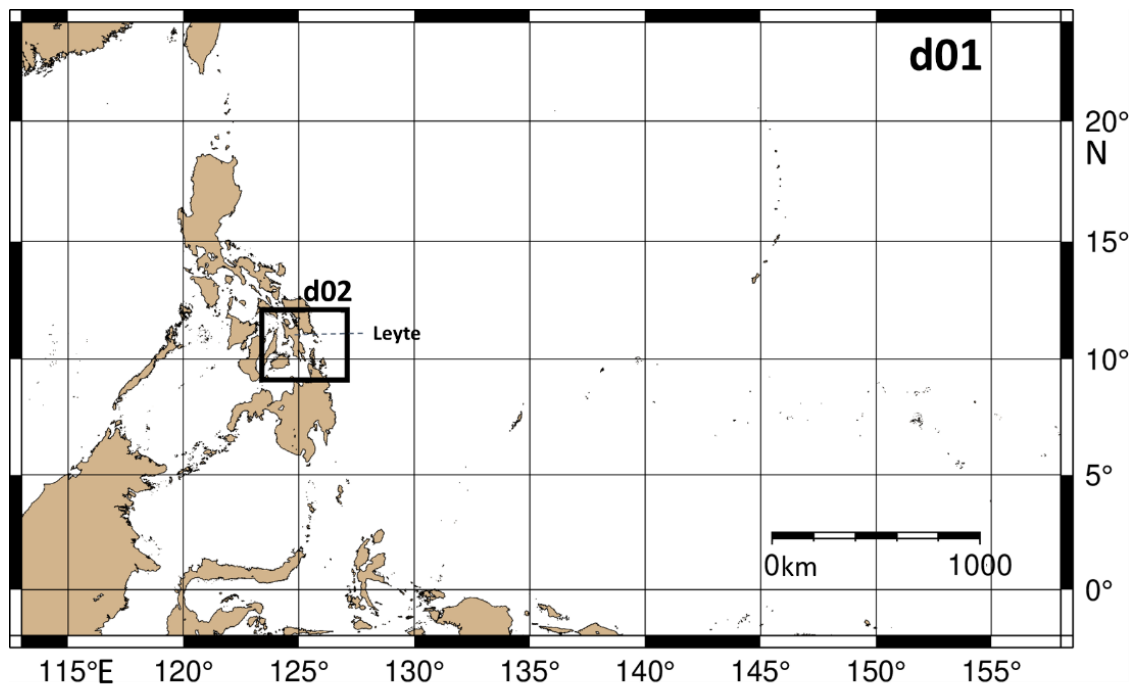

Figure 10. WRF Domain Set-up (Haiyan).

The simulation period for the parent domain (d01) was from 04 November 2013 18:00 UTC to 09 November 2013 06:00 UTC, while for the nested domain (d02) it ranged from 6 November 2013 18:00 UTC to 09 November 2013 06:00 UTC. The meteorological files used for this study were the 6-hourly Global Forecast System (GFS) 0.5º x 0.5º resolution data of the NCAR Research Data Archive (NCEP et al. 2003). The physics settings used are shown in **Table 1**. Two simulations were performed (with and without TC-Bogussing scheme) to investigate the effects of TC Bogussing scheme and the simulated MSLP, maximum wind speed, and track of Haiyan were recorded and compared with the JMA observed data.

Table 1. Numerical condition set-up (Haiyan).

WRF Set-up		
Domain	**d01**	**d02**
Simulation Start Time (UTC)	2013 November 04, 18:00	2013 November 07, 06:00
Simulation End Time (UTC)	2013 November 08, 18:00	2013 November 08, 18:00
Latitude and Longitude	2º S - 24º N, 113º E - 158º E	9.1º N - 12.1º N, 123.4º E - 127.1º E
Grid Size	9,000 m x 9,000 m	3,000 m x 3,000 m
Microphysics	Purdue Lin Scheme	
Planetary Boundary Layer	Quasi-normal Scale Elimination (QNSE) Scheme	
Cumulus Parametrization	Kain-Fritsch Scheme	
Shortwave and Longwave	RRTMG Scheme	
Land Surface	Noah-MP Land Surface Model	
Surface Layer	QNSE Scheme	

Vertical Layers	30
Meteorological Data	Global Forecast System (GFS) 0.5º x 0.5º 6-hourly data
FVCOM Set-up	
Simulation Time (UTC)	2013 November 07, 06:00 - 2013 November 08, 18:00
Mesh System	147,594 nodes; 274,971 triangular elements
Mesh Size	5 m – 1,000 m
Coastline Data	Global Self-consistent, Hierarchical, High-resolution Geography (GSHHG) Version 2.3.7 Database
Elevation Data	General Bathymetric Chart of the Oceans (GEBCO) 2014 30-arc second grid; and digitized NAMRIA maps (NAMRIA 2014)
Building Location Data	OpenTopoMap
STAAD.Pro Set-up	
Reference Design Code	2015 NSCP

3.2.1.2 FVCOM Set-up

The Global Self-consistent, Hierarchical, High-resolution Geography (GSHHG) Version 2.3.7 Database (Wessel and Smith 1996) and the General Bathymetric Chart of the Oceans (GEBCO) 2014 Grid with a 30-arc second resolution (GEBCO 2014) were used for the mesh domain generation of the base coastline and bathymetry data, respectively. This was further improved by including local information from digitized maps (**Table 2**) of the National Mapping and Resource Information Authority (NAMRIA), the central mapping agency of the Philippines. The contours and data points from the maps were plotted in SMS and were interpolated into a 50-meter by 50-meter fine grid dataset. For the location of the buildings, OpenTopoMap data was used. For simplification, some buildings that are located closer to each other were aggregated (modelled) as one building (as it was not possible to

reproduce narrow roads passing between buildings using a 5-m mesh size), as seen in **Figure 11**. Another assumption is that all the buildings were modelled to be taller than the surge since it is difficult to set each one to their actual heights. The perimeter of the buildings was modelled using closed boundary conditions, thus affecting the wind and flow over the triangular mesh domain. An average of 5-meter segments were drawn for the outlines of the buildings.

Table 2. List of digitized NAMRIA maps (NAMRIA 2014).

Type	Map Area	Scale
Nautical	Leyte Gulf and Approaches	1:150,000
Topographic	Tigbao	1:10,000
Topographic	Tacloban City	1:10,000
Topographic	Pawing	1:10,000
Topographic	Tanauan	1:10,000
Topographic	San Antonio	1:10,000
Topographic	Basey	1:10,000

For the FVCOM simulation a single domain, encompassing the coastline of Leyte Gulf and downtown Tacloban, was set up. Details about this domain are given in **Table 1**, and the mesh system is presented in **Figure 11**. The bottom drag coefficient C_B used to compute the bottom shear stress was obtained from:

$$C_B = \max\left[\frac{\kappa^2}{\ln\left(\frac{z_{ab}}{z_o}\right)^2}, 0.0025\right] \qquad (13)$$

where κ is the Von Karman constant (= 0.4), z_{ab} is the height from the logarithmic bottom layer to the model layer, and z_o is the bottom roughness parameter. A value of 0.025 m

(default value for FVCOM) was used for z_o in the coastal area, while 0.04 m was set for the land area, following Nakamura, Mäll, and Shibayama (2019).

Tide effects during the passage of the typhoon were considered negligible and thus were not included in the simulation, as the event occurred when the water surface was around the mean sea level. The simulated storm surge heights were validated with recorded watermarks at selected locations close to the coastline that were obtained from the results of field surveys (Tajima et al. 2014; Mikami et al. 2016; Takagi et al. 2016). The location of Panalaron Central School, as indicated in **Figure 11**, was selected as the case study structure to be analyzed, and thus the simulated inland wind speed at 10 m elevation, inundation depth, and horizontal flow velocity at this location were recorded. The inland part of downtown Tacloban generally did not experience significant structural damage compared to the coastal areas, which were heavily affected by the wind and surge (Mas et al. 2015). To further check the influence of flooding, another hypothetical structure of the same characteristics was set at Libertad, a location near the coast of Tacloban where a higher storm surge height was expected (shown in **Figure 11**) and compared with that at Panalaron.
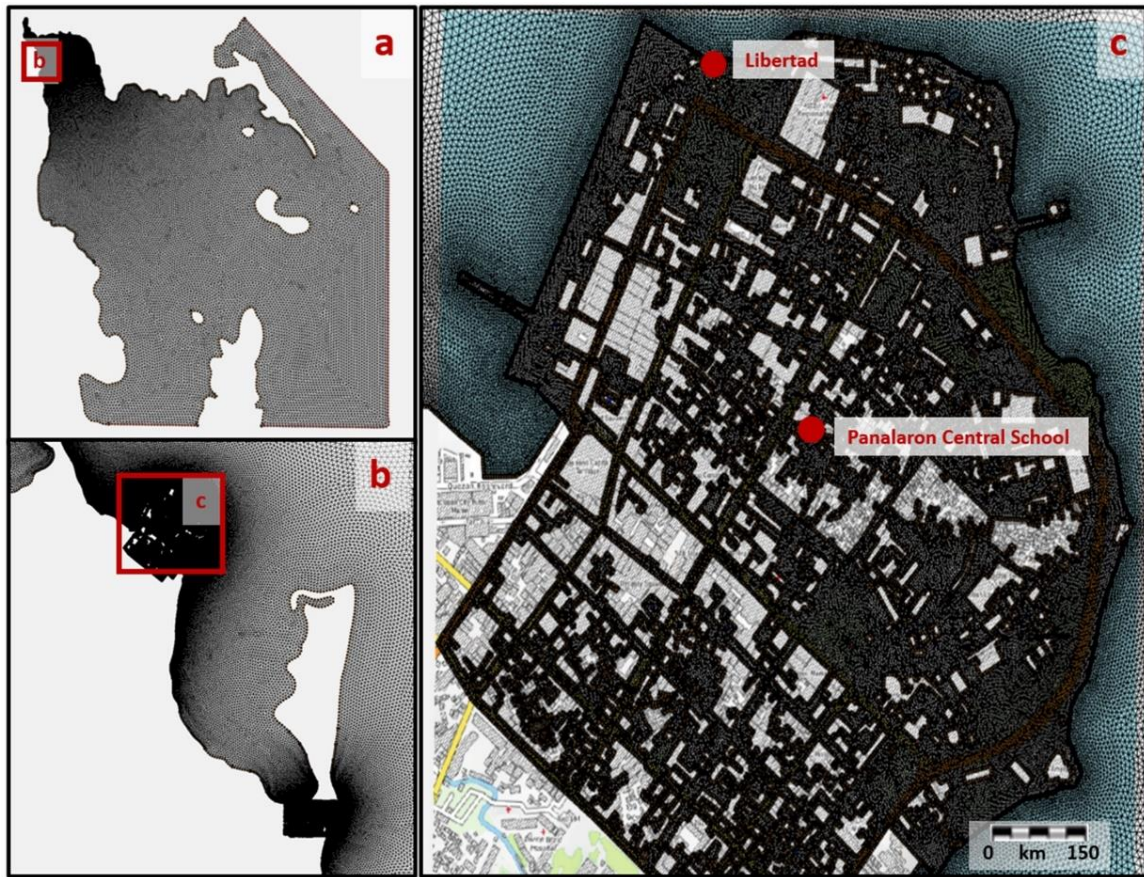
Figure 11. (a) Entire FVCOM domain; (b) Location of Downtown Tacloban; (c) Location of Panalaron Central School and Libertad.

3.2.1.3 STAAD.Pro Set-up

Panalaron Central School (a 4-floor public school building) was modelled in STAAD.Pro. As precise information about the school was not available, its geometry was determined based on information available on architectural and structural plans for a typical 4-story reinforced concrete public school building designed by DPWH, as shown in **Figure 12**. The square column C1 was selected as the structural member to be analyzed.

For the analysis of forces like those that would have been applied by a typhoon Haiyan level event, two general loading types were considered: wind loads and flood loads. The FVCOM results at the selected location in Tacloban were used for the wind and flood

forcing. The flood loads in this study were composed of hydrostatic, hydrodynamic, and breaking wave loads. While surge loads can be applied from many directions, in the present work and in order to simplify the authors applied the wind and flood loads to the structure model in three directions: along the positive global X axis, along the positive global Z axis, and along both the positive global X and positive global Z axes. These loads were applied perpendicular to the structural members for each loading direction. The axial, shear, and bending moment envelopes at C1 were calculated by obtaining the maximum values of the internal forces along the member for both positive (+ dir) and negative (- dir) X and Z axes.
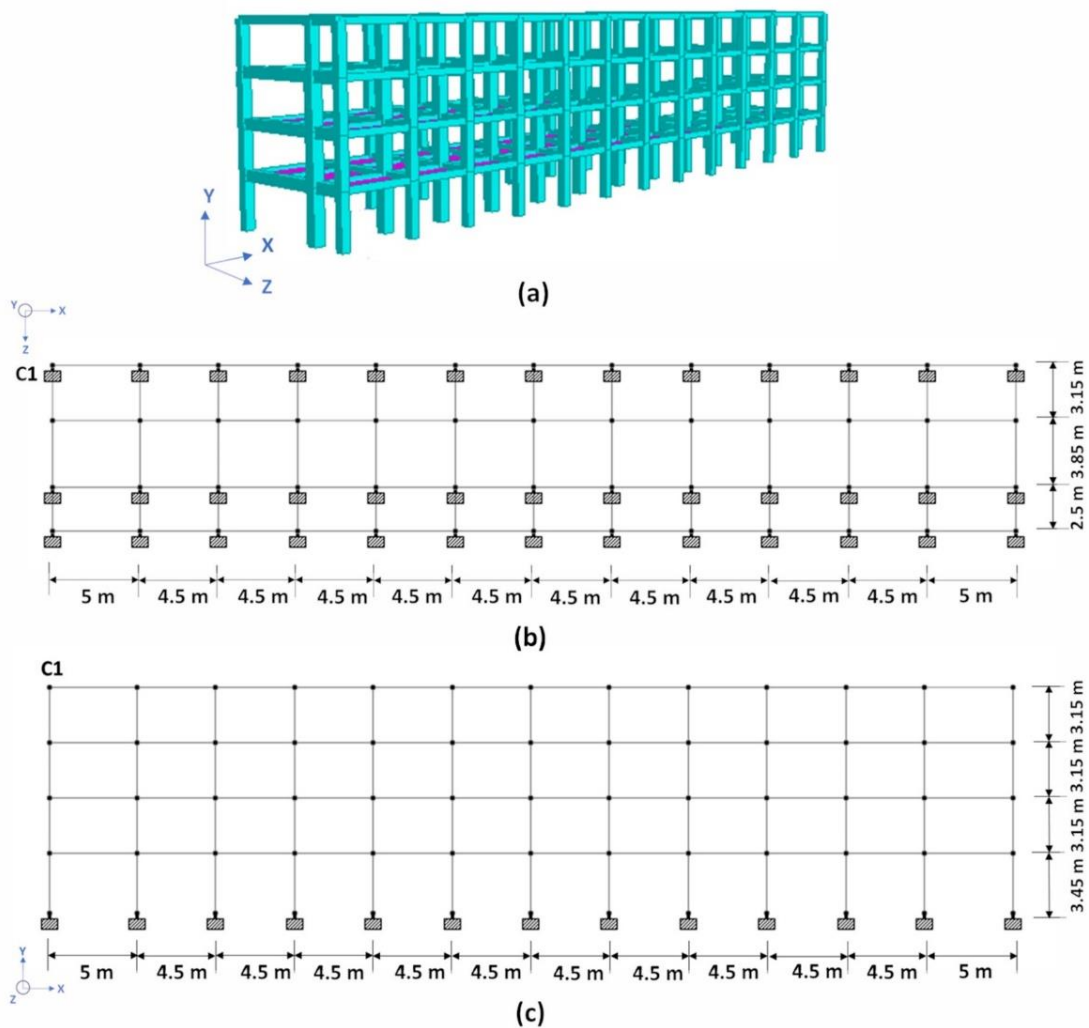

Figure 12. (a) 3-D model of the 4-floor school building; (b) Top view and (c) Front view of the model.

The wind loads were calculated as wind speed pressure over the exposed areas of the structure (above the inundation level) according to the procedures described in Section 207 of the 2015 NSCP, downscaling the 10 m wind speed obtained from the FVCOM results along the height of the model. The velocity pressure q_z (N/m²) at a given height z was given by:

$$q_{z=}0.613K_z K_{zt} K_d V^2 \tag{14}$$

where K_z is the velocity pressure exposure coefficient (= 0.773 for building height of 12.9 m), K_{zt} is the topographic factor (= 1 for no abrupt changes in the general topography), K_d is the wind directionality factor (= 0.85 for main wind force resisting system), and V is the wind speed (m/s). The wind speed pressure p (N/m²) for the main wind-force resisting system of the structure was obtained from:

$$p = q_z[(GC_p) - (GC_{pi})] \tag{15}$$

where G is the gust effect factor (= 0.85 for a rigid structure), C_p is the external pressure coefficient (based on Section 207C.4.1.1 of the 2015 NSCP), and GC_{pi} is the internal pressure coefficient (±0.18 for enclosed buildings).

The hydrostatic loads were composed of the lateral hydrostatic force and buoyant force. The lateral hydrostatic force F_h (kN) was computed by:

$$F_h = \frac{1}{2}\gamma_w b h_{max}^2 \tag{16}$$

where γ_w is the unit weight of water (10.05 kN/m³ for salt water), b is the width subjected to the force (m), and h_{max} is the maximum inundation depth (m). While 2015 NSCP specifies the need to consider hydrodynamic loads, a detailed methodology to do so was

not provided. For the specific case of Haiyan storm surge these were assumed to be a bore (though it should be noted that storm surges do not always produce bores, and that this was something particular to the case of this event). -Hence, the hydrodynamic loads were calculated based on the American Society of Civil Engineers (ASCE) 7-16 Tsunami Load provisions (ASCE/SEI 2017), with the assumption that the inland flow of the storm surge is similar to that of a tsunami.

The lateral hydrodynamic drag force F_d (kN), considering a tsunami-like bore, was computed by:

$$F_d = \frac{3}{4}\rho_w C_D b(h_e u^2)_{bore} \tag{17}$$

where ρ_w is the density of water (1127.50 kg/m^3 for salt water), C_D is the drag coefficient (2.25 for rectangular columns), h_e is the inundated height at the structure element, and u is the flow velocity (m/s). An equation to calculate breaking wave loads on columns F_w (kN) acting at the still water elevation is provided by 2015 NSCP as follows:

$$F_w = \frac{1}{2}\gamma_w C_D \phi H_B{}^2 \tag{18}$$

where C_D is 2.25 for rectangular columns, ϕ is the column diameter (= 1.4 times the width of a rectangular column in meters) and H_B is the breaking wave height (= 0.78 times the instantaneous flood depth in meters).

3.2.2 Typhoon Rai

3.2.2.1 WRF Set-up

Two numerical models were used in this Typhoon Rai study: WRF version 4.2 for the simulation of Typhoon Rai and FVCOM SWAVE version 4.1 for the simulation of its storm

surges and waves at Tubigon (**Figure 13**). The WRF Model was also used to hindcast Typhoon Rai with the 6-hourly GFS 0.25º x 0.25º meteorological data (NCEP et al. 2015). A two-way nested domain was set-up over the Pacific Ocean and the central Visayas with a simulation period from 2021 12 December 00:00 to 2021 18 December 00:00 UTC. Three domains were set-up for this simulation (**Figure 14**) and the physics settings used are shown in **Table 3**. Unlike the Typhoon Haiyan case, the TC-Bogussing scheme was not employed in the Typhoon Rai simulation.
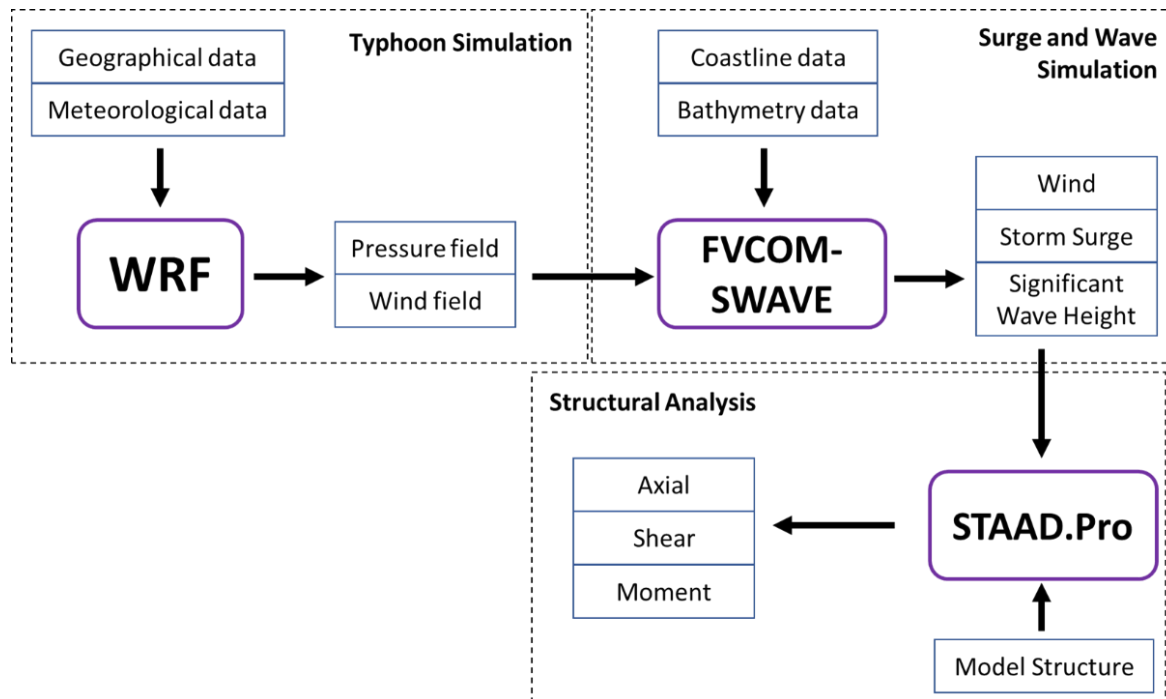

Figure 13. Flowchart of numerical models used in the Typhoon Rai study.
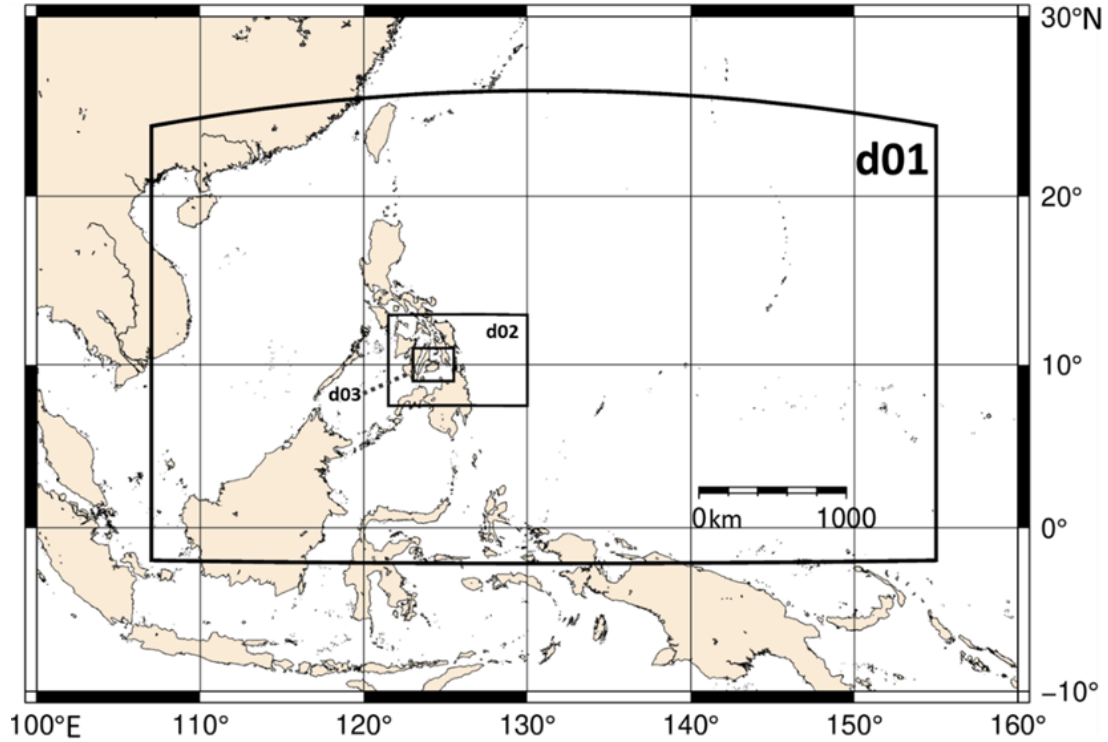
Figure 14. WRF Domain Set-up (Rai).

Table 3. Numerical condition set-up (Rai).

WRF Set-up			
Domain	**d01**	**d02**	**d03**
Simulation Start Time (UTC)	2021 December 13, 00:00	2021 December 15, 00:00	2021 December 16, 00:00
Simulation End Time (UTC)	2021 December 18, 00:00	2021 December 17, 12:00	2021 December 17, 00:00
Latitude and Longitude	2º S - 24º N, 107º E - 155º E	7.5º N - 13º N, 121.5º E - 130º E	9º N - 11º N, 123º E – 125.5º E
Grid Size	9,000 m x 9,000 m	3,000 m x 3,000 m	1,000 m x 1,000 m
Microphysics	Purdue Lin Scheme		
Planetary Boundary Layer	Quasi-normal Scale Elimination (QNSE) Scheme		
Cumulus Parametrization	Kain-Fritsch Scheme		

Shortwave and Longwave	RRTMG Scheme
Land Surface	Noah-MP Land Surface Model
Surface Layer	QNSE Scheme
Vertical Layers	35
Meteorological Data	Global Forecast System (GFS) 0.25º x 0.25 º 6-hourly data
FVCOM-SWAVE Set-up	
Mesh System	59,991 nodes; 117,047 triangular elements
Mesh Size	1,000 m (open boundary) to 100 m (Tubigon)
Simulation Time (UTC)	2021 December 16, 00:00 – 2021 December 17, 00:00
Coastline	Global Self-consistent, Hierarchical, High-resolution Geography (GSHHG) Version 2.3.7 Database
Bathymetry	General Bathymetric Chart of the Oceans (GEBCO) 2021 30-arc second grid, and field survey data
WRF Set-up	
STAAD.Pro Set-up	
Reference Design Code	2015 NSCP

3.2.2.2 FVCOM Set-up

A 1000-m to 300-m unstructured triangular mesh covering the sea between Cebu and Bohol islands (**Figure 15**) was set up using SMS to simulate potential storm surges. The GEBCO 2021 Grid (GEBCO Compilation Group 2021) and bathymetry survey data from Esteban et al. (2022) were interpolated for bathymetry data and the GSHHG Database (Wessel and Smith 1996) was used for the coastline data. It should be noted that all coastlines, including the small islands of Pangapasan, Ubay, and Batasan, were modelled with closed boundaries. Thus, the condition wherein these islands are inundated during high water levels was not

simulated and is considered a limitation of this study. The time-history surges and significant wave heights were calculated at four locations in Tubigon (Tubigon Port, Pangapasan, Ubay, and Batasan) and then compared with measured watermarks. Tidal effects were not included in this study to focus more on the influence of surge and waves in the water elevation.
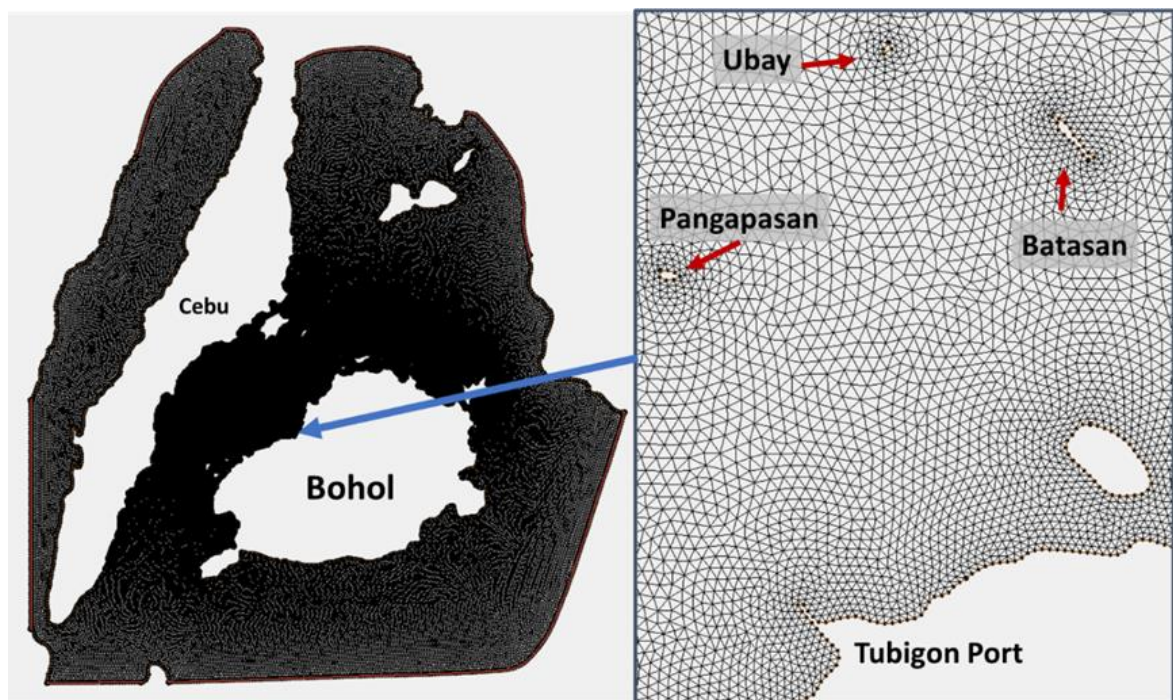

Figure 15. FVCOM Domain Set-up for Rai at Cebu and Bohol.

3.2.2.3 STAAD.Pro Set-up

Similar structural analysis done in the Typhoon Haiyan case was applied in the Typhoon Rai case with some modifications, mainly the public school building was replaced with a 3 meter-long, 3-meter wide, and 6-m high representative 2-storey concrete house structure (**Figure 16**). Pangapasan Island was selected to be the hypothetical location of the structure. Since only the surge as it approached the coastline was modelled and not the inundation over land, the computation of flood loads was treated differently. The inundation height

was assumed to be the maximum potential water level which is the peak simulated surge height plus half of the peak simulated significant wave height. The values of surge, wind, and wave were taken from a nearby node and elements off the island.
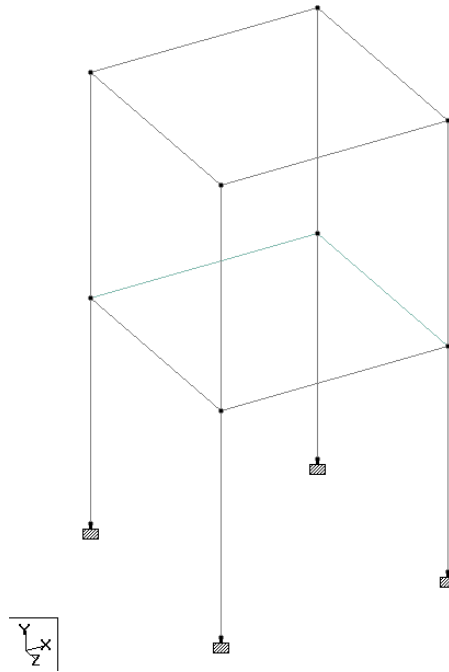

Figure 16. Representative two-storey house structure modelled in STAAD.Pro.

3.2.3   Cyclone Batsirai

3.2.3.1 WRF Set-up

For the Cyclone Batsirai case, the 6-hourly Climate Forecast System Version 2 (CFSv2) 0.5º x 0.5º meteorological data from the National Centers for Environmental Prediction (NCEP) was used in the WRF simulation with the physics settings shown in **Table 4** (Saha et al. 2011)**.** A 9-km by 9-km parent domain was set-up over the Indian Ocean including the islands of Mauritius, Réunion, and Madagascar and a 3-km by 3km nested domain over Mauritius (**Figure 17**) with a simulation period from 2022 31 January 12:00 to 2022 05 February 12:00 UTC. The WRF results of the nested domain were used as boundary conditions for the FVCOM simulation over Mauritius waters.
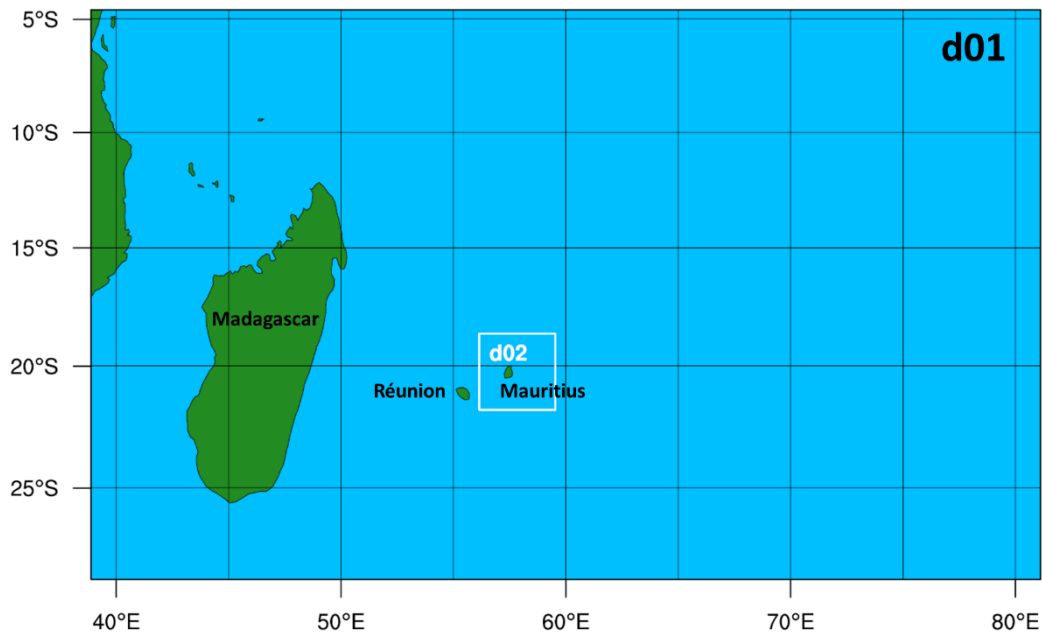
Figure 17. WRF Domain Set-up (Batsirai).

Table 4. WRF numerical condition set-up (Batsirai).

WRF Set-up		
Domain	**d01**	**d02**
Simulation Start Time (UTC)	2022 January 31, 12:00	2022 February 01, 12:00
Simulation End Time (UTC)	2022 February 05, 12:00	2022 February 05, 00:00
Latitude and Longitude	28º S - 6º S, 42º E - 77º E	22º S – 18.5º S, 56.5º E – 59.5º E
Grid Size	9,000 m x 9,000 m	3,000 m x 3,000 m
Microphysics	WRF Single-Moment 6-Class (WSM6)	
Planetary Boundary Layer	Quasi-normal Scale Elimination (QNSE) Scheme	
Cumulus Parametrization	Tiedtke Scheme	

Shortwave and Longwave	RRTMG Scheme
Land Surface	Noah-MP Land Surface Model
Surface Layer	QNSE Scheme
Vertical Layers	45
Meteorological Data	Climate Forecast System Version 2 (CFSv2) 0.5º x 0.5º 6-hourly data

3.2.3.2 FVCOM Set-up

A mesh domain surrounding the Mauritius main island was set up for FVCOM simulation using the SMS software (**Figure 18**) and the simulation properties are listed in **Table 5**. The mesh sizes ranged from 1000 m along the open boundary in the Indian Ocean to 100 m along the coast of Port Louis. The simulated change in water level due to the passage of Cyclone Batsirai at the domain was recorded.
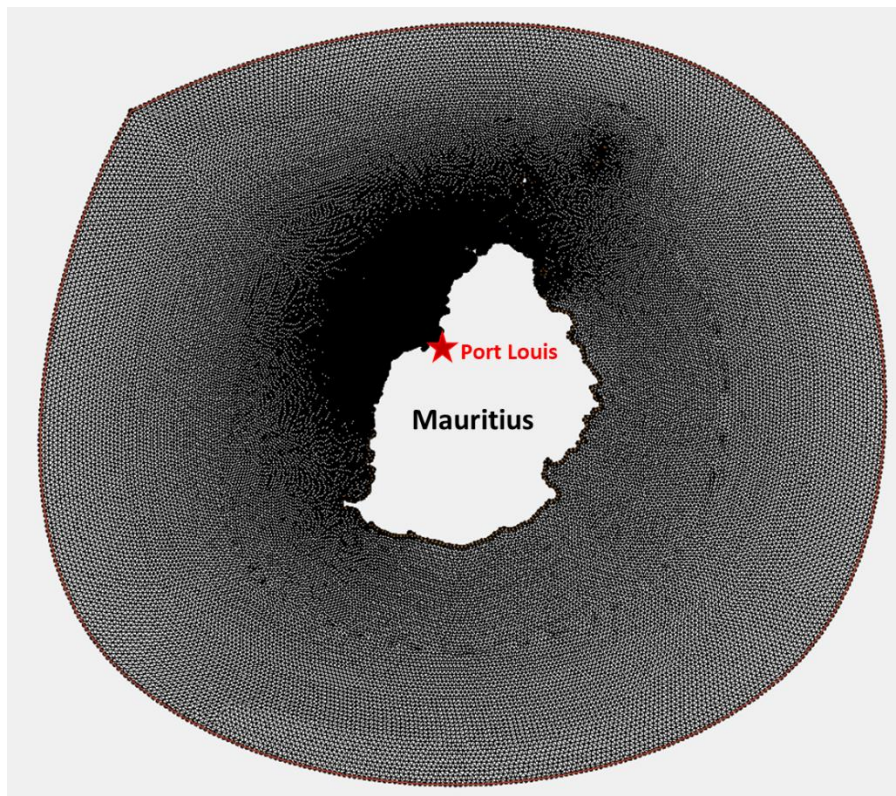
Figure 18. FVCOM Domain Set-up (Batsirai).

Table 5. FVCOM numerical condition set-up (Batsirai).

FVCOM Set-up	
Mesh System	54,792 nodes; 108,249 triangular elements
Mesh Size	1,000 m (open boundary) to 100 m (Port Louis)
Simulation Time (UTC)	2022 February 01, 12:00 – 2022 February 05, 00:00
Coastline	GSHHG Version 2.3.7 Database
Bathymetry	GEBCO 2022 15-arc second grid

CHAPTER 4: RESULTS

4.1 Typhoon Haiyan

4.1.1   WRF Typhoon Simulation

The WRF wind field results showed that the direction of the wind as the storm crossed Leyte province was towards Tacloban (**Figure 19**), producing a positive surge in that area. The comparison of the simulated typhoon tracks with the observation data over the parent (d01) and nested (d02) domains is presented in **Figure 20**, showing a slight deviation between them over the Pacific Ocean. Without TC-Bogus, the deviation in the simulated track increases as the typhoon approaches the Philippines and would result in different pressure and wind fields over San Pedro Bay, compared to the actual event. With TC-Bogus the track is significantly improved, and the storm makes landfall at Leyte with a deviation of around 10 km from the observed location (**Figure 20**).
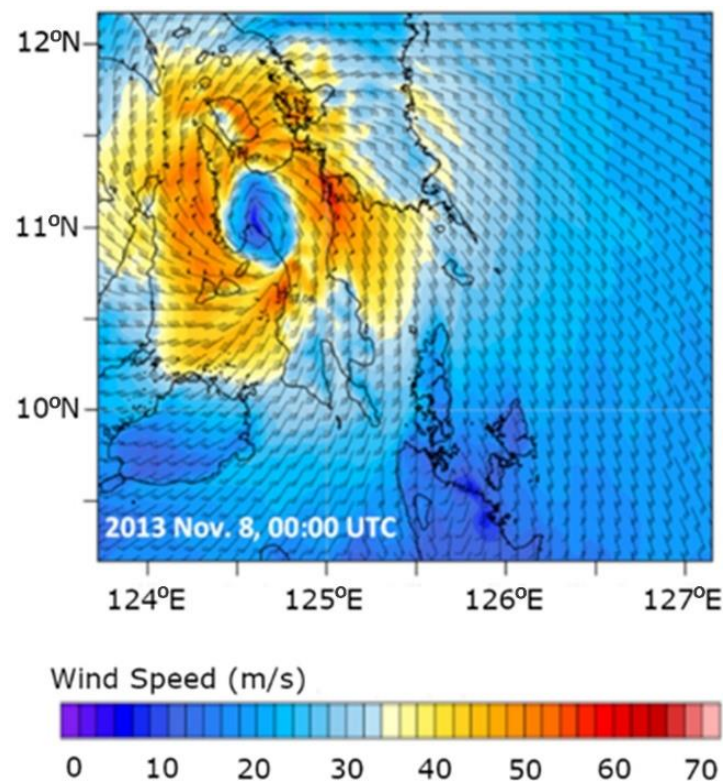

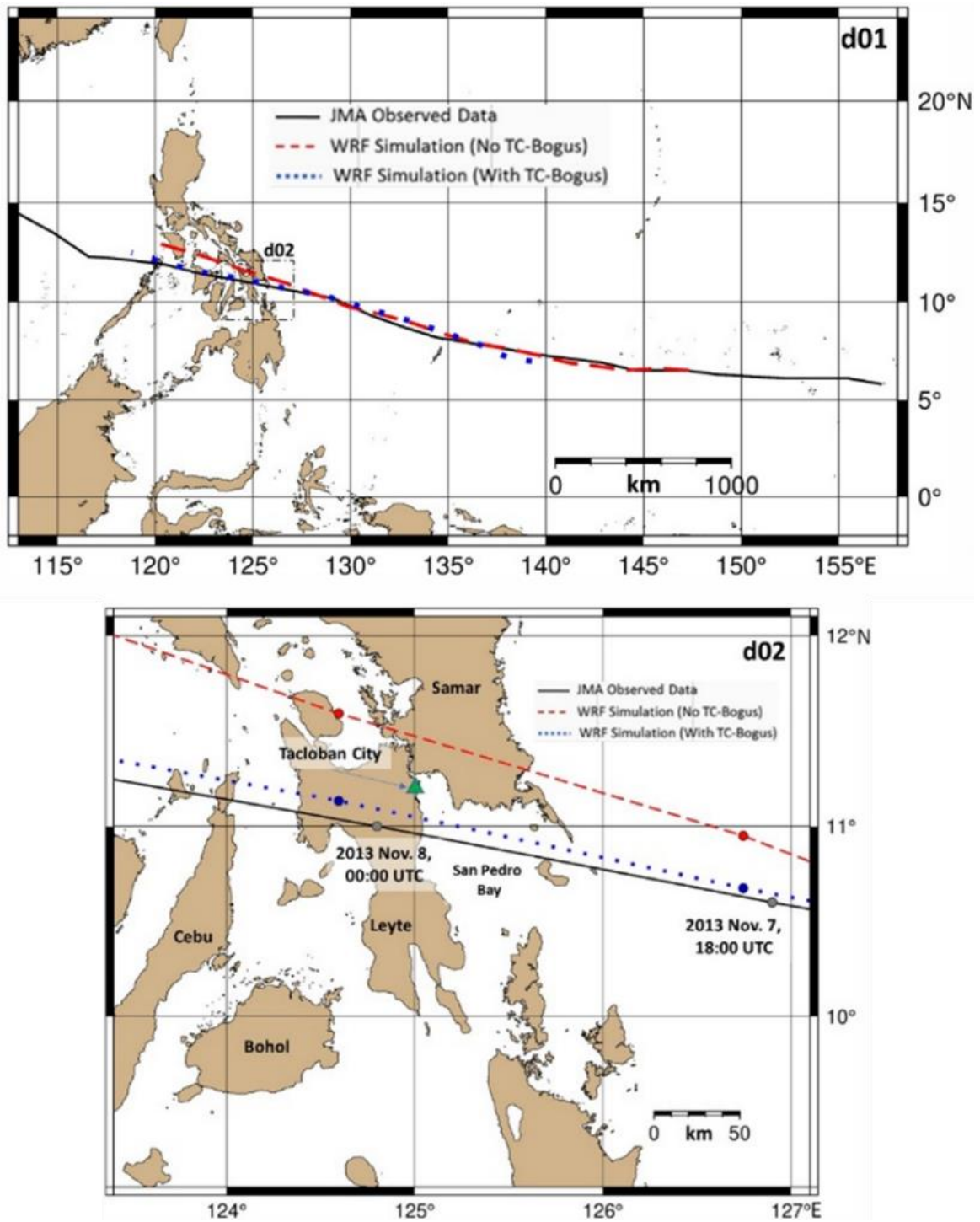**Figure 19.** Simulated WRF wind field results.

Figure 20. Comparison of simulated tracks with observed data at d01 (top) and d02 (bottom).

The MSLP and maximum wind speed obtained from the simulations and the observed data are shown in **Figure 21**. As stated earlier, the peak observed MSLP and maximum wind

speed of Typhoon Haiyan was 895 hPa and 64 m/s, respectively, on 07 November 2013 12:00-18:00 UTC. For the WRF simulation without TC-Bogus, the MSLP is initially lower than the observed one but becomes higher by 06 November 2013 06:00, only reaching 911.2 hPa. The maximum wind speed is initially overestimated, though it is then underestimated as the typhoon approached the Philippines, peaking at 59.4 m/s. For the TC-Bogus case, the MSLP is initially higher than the observed one but reached a low of 897.9 hPa. The maximum wind speed agrees well with the observation data, peaking at 62.0 m/s. Additionally, the simulated MSLP and maximum wind speed around the time of landfall at Leyte (8 November 2013 00:00 UTC) only has discrepancies of +7.5 hPa and -0.6 m/s, respectively, with the observed data. Thus, the WRF results with TC-Bogus were used as inputs into the FVCOM simulation.
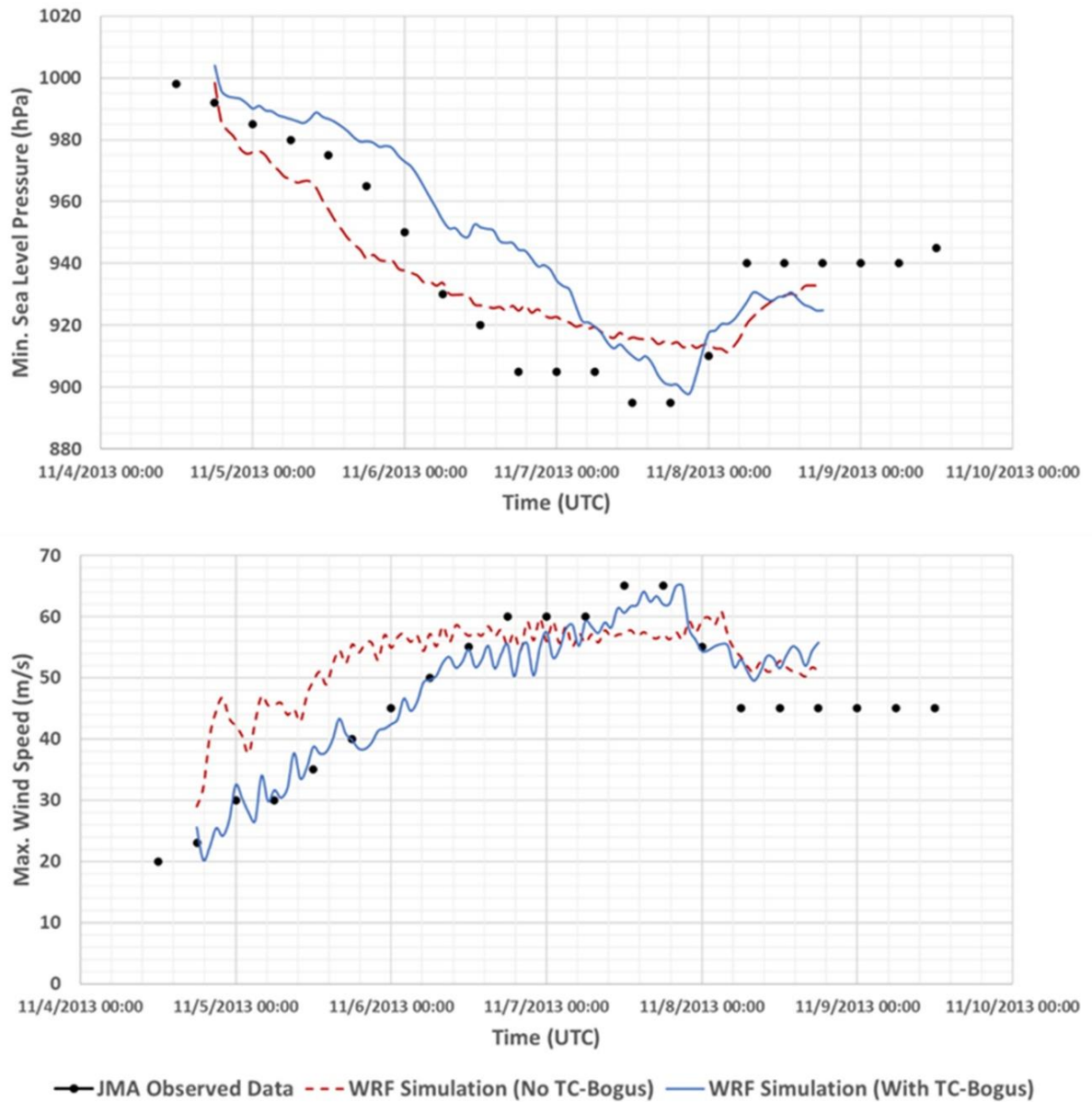
Figure 21. Comparison of MSLP (top) and maximum wind speed (bottom) of simulation results with observed data.

4.1.2 FVCOM Storm Surge Simulation

The results of the storm surge simulation were validated by comparing them with 77 inundation water level trace marks provided by Tajima et al. (2014), Takagi et al. (2016) and Mikami et al. (2016), as shown in **Figures 22-24**. However, there was no measured data at the exact location of Panalaron Central School. Thus, to validate the storm surge

height at this area, the time histories of the simulated storm surge heights at three representative locations (namely Tacloban Airport, Tacloban City Convention Center, and around Paterno Street) in Tacloban are also shown in **Figure 23**, together with the maximum observed water trace level there (obtained from Mikami et al., 2016). The maximum simulated storm surge heights at these three locations are within 1 meter from the recorded heights, though it should be noted that as the distance to this city increases, they are progressively underestimated. The flow velocity results provided by the storm surge simulation were validated using analysis from a video taken near Alejandro Hotel at Paterno Street (see Takagi et al. 2016), with **Figure 25** showing that there was a good agreement between them (Points 1-5 refer to the triangular elements in the computational grid that were situated just in front of the hotel).
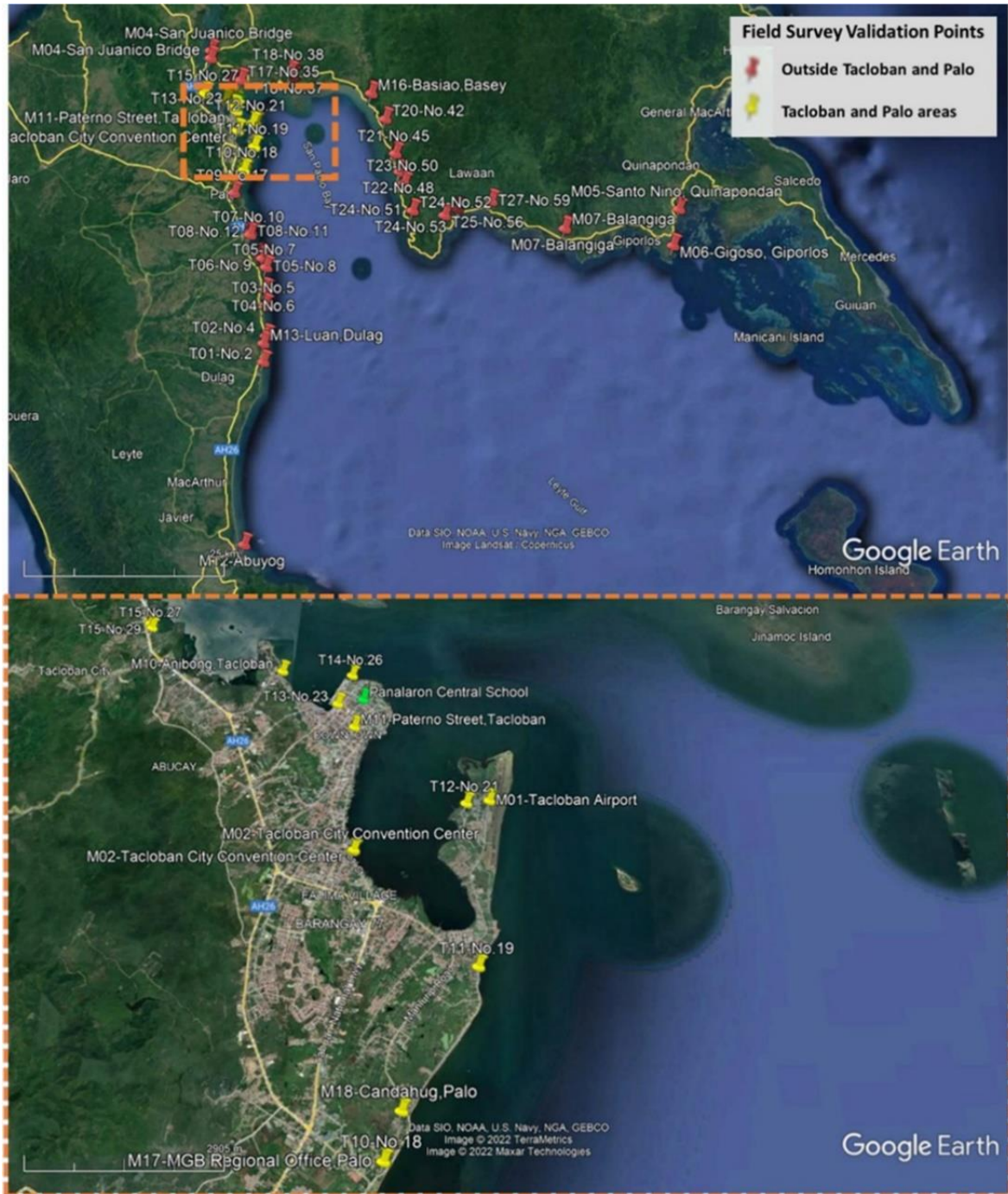
Figure 22. Approximate locations of the data points taken from field surveys. (Google Earth). The green pin shows the location of Panalaron Central School.
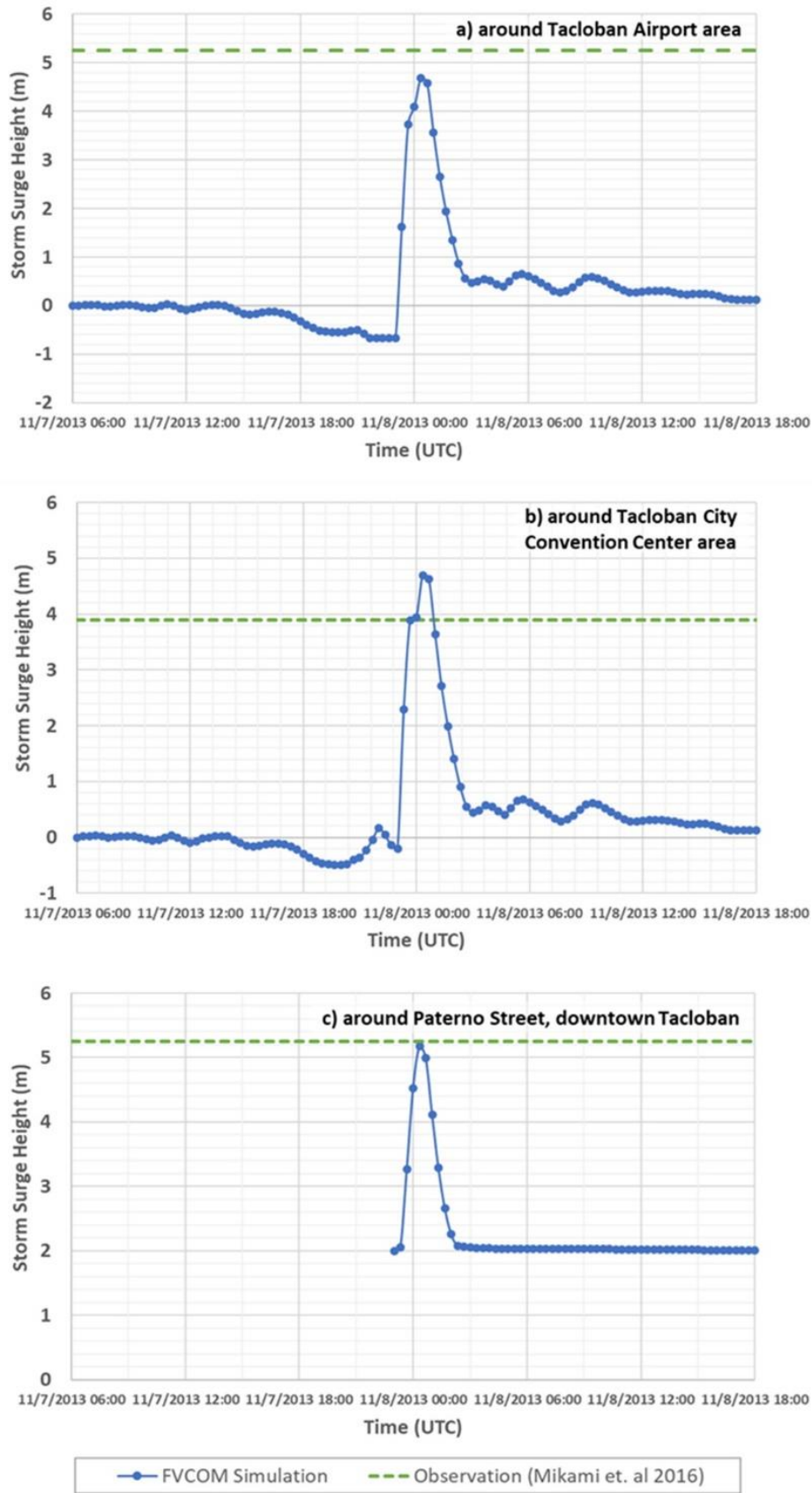
Figure 23. Simulated time-series of surge height at three locations in Tacloban, together with recorded trace water heights from post-disaster field surveys (Mikami et al. 2016).
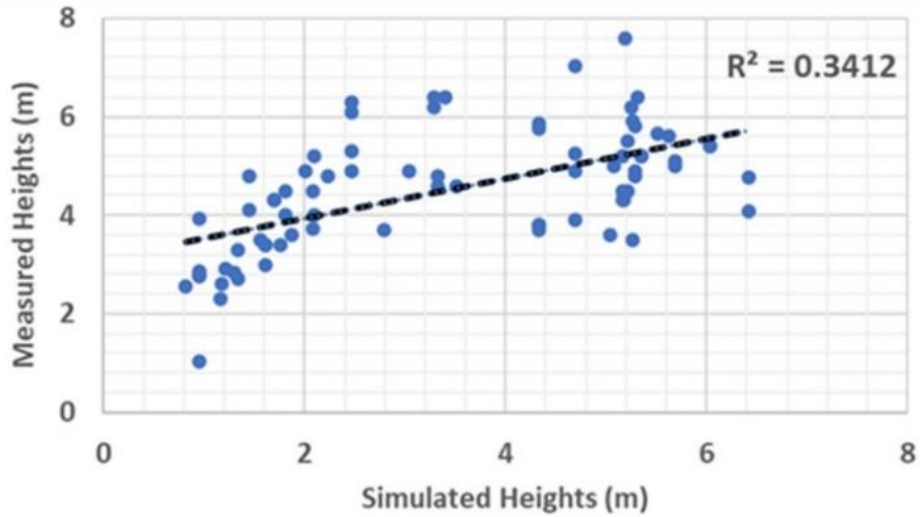
Figure 24. Comparison of simulated and measured storm surge heights.
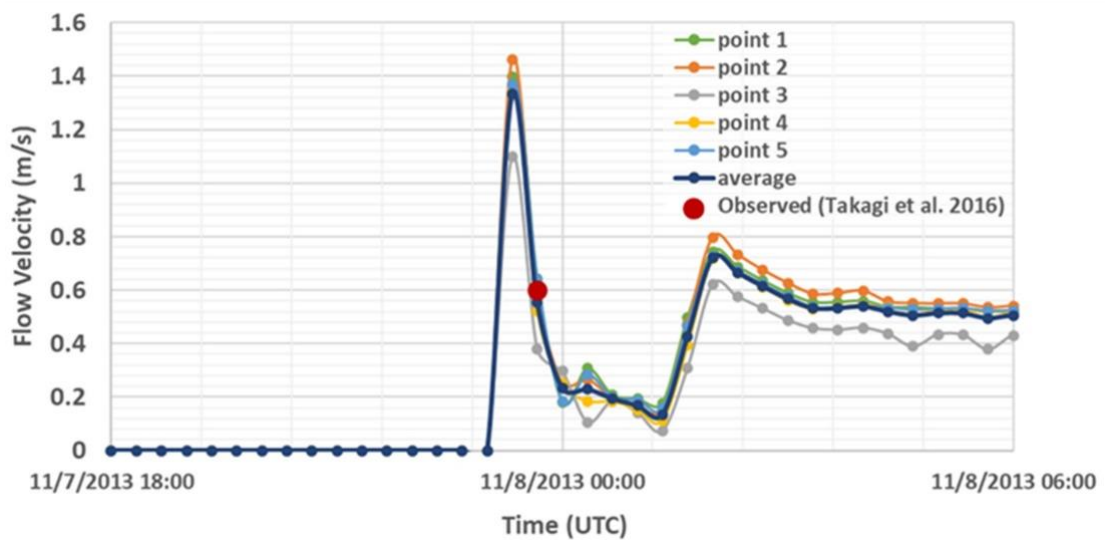
Figure 25. Validation of simulated flow velocity near Alejandro Hotel with analysis of recorded velocity (see Takagi et al. 2016).

The time-series of the 10-meter wind speed, depth, and horizontal flow speed of the surge at the location of Panalaron Central School was obtained from the FVCOM results (**Figure 26**), which peaked at 52.56 m/s, 3.45 m, and 0.39 m/s, respectively. The values during three time periods (start of inundation, during maximum wind speed, and during maximum inundation), as indicated in **Figure 26**, were used as inputs for the wind and flood loads in

the STAAD.Pro computation. To compare the significance of flood loads with that of wind loads, a maximum wind with no flooding case was also included in the analysis and included. For comparison, the FVCOM results at Libertad are shown in **Figure 27**, with peak values of 52.78 m/s, 5.23 m, and 0.53 m/s for wind speed, inundation, and flow speed, respectively. For this case, the maximum inundation depth was higher than the level at the location of Panalaron Central School and reached the second floor of the structure.

Figure 26. (a) Time-series FVCOM results at Panalaron Central School. (b) Selected time periods for the calculation of wind and flood forces.

Figure 27. (a) Time-series FVCOM results at Libertad. (b) Selected time periods for the

calculation of wind and flood forces.

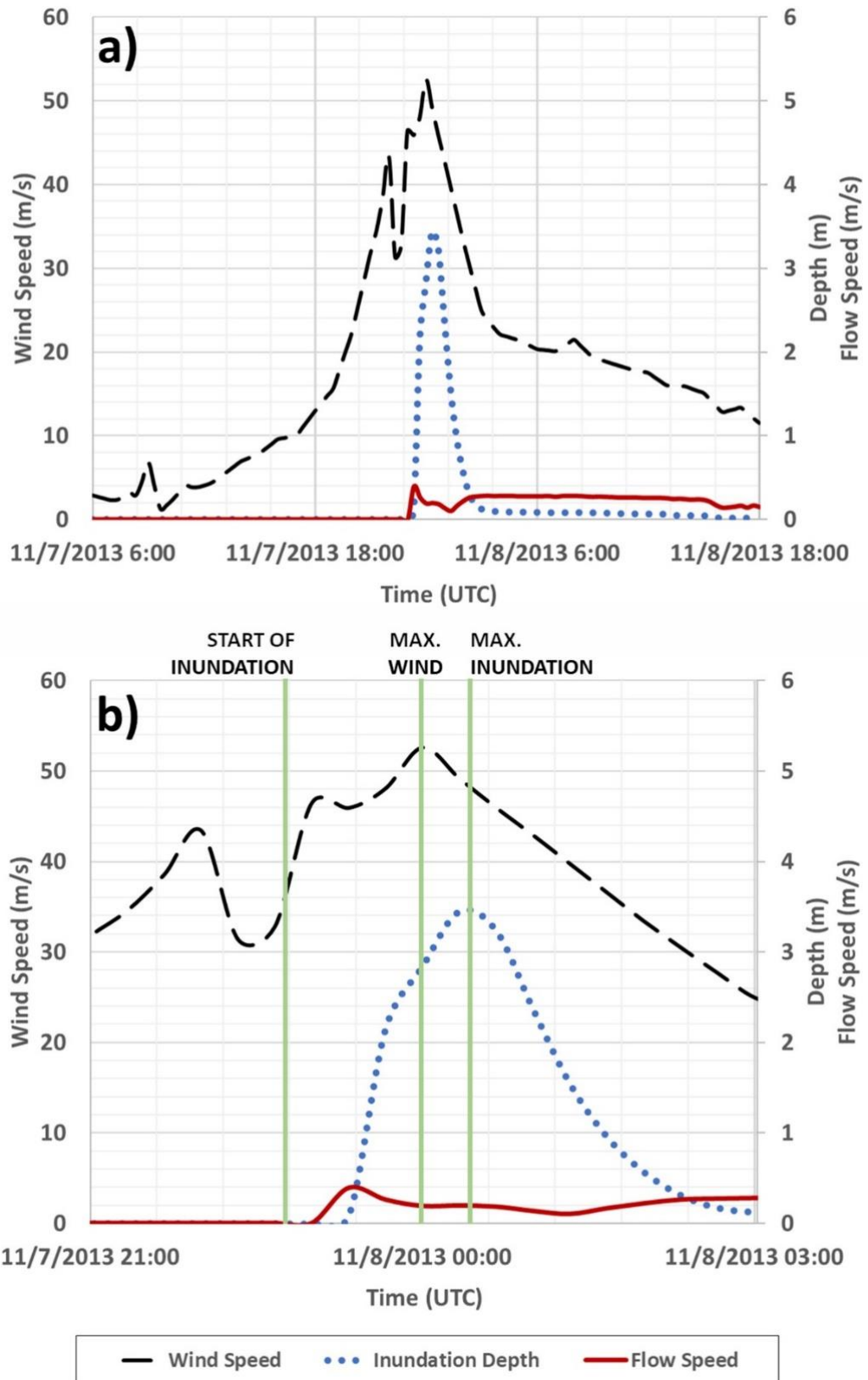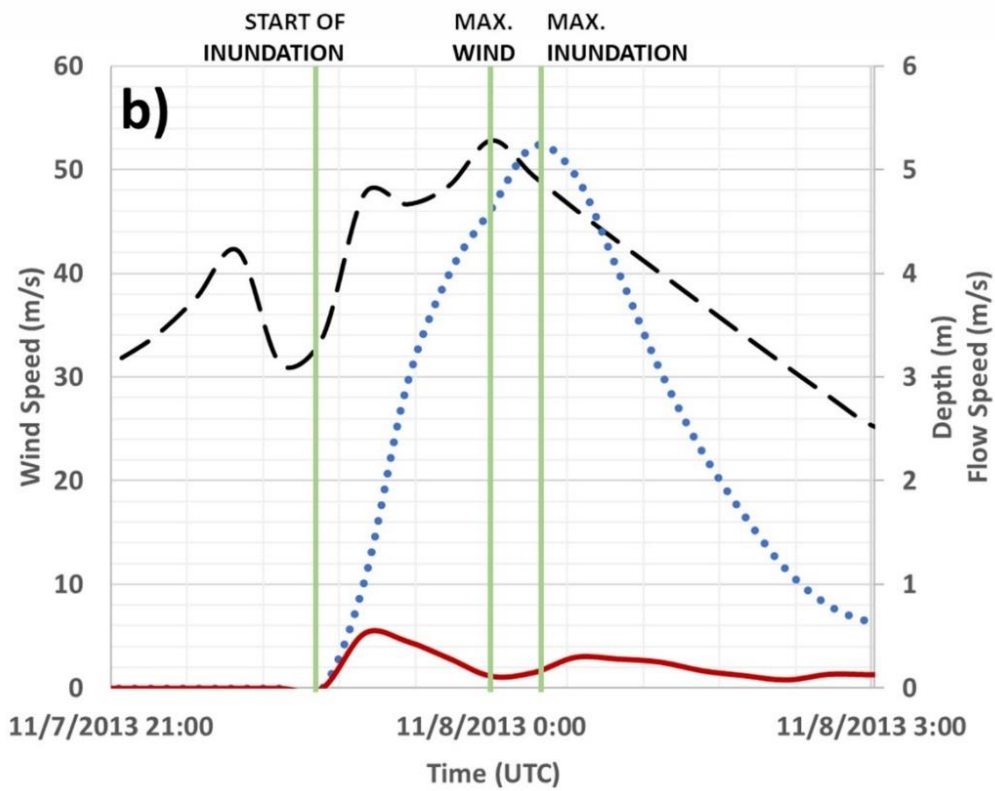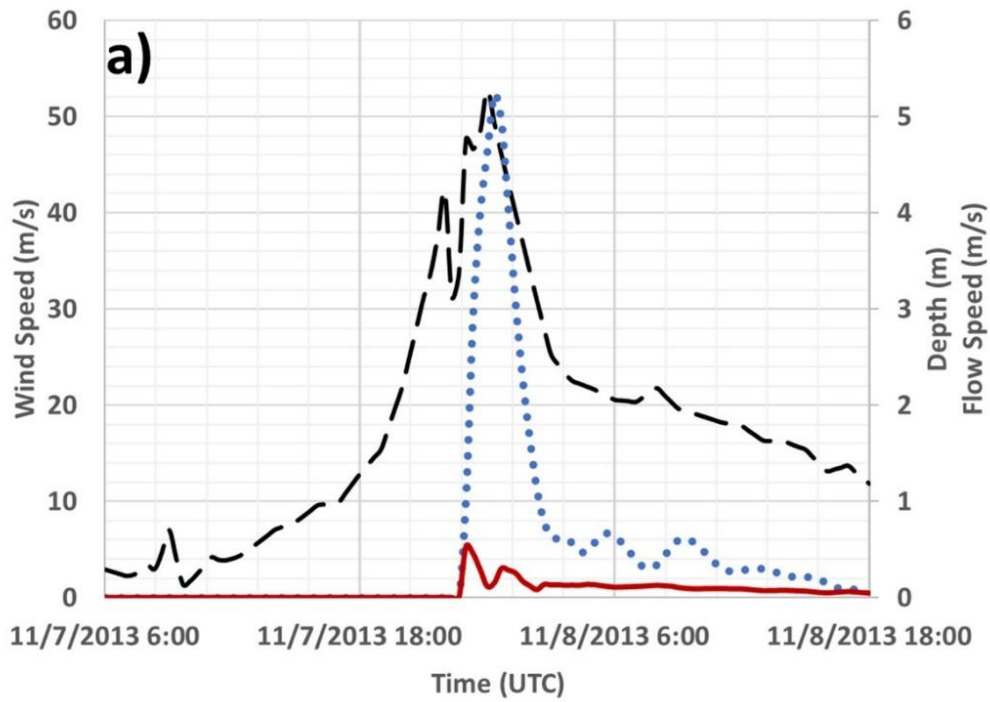### 4.1.3   STAAD.Pro Structural Analysis

The STAAD.Pro model was able to calculate the loads applied to the model structure by the storm surge and calculate the resulting axial, shear, and moment envelopes. The corner column (C1 in **Figure 12**) was determined to be a critical component, as this member would simultaneously experience both wind and flood loads. The peak inundation depth simulated at the target location would inundate the school to a depth of 3.45 m, nearly submerging the ground floor level.

The axial, shear, and moment envelopes during the four cases for column C1 are shown in **Figure 28**. The black lines show the results at the start of inundation (case 1), the red lines show the results at the time when the peak wind speed during the inundation takes place (case 2), the blue lines show the results at the peak inundation (case 3), and the green lines show the results at the peak wind speed but without inundation only the forces exerted at the time when the peak wind speed takes place but ignoring the effect of the inundation (case 4). The directions are based on the global axis orientation of the whole structure (refer to **Figure 12**). The axial, shear, and moment at the ground floor column (0.00-3.45 m from the ground) significantly increased as the flooding occurred around the structure. Also, the shear force significantly increased at the upper part of the ground floor column (3.45 m from the ground) during the maximum inundation. The maximum calculated axial force was obtained from case 3 (27.05 kN), which was 2.35 kN greater than case 4. The maximum calculated shear force was also from case 3 (67.78 kN) and was 51.36 kN greater than case 4. Finally, the maximum bending moment was also from case 3 (82.02 kN-m), 44.09 kN-m greater than case 4. These results show the importance of flood loads in calculating forces during a storm surge event.

54
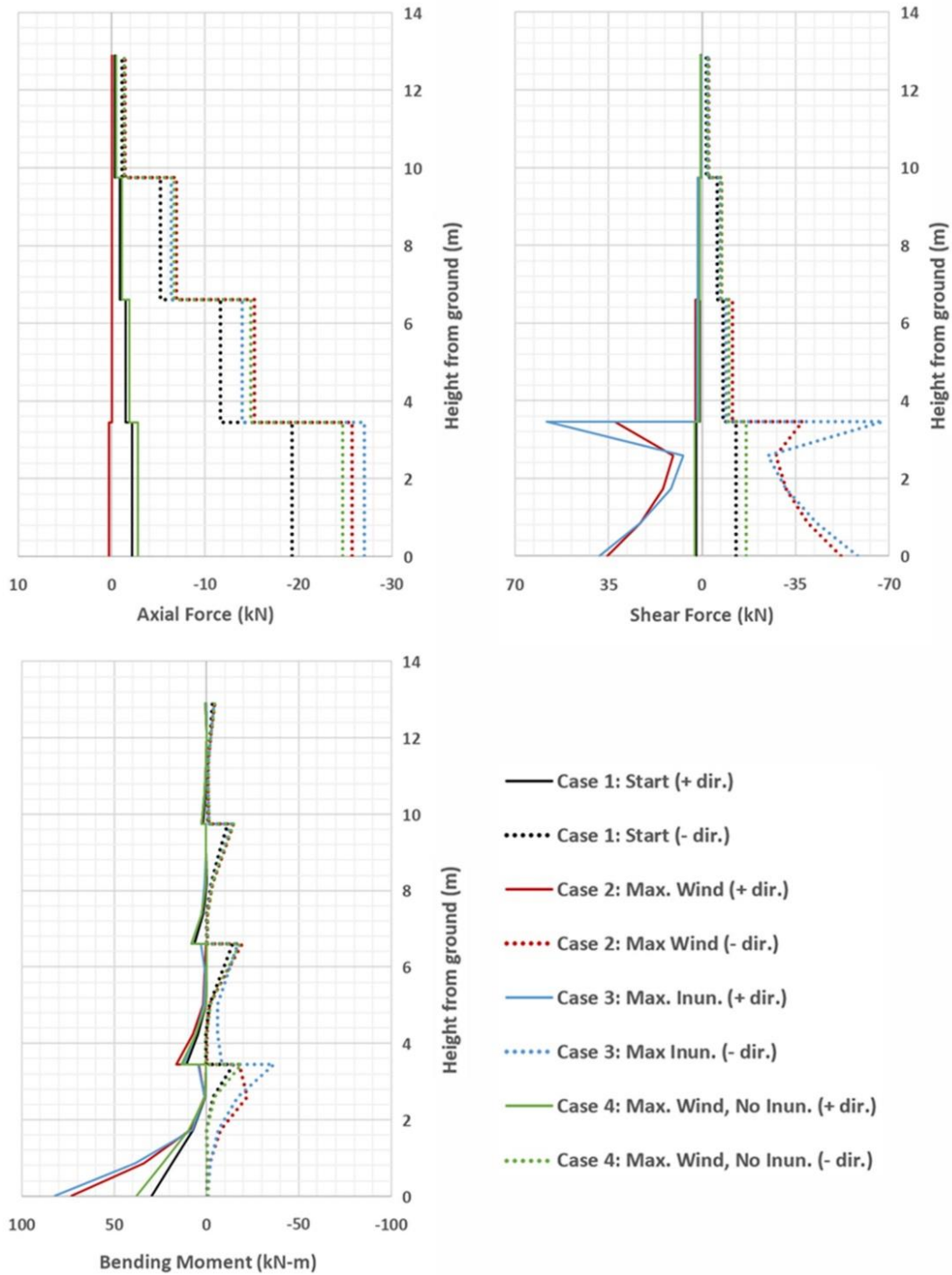
Figure 28. Axial, shear, and bending moment envelopes for column C1 of the 4-floor public school building at Panalaron.

To show the change in these internal forces as the wind speed and flood levels reached their peak, a time series of the forces at the bottom (0.00 m) and top (3.45 m) of the ground floor

column are shown in **Figure 29**. Although there was no drastic change in the axial force at the ground floor column as the storm surge first arrived, there was a significant increase in both shear force and moment at the time of maximum inundation and 20 minutes after the peak wind speed. These changes were more evident at the top of the ground floor column when the maximum water level was reached.

Figure 29. Time series of (a) axial, (b) shear, and (c) bending moment at the top and bottom of ground floor part (0.00 – 3.45 m) of column C1 at Panalaron. The same time series of wind speed, inundation, and flow speed was shown in all figures for reference.

If the structure was located at Libertad, it would have been inundated up to the second floor. For this location, the axial, shear, and moment envelopes for column C1 are shown in **Figure 30**. The location of the maximum axial force (54.48 kN) still occurred along the ground floor part of the column. For the shear force, the maximum value (105.19 kN) was at the top of the ground floor part of the column, an increase of 37.41 kN compared to the school at Panalaron. **Figure 30** shows the change in the distribution of shear force at the second-floor part of the column (3.45-6.60 m from the ground) from case 2 to case 3 as the surge reached its 5.23-m peak inundation depth. A similar observation was also seen for the moment at the second-floor column part for case 3, but the maximum moment was still at the bottom of C1. **Figure 31** presents the time-series of these forces, and all three (axial, shear, moment) significantly increased as the water level rose, and reached their maximum values at the time of the peak inundation depth.
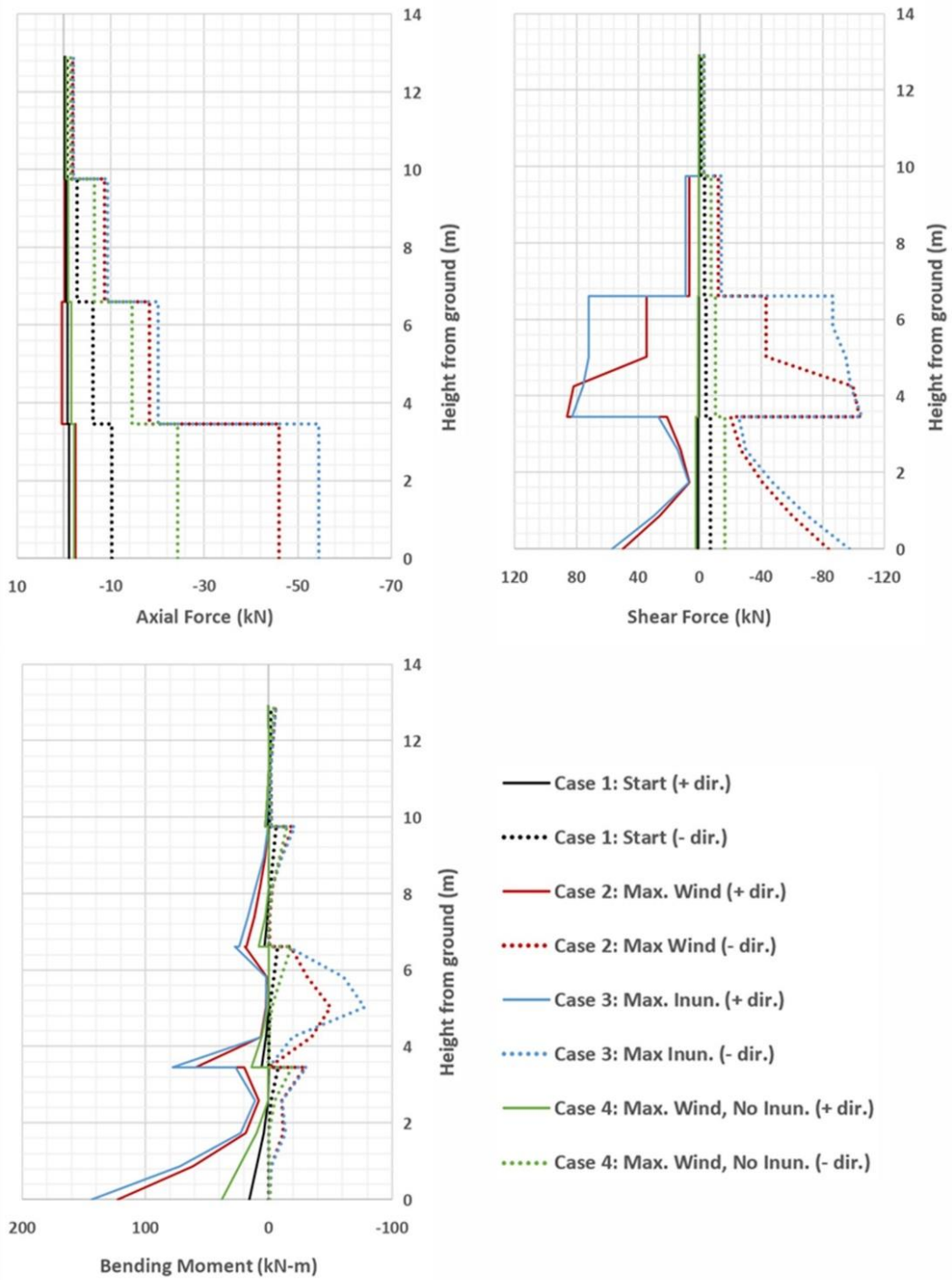
Figure 30. Axial, shear, and bending moment envelopes for column C1 if the 4-floor
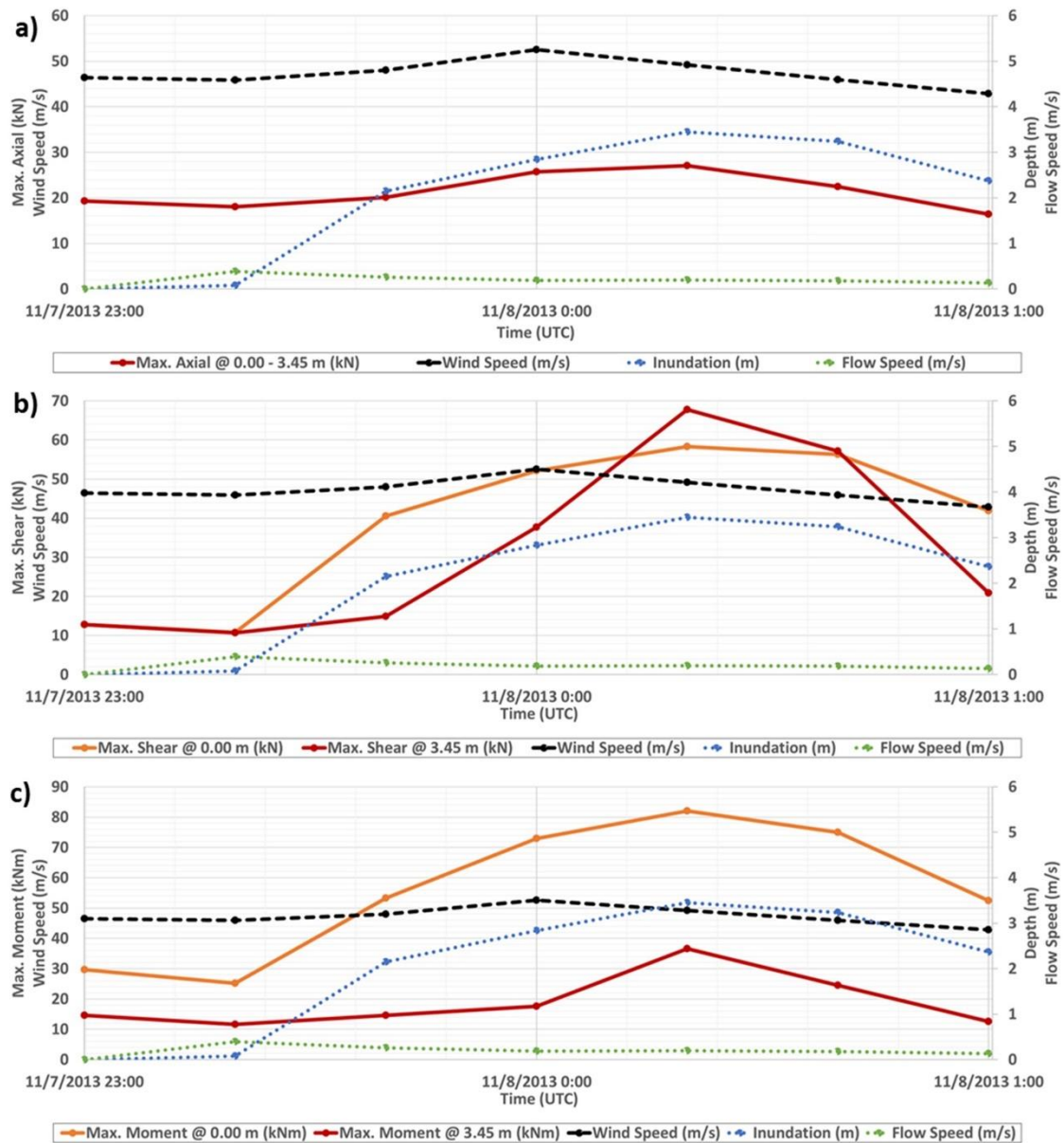
public school building was at Libertad.
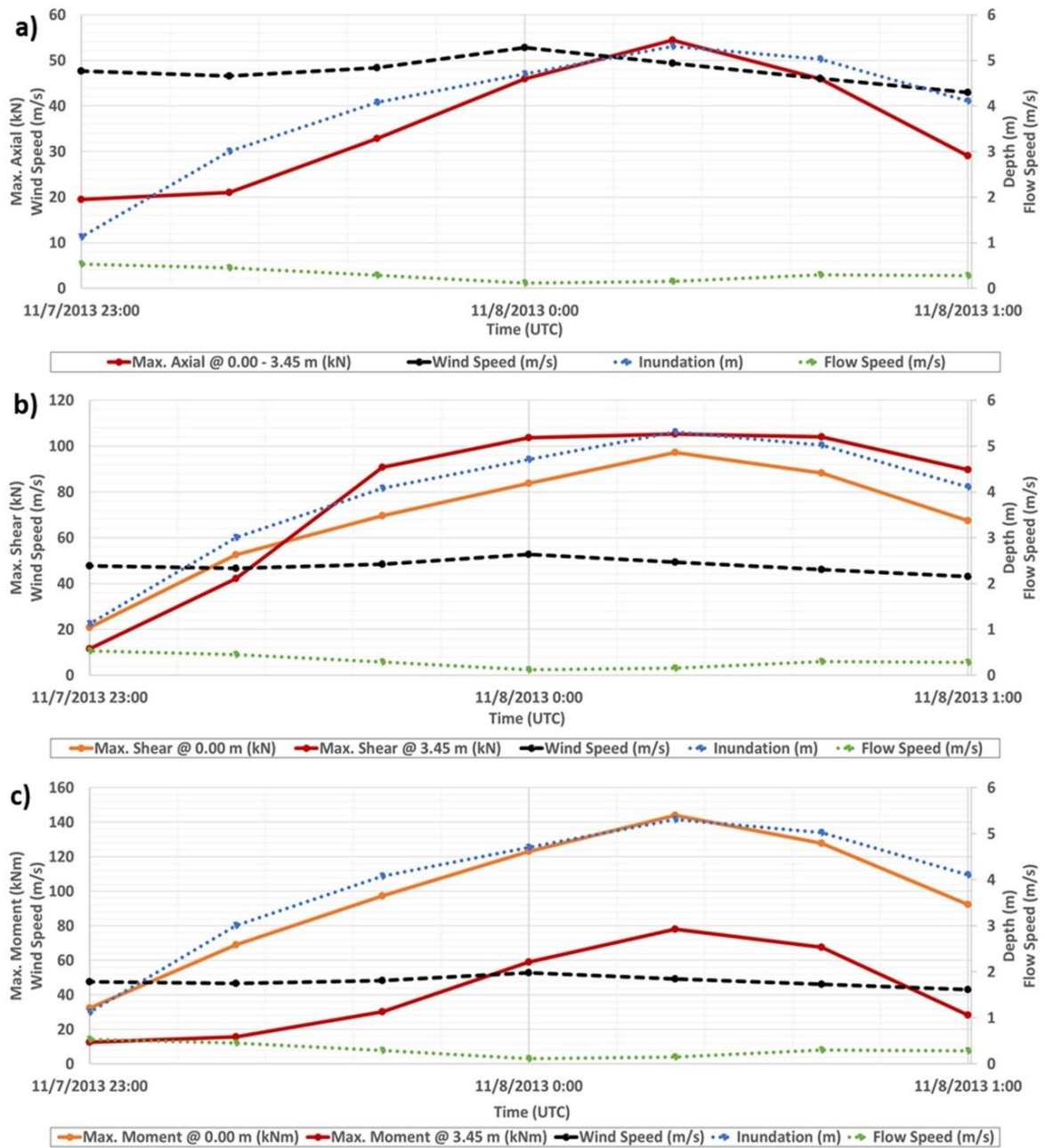
Figure 31. Time series of (a) axial, (b) shear, and (c) bending moment at the top and bottom of ground floor part (0.00 – 3.45 m) of column C1 at Libertad. The same time series wind speed, inundation, and flow speed was used in all figures.

4.2 Typhoon Rai

4.2.1   WRF Typhoon Simulation

The JMA observed and WRF simulated tracks of Typhoon Rai are compared in **Figure 32**. Although there were noticeable deviations of the track during the movement of Typhoon Rai over the Pacific Ocean, the track was simulated better as the typhoon reached the Philippines before diverging as it leaves the country. At Bohol, there was a deviation of the simulated track northward, shifting away from the study area of Tubigon by around 15 km. For the typhoon intensity, the simulation results of central pressure and maximum wind speed generally showed good agreement with the observed data over the whole simulation period. The simulated minimum central pressure (931.34 hPa) was 16.34 hPa higher than the observed value, while the simulated and observed peak wind speeds (55.94 m/s and 54.02 m/s, respectively) had a negligible difference (**Figure 33).** It can be also seen that the typhoon wind speed at around 2021 December 16 12:00 UTC, where Typhoon Rai was over Bohol (**Figure 32**), were simulated well but with a difference of around 11.64 hPa in the central pressure (**Figure 33**). Despite the slight deviations, the WRF results were deemed acceptable, and the output pressure and wind fields were used as boundary conditions for the storm surge simulation.
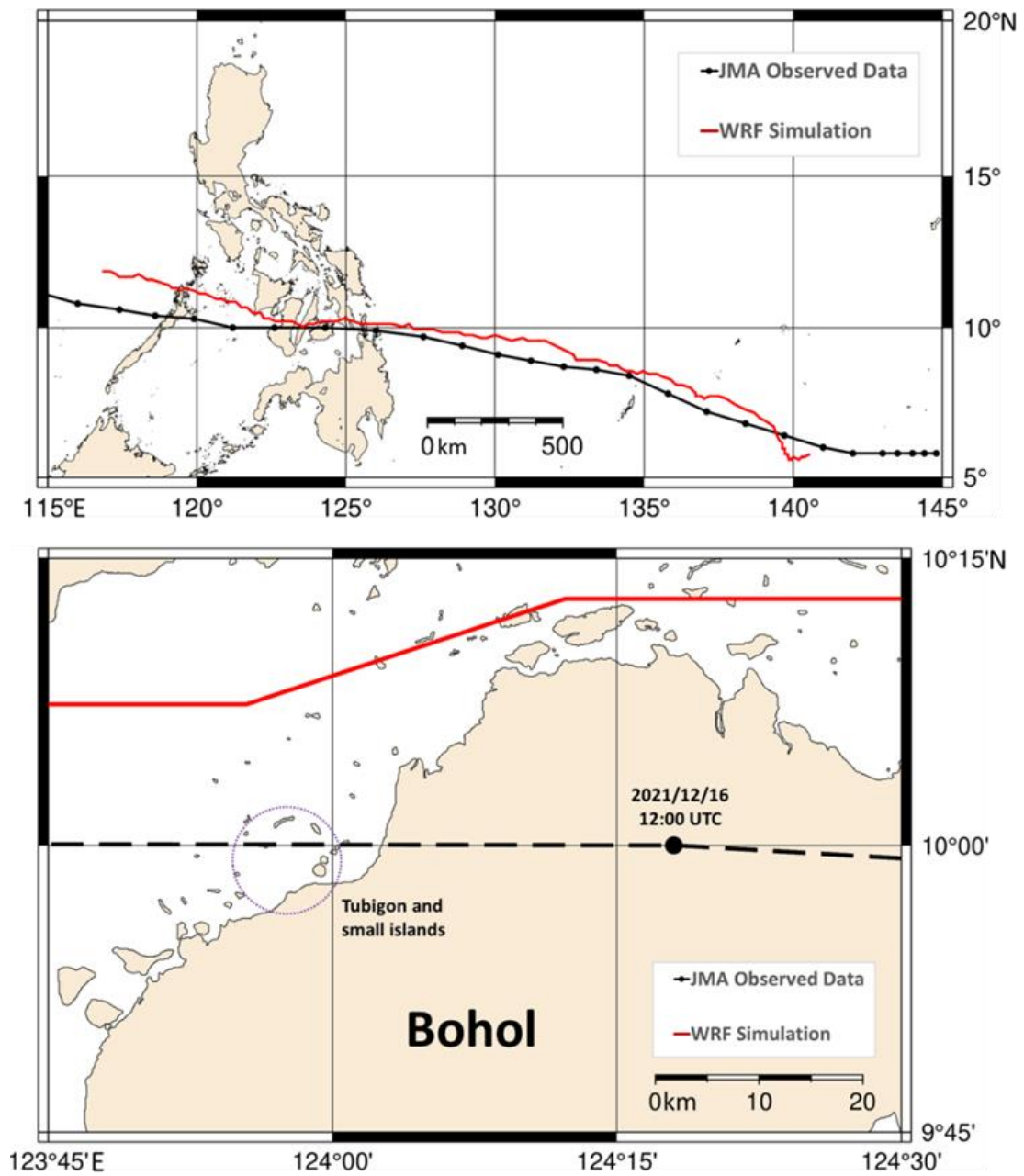
Figure 32. Comparison of observed and simulated typhoon tracks for the whole path during the simulation period (above) and close-up near the study area (below).
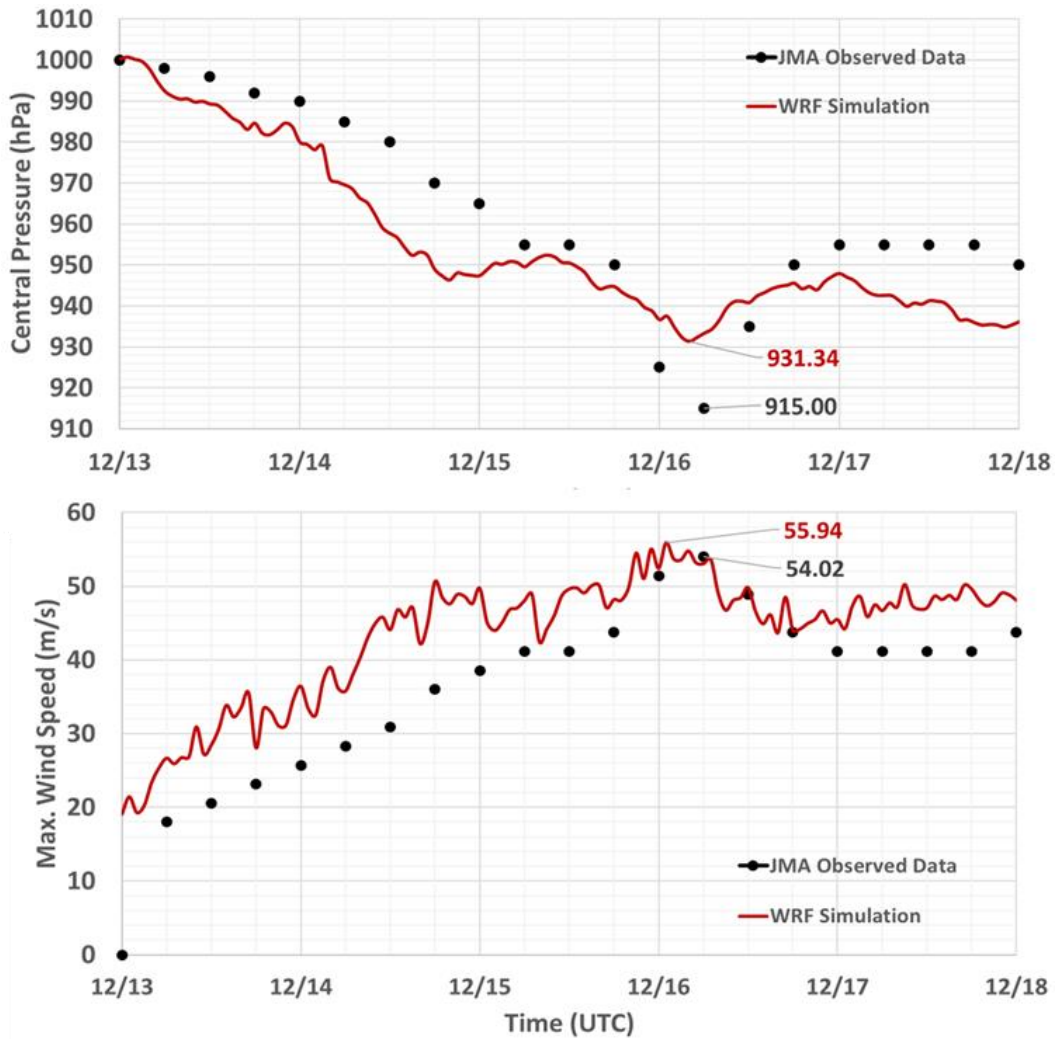
Figure 33. Observed and simulated Typhoon Rai central pressure (above) and maximum

wind speed (below).

4.2.2   FVCOM Storm Surge and Wave Simulation

4.2.2.1 Tubigon

The simulated storm surge and significant wave heights near the Tubigon Port are shown

in **Figure 34**. From the field survey of Esteban et al. 2023, the measured storm surge height

at a nearby house in Tubigon Port after removing the astronomical tide was 3.83 meters.

For clarification, the survey data shown as a gray horizontal line in **Figure 34** does not

represent a constant surge height of 3.83 meters throughout the period but only at a

particular moment. The simulated significant wave height taken at a point near the port

(shown as a green dotted line in **Figure 34**) peaked at 3.70 meters. The results showed that a relatively small surge of 0.94 m may have arrived at Tubigon Port, which was way below the watermark level of 3.83 m, but high waves of more than 3 m were generated off the coast.
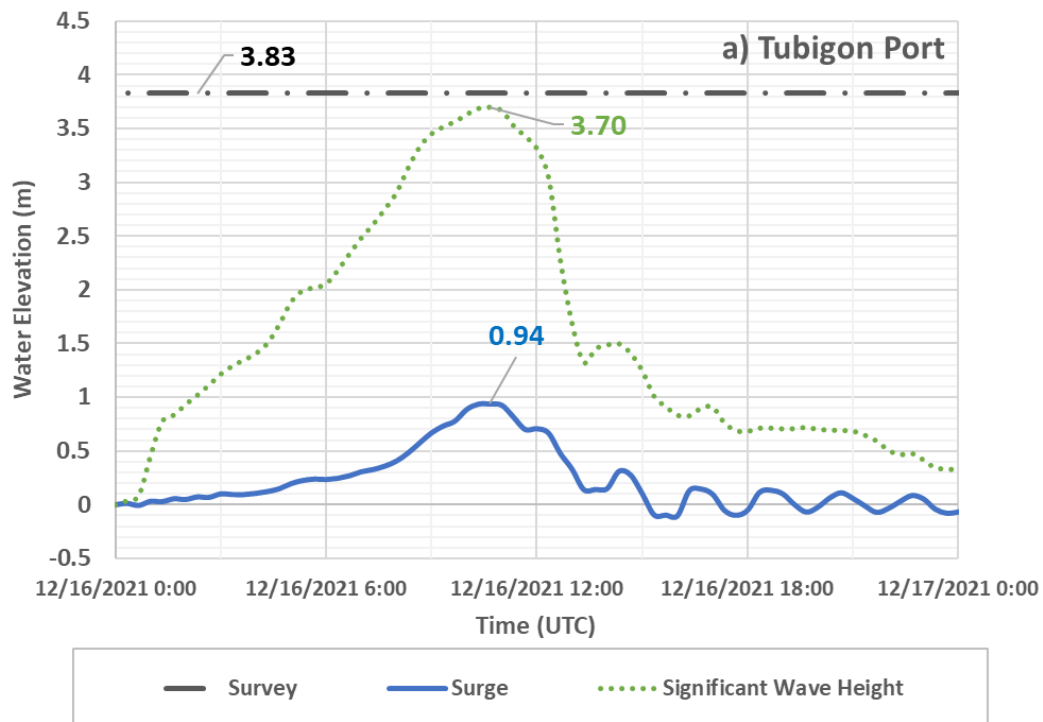
Figure 34. Simulated storm surge and significant wave height near Tubigon Port.

4.2.2.2 Small Islands

The simulated storm surge and significant wave heights near Pangapasan, Ubay, and Batasan islands are shown in **Figure 35** and compared with the field survey measurements from Esteban et al. 2023. At Pangapasan, the maximum simulated storm surge and significant wave heights were 0.81 m and 2.87 m, respectively. This storm surge height was relatively low, which was 1.56 m less than the measured watermark of 2.37 m at Pangapasan. For the case of Ubay, the maximum simulated storm surge and significant

wave heights of 0.72 m and 2.73 m, respectively, resulted in a difference of 1.64 m between the surge and watermark heights. Lastly, the maximum simulated storm surge and significant wave heights at Batasan were 0.84 m and 2.34 m, respectively. The lowest watermark among the islands was recorded at Batasan (2.01 m) which had the least difference with the simulated surge height (1.17 m discrepancy). Overall, the simulated storm surge heights at the islands were closer to its nearby watermarks compared to the Tubigon Port case. Also, relatively high significant wave heights were simulated compared to the simulated storm surge heights.
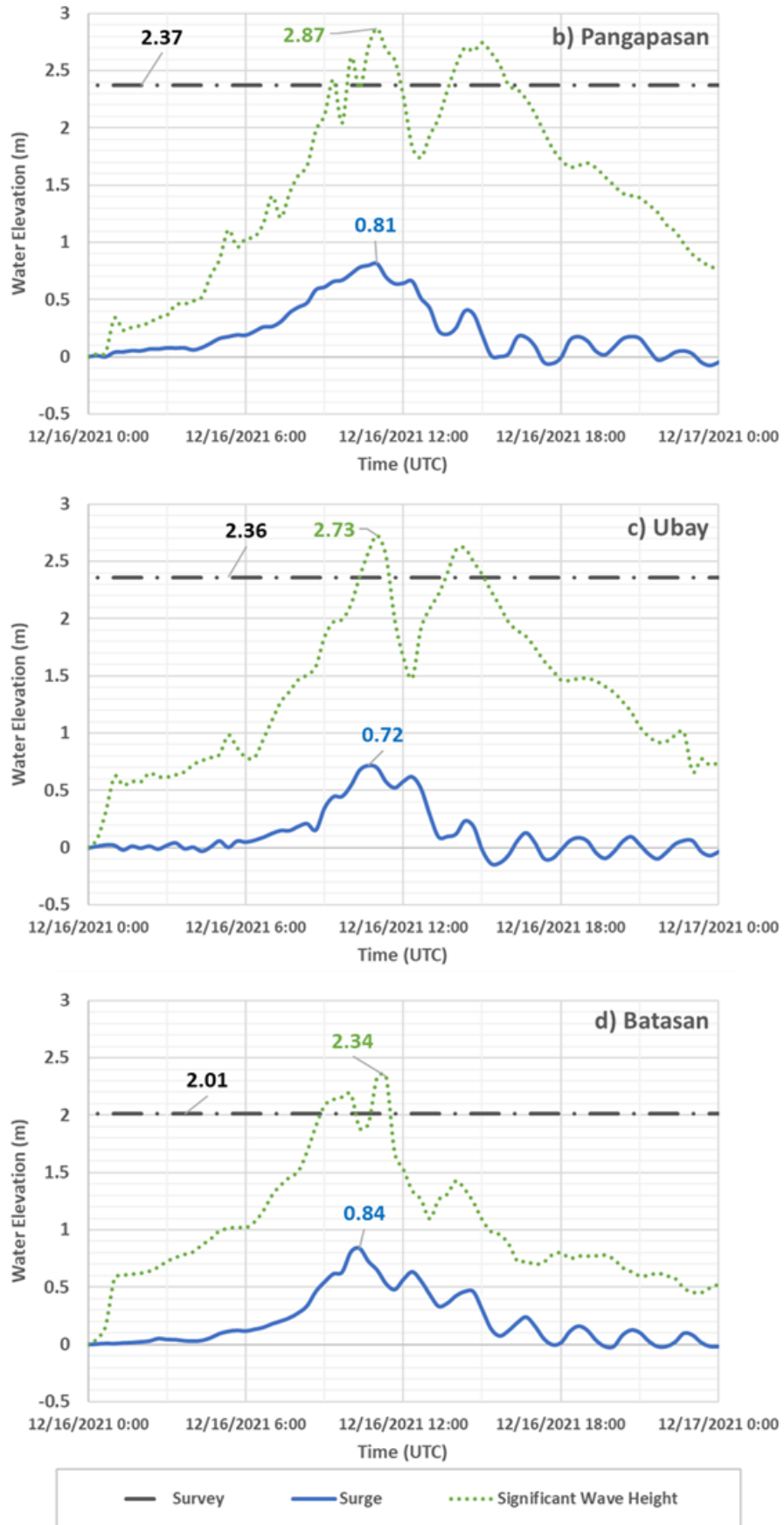
Figure 35. Simulated storm surge and significant wave height near the small islands.

4.2.3   STAAD.Pro Structural Analysis

Similar to the study of the public school building in the Typhoon Haiyan case, the STAAD.Pro model was able to calculate the loads applied to the two-storey house structure at Panalaron by the storm surge and waves, and calculate the resulting axial, shear, and moment envelopes. A corner column which would experience both wind and flood loads in two directions (X and Z axes) was selected for the force analysis. The whole column is composed of two elements: the ground floor column member (0.00 m to 3.00 m from ground level) and the second-floor column (3.00 m to 6.00 m). For simplicity, the simulated peak wind speed of 55.94 m/s was used as reference for the computation of wind loads, while the simulated surge height of 0.81 m was used as the reference inundation depth for the flood loads. Additionally, the simulated maximum significant wave height of 2.87 m was used as the reference for the wave loads hitting the house structure.

The axial, shear, and moment envelopes for the house structure column at the peak wind and flood conditions are shown in **Figure 36**. The solid black lines show the peak values of axial, shear, and moment at the positive axis directions, representing the maximum envelope. On the other hand, the dashed black lines show the peak values of axial, shear, and moment at the negative axis directions, representing the minimum envelope. The greatest absolute values from the envelopes then correspond to the critical axial, shear, and moment for the structural element.

From the results, the maximum axial, shear, and moment for the ground floor column (0.00 m to 3.00 m) were 27.01 kN. 24.50 kN, and 33.24 kN-m, respectively. These values were the maximum over the whole column (0.00 to 6.00 m) were located at the base, making it the critical point of the column. The maximum internal forces for the second-floor column

were also determined: axial force of 26.10 kN, shear force of 9.05 kN, and moment of 15.04

kN-m. Overall, the STAAD.Pro model was able to determine the maximum axial, shear,

and moment along the column members subjected to wind and flood loads from Typhoon

Rai.
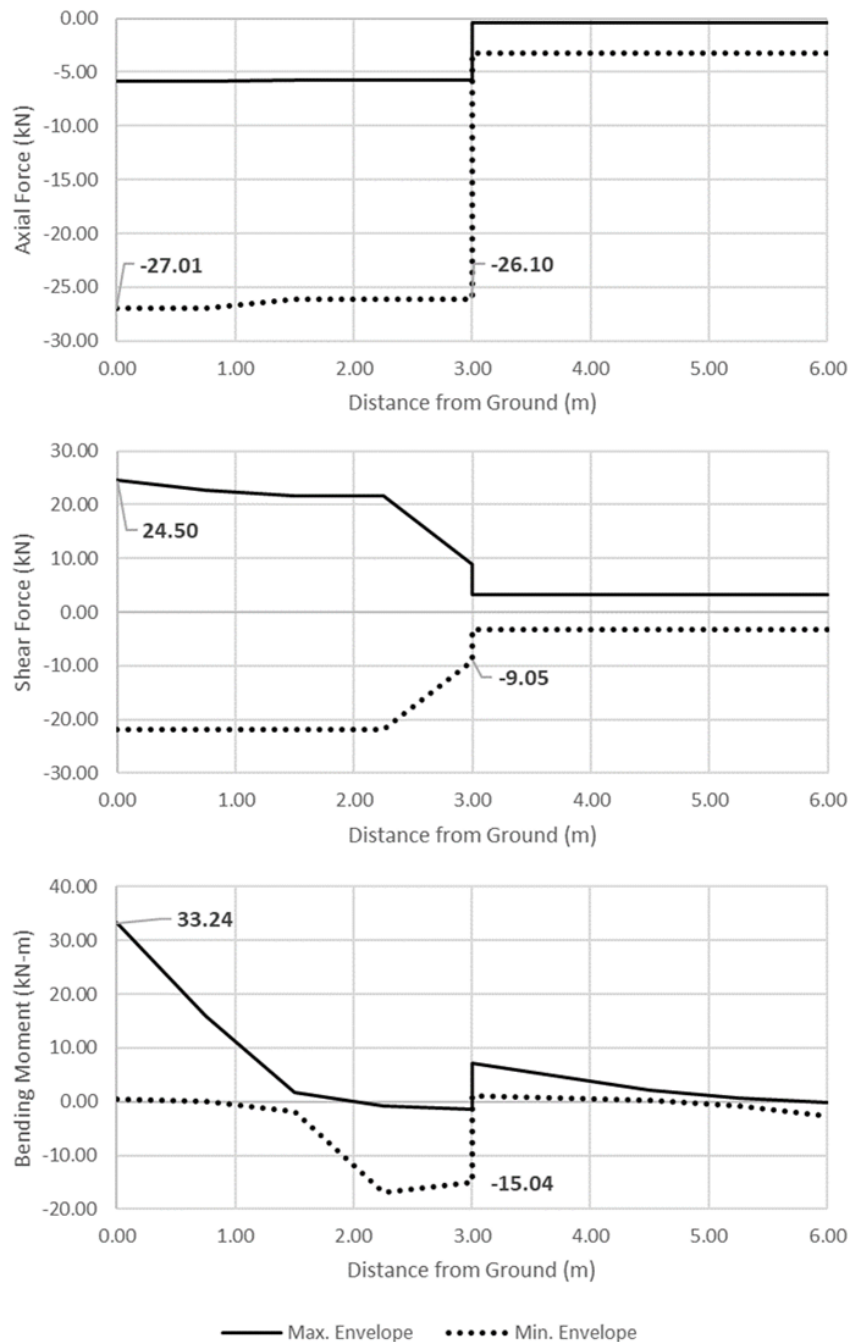
Figure 36. Axial, shear, and bending moment envelopes for the column of the model

house structure at Pangapasan Island.

4.3 Cyclone Batsirai

4.3.1   WRF Cyclone Simulation

The simulated MSLP and maximum wind speed of Cyclone Batsirai are shown in **Figure 37**. The MSLP was simulated with good agreement with the observed data up to the simulated time of 2023 February 02 UTC before the discrepancy increased (simulated cyclone became stronger when the observed cyclone weakened as it moved farther from Mauritius). Since Cyclone Batsirai was near Mauritius around 2023 February 02 UTC, the simulated MSLP was acceptable for this study despite not capturing the weakening state of the cyclone as it moved away. The maximum wind speed was simulated relatively well at the beginning phase of the modelling. However, there was discrepancy between the simulated and observed wind speeds as the cyclone approached Mauritius, reaching to around 5 m/s underestimation at the simulation time of 2023 February 02 UTC. Also, the simulated track shifted north of the observed track of around 100 km as Cyclone Batsirai travelled towards Mauritius before shifting south as it passed near Réunion (**Figure 38**). Nonetheless, the WRF simulation was used to investigate the possible change in water level or storm surge at Mauritius due to Cyclone Batsirai.
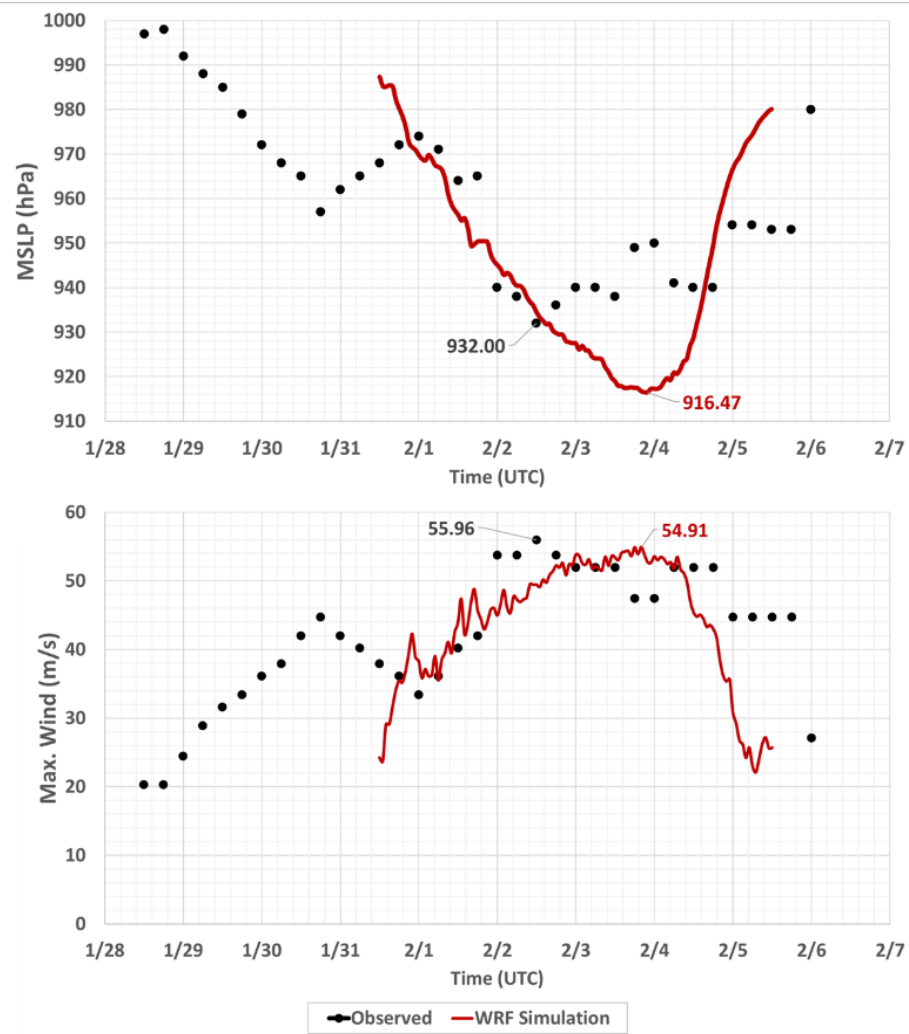
Figure 37. Simulated and observed MSLP (top) and max. wind speed (bottom) of

Batsirai.
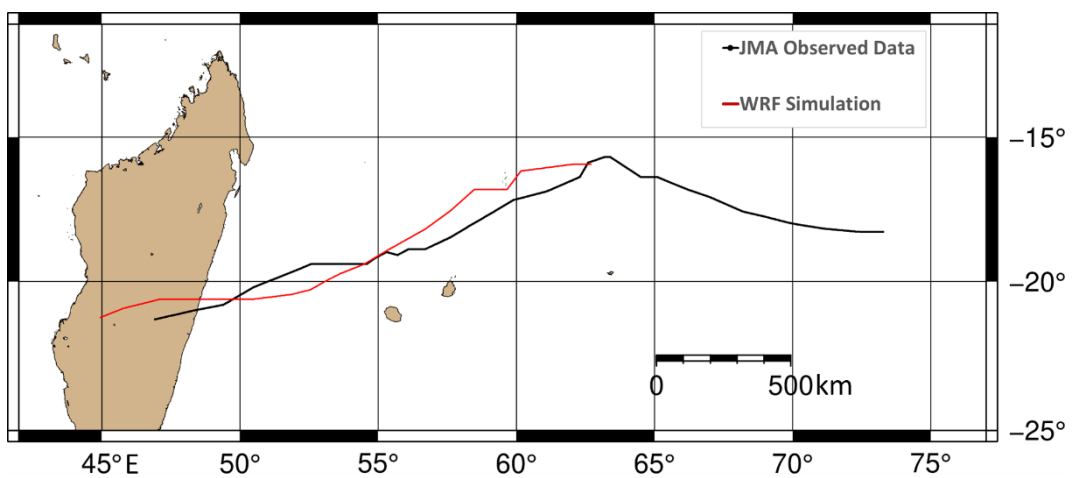
Figure 38. Simulated and observed track of Batsirai.

69

4.3.2 FVCOM Storm Surge Simulation

The change in water level from to a possible storm surge generated by Cyclone Batsirai over the simulation period at a point around Port Louis is shown in **Figure 39**. The graph shows that the storm surge was very small compared to the other simulations in this study (Typhoon Haiyan and Typhoon Rai). The water level first increased to 0.06 m before decreasing to -0.03 m then maintaining an increased water level to around 0.05 m after the passage of Cyclone Batsirai. Checking the observed track, the cyclone seemed far from Mauritius to generate a significant storm surge in Port Louis. Also, the discrepancy in the simulated and observed tracks could have further affected the storm surge simulation. Nonetheless, the model was able to capture in the simulation a small storm surge and the change in water at Mauritius due to Cyclone Batsirai.
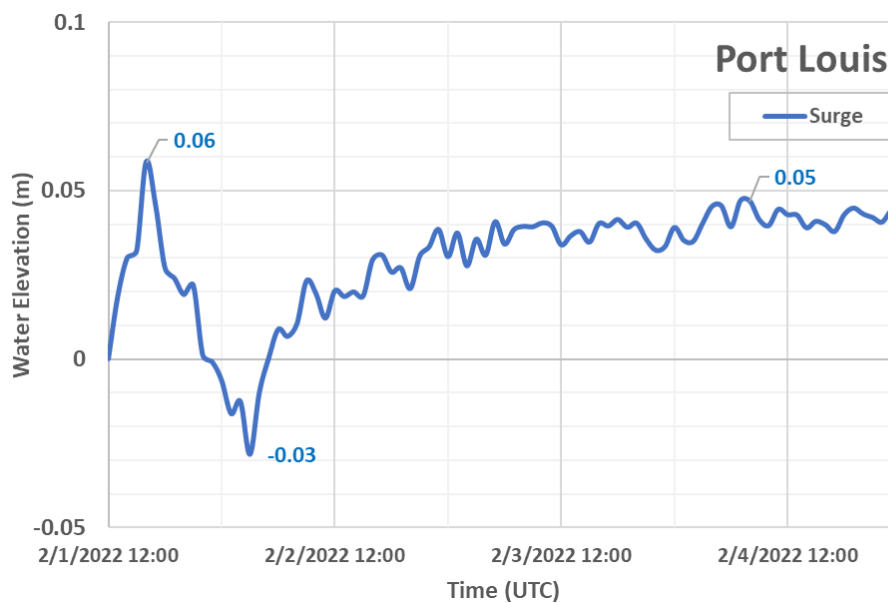
Figure 39. Simulated storm surge around Port Louis due to Cyclone Batsirai.

CHAPTER 5: DISCUSSION

5.1 Typhoon Haiyan Simulations

The WRF model could hindcast Typhoon Haiyan well in terms of intensity and track. Although using the TC-Bogussing scheme produced an underestimation of the mean sea level pressure at the beginning of the simulation (see **Figure 21**), it was able to eventually replicate the observed conditions before landfall. The FVCOM model was able to hindcast well the storm surge along the Tacloban area, though generally underestimated it in adjacent coastal areas. It is important to note at this point that the recorded storm surge heights at each location can vary significantly due to local topographic effects and human errors, and hence such discrepancies are to be expected. Variations of up to 1 meter at Tacloban (**Figure 23**) could be the result of the assumptions made regarding the inundation mesh (i.e. buildings that are very close aggregated together, or the 5 m mesh size). Another reason to explain this discrepancy is that the mesh grid size becomes coarser away from Tacloban, thus increasing the error in the estimation of the storm surge heights. Although only one validation point was available for the flow speed (at Paterno Street near Alejandro Hotel), it can be acceptable since it is an actual video of the surge and is within downtown Tacloban where Panalaron area is located. Considering these limitations, the FVCOM results were deemed acceptable. However, the results at the actual location of the school should be treated with some caution as the simulation environment was simplified (the inland topography of the inundation area was assumed to have a uniform bottom roughness), and no validation at that precise point could be made (since there was no record of trace water levels there in any of the post-disaster field surveys of the event).

In the structural analysis, the shear force at the ground floor column at Panaalron significantly increased at the time when the maximum inundation took place. Additionally,

the axial, shear, and moment at the column is significantly higher for the cases when flooding was considered, compared to when only wind loads were applied. This was more evident for a hypothetical school located at Libertad, where the surge would have reached the second floor. Significant increases in axial, shear, and moment were observed at column C1 as the inundation depth rapidly rose, though there were no significant changes in the wind speed. For this case, the second-floor part of the column was considered as a critical member, due to the increase in shear force along it. Overall, the results highlighted the importance of considering flood forces in structural analysis, which is supported by the statistical analysis of Chaivutitorn et al. (2020), where wind speed was not a significant factor in the damage to structures at Tacloban, compared to that due to flooding and other factors such as debris and topography. Since the design of structures in the Philippines usually does not consider flood loads (except the 2015 NSCP), there may be a possibility that the capacity of structural members may not be sufficiently high against storm surges. While more in-depth structural analysis should be performed before any detailed structural recommendations can be made, it appears that the inclusion of flood loads is important in the design of structures, especially at areas near the coast and prone to storm surges. However, it is also important to note that the present study did not consider other flood loads such as debris impact, which could not be quantified in the storm surge simulation.

5.2 Typhoon Rai Simulations

The WRF model was able to simulate Typhoon Rai generally well, although there were some slight differences with the observed central pressure, wind speed, and track. It was difficult to simulate Typhoon Rai over the Pacific Ocean with the relatively coarse grids from the domains (9 km for d01 and 3 km for d02) which could have affected the accuracy of the resulting typhoon intensities and track. The observed minimum central pressure of

915 hPa on 12 December 06:00 UTC, occurring before Typhoon Rai made landfall at mainland Bohol, was not reached by the modelled typhoon (931.34 hPa). The modelling improved when Typhoon Rai approached d03 (after 12 December 06:00 UTC) which had a 1 km grid size. During the passage at mainland Bohol (12 December 12:00 UTC), the difference between the observed and simulated central pressure was only around 5.8 hPa, likely decreasing the storm surge height negligibly by 0.05-0.06 m. On the other hand, the maximum wind speed of Typhoon Rai over the study area was well simulated, which was a main factor in generating a storm surge. However, there was a deviation of the simulated track northward from the islands and could have affected the wind direction at Tubigon where Typhoon Rai directly passed over. Nonetheless, the results generally showed good agreement with observation data as it passed over the study area and were usable for storm surge simulation.

The FVCOM-SWAVE storm surge simulations resulted in heights much lower than expected, especially in Tubigon Port. The simulated maximum surge height was only around 0.94 m. However, the simulated significant wave height rose to around 3.70 m near the shore during the peak of the typhoon. This result shows that although the surge height was small, the storm waves had a major influence in the increase of water level at Tubigon. At the estimated time of passage of Typhoon Rai, the astronomical tide was around 1.4 m above mean sea level (Esteban et al. 2023). This increase in the water level, although not reflected in the simulation, could have aggravated the inundation at Tubigon.

A similar pattern was observed at the three islands, a relatively small surge height and high significant wave height. The surge heights were closer to the watermarks in these islands compared to the Tubigon Port case, however these were still far from the recorded marks

(1.17 m to 1.64 m difference). Although there were discrepancies from the simulation to the measured watermarks, the wave run-up is highly influenced by local factors such as the slope near the shore and wave splashing. Also, it was difficult to hydrodynamically simulate over the complex reef bathymetry of Tubigon with 30-arc second grid data and relatively limited field survey measurements compared to the whole study area. These could not be accurately captured in the model set up, and it is accepted as a limitation of the study. Additionally, the storm surge underestimation was probably mainly due to the discrepancies in the typhoon simulation, particularly on the track and resulting wind field which is the main driving force in generating surges. It was difficult to simulate the typhoon over the archipelagic and mountainous area, resulting to slight deviation in track as Typhoon Rai passed over central Philippines.

By including the STAAD.Pro model to do structural analysis, the wind, surge, and wave data from the FVCOM-SWAVE model could be used to investigate the driving forces on a house structure at a small island due to Typhoon Rai. The maximum axial, shear, and moment envelopes at a column of a representative two-storey structure at Pangapasan were evaluated to determine the critical values at each structural member. With the flexibility of the models, the structural analysis can be done at the other islands as well with different structural configurations. This is useful since houses typically have different designs depending on the construction set by the owner and it will also aid in determining which structural members are critical during typhoon events.

Overall, the results verified that there was a surge that occurred in Tubigon, and high wind waves were experienced. The numerical model was able to show the storm surge and significant wave height which mainly influenced the measured watermarks at Bohol from

Typhoon Rai. Also, the model showed the sensitivity of typhoon track when simulating storm surges, especially at Tubigon where Typhoon Rai passed directly over the study area. Although the storm surge was not as high as that of Typhoon Haiyan in 2013, this recent Typhoon Rai event should be considered in disaster mitigation plans in the Philippines. The modelling methodology presented in this study could be used to investigate storm surges and waves, especially around small islands such as at Tubigon.

5.3 Cyclone Batsirai Simulations

The simulation model was then attempted to be applied in Mauritius, a different region from the previous two simulations in the Philippines, thus a rough set-up in terms of the domain and physics was used. With little experience in simulating cyclones in the Indian Ocean (as the path could vary widely from cyclone to cyclone), it was a challenge to simulate Cyclone Batsirai. Due to this set-up limitation, there were discrepancies in the simulation of Cyclone Batsirai in WRF, particularly the wind speed and track. The present simulation set-up was not able to capture the rapid change in intensity of Cylone Batsirai as it passed the study area. However, the MSLP was simulated with good agreement as the cyclone moved near Mauritius. Nonetheless, the WRF results were used as input parameters for the FVCOM model.

Although a small surge was captured in the FVCOM simulation model, the present study was not able to validate the reported flooding in coastal areas of Mauritius due to Cyclone Batsirai, which was the limitation coming from the relatively rough numerical set-up of this study. High wave attack could have had a major influence in coastal flooding in Mauritius, which was not part the scope of this particular FVCOM simulation of Cyclone Batsirai. With more accurate runs (by conducting more sensitivity analysis), including the

improvement of WRF simulation physics settings selection and the use of FVCOM-SWAVE instead of FVCOM, the numerical methodology can potentially aid in understanding the coastal flooding brought forth by Cyclone Batsirai. Then, the STAAD.Pro model could be used to evaluate the driving forces of the cyclone, similar to the methodology done in the Typhon Haiyan and Typhoon Rai simulations. Eventually, the methodology in this dissertation is targeted to serve as one of the references for capacity building in Mauritius for modelling of cyclones and surges.

5.4 Performance of Weather-Surge-Structure Model

In general, the weather-surge-structure model was able to simulate with a degree of good agreement Typhoon Haiyan and Typhoon Rai in the Philippines. The case of Cyclone Batsirai had some significant discrepancies due to certain limitations such as only a single domain was initially used, and few simulation test runs have been conducted. Despite such shortcomings, the coupled numerical model was able to show that it is possible to calculate wind and flood loads from a storm surge event and perform a simple structural analysis of a given structure. In the future it is recommended that such analysis includes other flood loads to provide a more realistic simulation of how structures might perform under a storm surge event. A better outlook on the performance of the weather-surge-structure can be provided once all the planned simulations in this research are completed.

5.5 Importance of Numerical Modelling in Philippines and Mauritius

When a strong typhoon such as Haiyan or Rai makes landfall, it is crucial for coastal engineers to determine whether a storm surge or high wave attack occurred in a coastal area as soon as possible. This can be done by numerical simulations and field surveys. Conducting numerical simulations to grasp an overview of what an area experienced during

a typhoon seems to be not usually the immediate focus of the authorities as the priorities are more on recovery and relief operations. By the time field surveys can be done, evidence of watermarks and debris could have already been cleaned up by the residents.

Adding the fact that the Philippines is an archipelago and travel restrictions were in effect due to the pandemic, it was difficult to conduct relief operations and surveys during this time. Government agencies can determine areas affected by storm surges that need immediate response by conducting accurate   preliminary simulations even if on-site investigations are restricted. The coupled WRF-FVCOM-STAAD.Pro numerical model allows hindcast any typhoon event immediately after the typhoon attack, check for potential storm surges at any location in the Philippines and evaluate flood forces on a structure. This method can be useful if travel restrictions continue to affect when another strong typhoon hits the country.

The similar case can be stated for Mauritius, where cyclones from the Indian has always been a threat. Over the years coastal erosion has become an issue such as in Belle Mare (**Figure 40**). As a country that highly depends on tourism in its beaches to drive its economy (like the Philippines), understanding coastal disaster threats has become of utmost importance. During the visit of the research team led by Professor Shibayama to Mauritius, it was expressed by the local counterparts that there is a desire to conduct capacity building on cyclone and storm surge prediction. The simulation of Cyclone Batsirai in this research is part of the planned research project in Mauritius.

Figure 40. Coastal erosion in Belle Mare, Mauritius.

CHAPTER 6: CONCLUSION

6.1 Typhoon Haiyan Simulation

An integrated weather-storm surge-structure model was utilized to simulate storm surge events and calculate the surge-induced axial, shear, and moment envelopes on a column of a 4-floor public school building in Tacloban during the passage of Typhoon Haiyan in 2013. The hindcast numerical simulation was performed using the TC-Bogussing scheme in the WRF model, which showed good agreement with observation data. Using the resulting wind speed and pressure data from the WRF results, the FVCOM model was utilized to simulate the wind driven and pressure surges. Observations from 3 post-disaster field surveys were used for validation, and the simulation showed good agreement around Tacloban area, though the accuracy of the estimation of inundation levels decreased with distance from this city. The time-series of flood simulation data at Panalaron Central School in downtown Tacloban was used as inputs for the wind and flood (hydrostatic, hydrodynamic, and breaking wave) loads, which were analyzed using STAAD.Pro model.

The axial, shear, and moment envelopes at column C1 of the public school building for two flooding scenarios at the start of the inundation, at the time of maximum wind speed (with and without inundation), and at maximum inundation were calculated using STAAD.Pro, showing the importance of considering flood forces in structural analysis. While the methodology employed could be further improved by applying it to different structure types (such as houses) and including other flood loads such as debris impact from other materials (such as vehicles) to provide a more realistic analysis, it appears accurate and robust enough to warrant its use for the design of structures against storm surges.

6.2 Typhoon Rai Simulation

Typhoon Rai, with local name Odette, made landfall in the Philippines in late 2021 and caused massive damage and flooding in the Visayas region. A field survey from Esteban et al. 2023 recorded storm surge watermarks at Tubigon and nearby islands of Pangapasan, Ubay, and Batasan in Bohol province. To verify the watermarks in Tubigon, selected as the study area, numerical modelling of the typhoon and its resulting storm surges and waves using the WRF model and FVCOM-SWAVE model, respectively. For the typhoon simulation, a three-domain set-up with simulation period from 2021 December 13-18 UTC using the GFS meteorological data was performed. The central pressure and maximum wind speed of Typhoon Rai was simulated with good agreement with observed data. However, there was a slight discrepancy in the typhoon track and its resulting wind field over the study area. Nonetheless, the WRF simulation results were deemed a good representation of Typhoon Rai and were used for hydrodynamic modelling.

To simulate the storm surge and waves in FVCOM-SWAVE, an unstructured triangular mesh domain was set up around the sea surrounding Bohol province. Mesh sizes around Tubigon Port and the islands of Pangapasan, Ubay, and Batasan were around 100 meters. Simulation results showed that the storm surge heights around the study area were small, ranging from 0.72 m at Ubay to 0.94 m at the port. However, the simulated significant wave heights ranged from 1.90 m to 2.79 m, indicating that high waves could have hit the area and aggravated the flooding. The discrepancy of the hydrodynamic modelling could be attributed mainly to the simulated typhoon track deviation in which the wind field plays a major influence in storm surge generation. Additional factors include localized effects such as wave splashing and simulating over a complex reef-island bathymetry. Nonetheless, the

overall numerical modelling was able to show that a storm surge occurred in Tubigon, Bohol and its nearby islands and that high storm waves hit the area. Also, the inclusion of the STAAD.Pro structural model was able to investigate the driving forces on a house structure at a small island due to Typhoon Rai. The structural analysis could be applied not only in analyzing the effect of typhoon-driven forces on a structure but also using the results as reference for designing more typhoon-resilient houses in the coastal areas.

6.3 Cyclone Batsirai Simulation

Finally, the numerical methodology was applied to a different region: Mauritius in the Indian Ocean. Cyclone Batsirai, which affected Mauritius in early 2022. A two-domain set-up was used in the simulation of the cyclone in WRF. The MSLP and wind speed were simulated with good agreement at the beginning of the simulation but had discrepancies as it passed near Mauritius. On the other hand, the cyclone track had deviations of around 100 km near the study area. With a rough simulation set-up and limited experience in simulating at the Indian Ocean, discrepancies occurred in the cyclone intensity and track which could be improved with more sensitivity analysis. Nonetheless, the WRF results were used for the purpose of simulating the change in water level at Mauritius due to a cyclone.

For the FVCOM simulation, an unstructured triangular mesh domain surrounding Mauritius with mesh sizes from 1000-m along the open boundary in the Indian Ocean and around 100-m along the coast of Port Louis (the capital of Mauritius). Using the wind and pressure fields from the WRF model, the FVCOM was able to simulate the change in water level due to the passage of Cyclone Batsirai. Although a small surge of around 0.05-0.06 m was captured in the FVCOM simulation model, the present study was not able to validate

the reported flooding in coastal areas of Mauritius due to Cyclone Batsirai, which was the limitation coming from the relatively rough numerical set-up of this study and discrepancy that arose from the cyclone simulation. Checking on the observed cyclone track and wind field of Batsirai, no significant storm surge was expected. However, high wave attack could have caused some coastal flooding in Mauritius which was not captured in the FVCOM model (but possible in FVCOM-SWAVE). With improvements in the cyclone simulation by addressing the limitations show in the present study, the methodology in this dissertation could eventually be targeted to serve as one of the references for capacity building in Mauritius for modelling of cyclones and surges.

REFERENCES

ASCE/SEI (American Society of Civil Engineers/Structural Engineering Institute). 2017. ASCE/SEI 7-16 Minimum Design Loads and Associated Criteria for Buildings and Other Structures. Reston, VA: ASCE.

ASEP (Association of Structural Engineers of the Philippines). 2016. National Structural Code of the Philippines 2015 Volume 1 Buildings, Towers, and Other Vertical Structures. Quezon City, Philippines: ASEP.

Bentley Systems. 2012. STAAD.Pro V8i (SELECTseries 4). Technical Reference Manual (DAA037780-1/0005). Accessed from: communities.bentley.com/products/ram-staad/m/structural_analysis_and_design_gallery/272213.

Bolanio K., Bermoy M., Gagula A., Vernante J., Boligor A., and Cabañelez J. 2022. "Analysis of the Super Typhoon Rai-induced infrastructure damage in severely affected Areas of CARAGA Region, Philippines using Sentinel -1 SAR imageries". ISPRS Ann. Photogramm. Remote Sens. Spatial Inf. Sci., X-3/W1-2022, 9-15. doi: 0.5194/isprs-annals-X-3-W1-2022-9-2022.

Bricker J., Takagi H., Mas E., Kure S., Adriano B., Yi C., and Roeber V. 2014. "Spatial Variation of Damage due to Storm Surge and Waves during Typhoon Haiyan in the Philippines". *J Jpn Soc Civil Eng Ser. B2 (Coastal Engineering)*, 70(2), I_231-I_235. doi:10.2208/kaigan.70.I_231.

Chen C., Liu H., and Beardsley R. 2003. "An Unstructured Grid, Finite-Volume Three-Dimensional, Primitive Equations Ocean Model: Application to Coastal Ocean and Estuaries". *J. Atmospheric and Oceanic Technology*, 20(1), 159-186. doi:10.1175/1520-0426(2003)020<0159:AUGFVT>2.0.CO;2.

Chen C., Beardsley R., Cowles G., Qi J., Lai Z., Guoping G., Stuebe D., Xu Q., Pengfei X., Ge J., Ji R., Hu S., Tian R., Huang H., Wu L., and Lin H. 2011. FVCOM User Manual (SMAST/UMASSD-11-1101. Accessed from: http://fvcom.smast.umassd.edu/wp-content/uploads/2013/11/MITSG_12-25.pdf.

Chock G., Robertson I., Kriebel D., Francis M., and Nistor I. 2013. Tohoku, Japan, Earthquake and Tsunami of 2011: Performance of Structures under Tsunami Loads. Reston, VA: ASCE.

Chaivutitorn T., Tanasakcharoen T., Leelawat N., Tang J., Caro C., Lagmay A., Suppasri A., Bricker J., Roeber V., Yi C., and Imamura F. "Statistical Analysis of Building Damage from the 2013 Super Typhoon Haiyan and its Storm Surge in the Philippines. *J. Disaster Research,* 15(7), 822-832. Doi: 10.20965/jdr.2020.p0822.

Dasallas L. and Lee S. 2019. "Topographical Analysis of the 2013 Typhoon Haiyan Storm Surge Flooding by Combining the JMA Storm Surge Model and the FLO-2D Flood Inundation Model". *Water*, 11(1), 144. doi:10.3390/w11010144.

Esteban M., Valenzuela V., Matsumaru R., Mikami T., Shibayama T., Takagi H., Thao N., and De Leon M. 2016. "Storm Surge Awareness in the Philippines Prior to Typhoon Haiyan: A Comparative Analysis with Tsunami Awareness in Recent Times". *Coastal Engineering Journal*, 58(1), 1640009-1-164000928. doi:10.1142/S057856341640009X.

Esteban M., Valdez J., Tan N., Rica A., Vasquez G., Jamero L., Valenzuela P., Sumalinog B., Ruiz R., Gera W., Chadwick C., Sparatu C., and Shibayama T. 2023. "Field Survey of 2021 Typhoon Rai – Odette - in the Philippines". Journal of Coastal and Riverine Flood Risk, 1. doi: 10.48438/jcrfr.2023.0001.

Ge J., Much D., Kapenberg J., Nino O., Ding P. and Chen Z. 2014. "Simulating storm flooding maps over HafenCity under present and sea level rise scenarios". *J. Flood Risk and Management*, 7(4), 319-331. doi:10.1111/jfr3.12054.

General Bathymetric Chart of the Oceans (GEBCO). 2014. "The GEBCO_2014 Grid, version 20141103. Accessed October 9, 2018. Available at: gebco.net.

Global Disaster Alert and Coordination System (GDACS). 2022. "Overall Red alert Tropical Cyclone for BATSIRAI-22". Accessed on 23 December 2022. Available at: gdacs.org/report.aspx?eventtype=TC&eventid=1000859.

Google Earth. (n.d.). [Map of Leyte and Samar]. Retrieved May 24, 2022, from Google Earth Pro v.7.3.4.8248.

Honda C. and Mitsuyasu K. 1980. "Experimental study on wind action on water surface". [In Japanese]. In *Proceedings of Coastal Engineering Lecture*, 27, 90-93. doi:10.2208/proce1970.27.90.

Hernandez J., Aquino R., Pacheco B., and Cruz E. 2015. "Damage Caused by Typhoon Haiyan in the Philippines, Review of Structural Regulations and Practice, and Research Developments in Wind Engineering". *Wind Engineers, JAWE*, 40(3), 270-274. doi:10.5359/jawe.40.270.

Hsiao L., Liou C., Yeh T. Guo Y., Chen D., Huang K., Terng C., and Chen J. 2010. "A Vortex Relocation Scheme for Tropical Cyclone Initialization in Advanced Research WRF". *Monthly Weather Review*, 138, 3298-3315. doi:10.1175/2010MWR3275.1.

International Research Institute of Disaster Science (IRIDes). 2014. "IRIDEs Fact-finding missions to Philippines". Tohoku University. Accessed May 4, 2022. https://irides.tohoku.ac.jp/media/files/IRIDeS_Report_Haiyan_20140527.pdf.

Islam T., Srivastava P., and Dai Q. 2015. "High-resolution WRF simulation of cloud properties over the super typhoon Haiyan: physics parametrizations and comparison against MODIS". *Theor Appl Climatol*, 126, 427-435. doi:10.1007/s00704-015-1575-y.

Jamero, L., Onuki, M., Esteban, M. and Tan, N. 2018. "Community-based adaptation in low-lying islands in the Philippines: Challenges and lessons learned", *Regional Environmental Change*, 8, 2249-2260. doi: 10.1007/s10113-018-1332-8.

Japan Meteorological Agency (JMA). 2014. RSMC Best Track Data – HAIYAN. Accessed from: https://www.jma.go.jp/jma/jma-eng/jma-center/rsmc-hp-pub-eg/besttrack.html.

Jia Y. and Sasani M. 2021. "Modeling Joint Probability of Wind and Flood Hazards in Boston". *Nat. Hazards Rev.*, 22(4), 04021047. doi:10.1061/(ASCE)NH.1527-6996.0000508.

Joint Research Centre. 2013. Red Tropical Cyclone alert for HAIYAN-13 in China, Viet Nam, Philippines, Palau from 04/11/2013 00:00 UTC to 11/11/2013 00:00 UTC. Accessed 30 September 2014. Available at: webcritech.jrc.ec.europa.eu/modelling/cyclonesurge/41058/final/locationsLight.kmz

Kim K. 2015. "Typhoon Storm Surge Simulation for Typhoon Haiyan." *Journal of International Development Cooperation*, 21, 17-25. ISSN 1341-0903.

Lapidez J., Tablazon J., Dasallas L., Gonzalo L., Cabacaba K., Ramos M., Suarez J., Santiago J., Lagmay A., and Malano V. 2015. "Identification of storm surge vulnerable areas in the Philippines through the simulation of Typhoon Haiyan-induced storm surge levels over historical storm tracks." *Nat. Hazards Earth Syst. Sci.*, 15(7), 1473-1481. doi:10.5194/nhess-15-1473-2015.

Li Y., van de Lindt J., Dao T., and Bjarnadottir S. 2012. "Loss Analysis for Combined Wind and Surge in Hurricanes". *Nat. Hazards Rev.*, 13(1), 1-10. doi:10.1061/(ASCE)NH.1527-6996.0000058.

Li F., Song J., and Li X. 2018. "A preliminary evaluation of the necessity of using a cumulus parametrization scheme in high-resolution simulations of Typhoon Haiyan (2013)". *Nat Hazards*, 92(2), 647-671. doi:10.1007/s11069-018-3218-y.

Malacañang Records Office. 1977. "Presidential Decree No. 1149". Accessed December 21, 2022. Official Gazette of the Republic of the Philippines website.

Mäll M., Suursaar Ü., and Nakamura R. 2017. "Modelling a storm surge under future climate scenarios: case study of extratropical cyclone Gudrun (2005)". *Nat Hazards*, 89(3), 1119-1144. doi:10.1007/s11069-017-3011-3.

MapAction. 2013. "Philippines Typhoon Haiyan (Yolanda) Damage – Tacloban City (as of 11-Nov-2013). Accessed May 4, 2022. https://maps.mapaction.org.

Mas E., Bricker J., Kure S., Adriano B., Yi C., Suppasri A., and Koshimura S. 2015. "Field survey report and satellite image interpretation of the 2013 Super Typhoon Haiyan in the Philippines". *Nat. Hazards Earth Syst. Sci.*, 15, 805-815. Doi: 10.5194/nhess-15-805-2015.

Meneses S. and Blanco A. 2022. "Rapid mapping and assessment of damages due to Typhoon Rai using Sentinel-1 Synthetic Aperture Radar data". Int. Arch. Photogramm. Remote Sens. Spatial Inf. Sci., XLIII-B3-2022, 1139–1146. doi: 10.5194/isprs-archives-XLIII-B3-2022-1139-202.

Mikami T., Shibayama T., Takagi H., Matsumaru R., Esteban M., Thao N., De Leon M., Valenzuela V., Oyama T., Nakamura R., Kumagai K., and Li S. 2016. "Storm Surge Heights and Damage Caused by the 2013 Typhoon Haiyan Along the Leyte Gulf Coast".

Coastal Engineering Journal, 58(1), 1640005-1-1640005-27. doi: 10.1142/S0578563416400052.

Mori N., Kato M., Kim S., Mase H., Shibutani Y., Takemi T., Tsuboki K., and Yasuda T. 2014. "Local amplification of storm surge by Super Typhoon Haiyan in Leyte Gulf". *Geophysical Research Letters*, 41(14), 5106-5113. doi:10.1002/2014GL060689.

Nakamura R., Shibayama T., Esteban M., and Iwamoto T. 2016. "Future typhoon and storm surges under different global warming scenarios: case study of typhoon Haiyan (2013)". *Nat Hazards*, 82(3), 1645-1681. doi:10.1007/s11069-016-2259-3.

National Centers for Environmental Prediction (NCEP)/National Weather Service/NOAA/U.S. Department of Commerce, European Centre for Medium-Range Weather Forecasts, and Unidata/University Corporation for Atmospheric Research. 2003, updated daily. "Historical Unidata Internet Data Distribution (IDD) Gridded Model Data". Research Data Archive at the National Center for Atmospheric Research, Computational and Information Systems Laboratory. doi:10.5065/549X-KE89. Accessed 16 April 2018.

National Centers for Environmental Prediction/National Weather Service/NOAA/U.S. Department of Commerce. 2015, updated daily. NCEP GFS 0.25 Degree Global Forecast Grids Historical Archive. Research Data Archive at the National Center for Atmospheric Research, Computational and Information Systems Laboratory. doi:10.5065/D65D8PWK. Accessed 16 September 2022.

National Disaster Risk Reduction and Management Council (NDRRMC). 2014. SitRep No. 108 Effects of Typhoon "YOLANDA" (HAIYAN). Available at: ndrrmc.gov.ph/attachments/article/1329/SitRep_No_108_Effects_of_Typhoon_Yolanda_HAIYAN_as_of_03APR2014_0600H.pdf.

NDRRMC. 2022. "Situational Report No. 46 for TC ODETTE (2021)". Accessed online on 25 Feb. 2022.

National Mapping and Resource Information Authority (NAMRIA). 2014. Nautical Chart of Leyte Gulf and Topographic Maps of Coastal Areas. Taguig City, Philippines.

Ohira K., Shibayama T., Esteban M., Mikami, T., Takabatake, T., and Kokado, M. 2012. "Comprehensive numerical simulation of waves caused by typhoon using a meteorology-wave-storm surge-tide coupled model". In *Proceedings of the 33rd International Conference on Coastal Engineering 2012*, 1(33), 52. doi:10.9753/ice.v33.currents.52.

Roughneen S. 2014. "Christmas in Tacloban: Locals count their mixed blessings" (January 7, 2014). Nikkei Asia. Accessed May 4, 2022. Available at: asia.nikkei.com.

Saha, S., et al. 2011, updated daily. NCEP Climate Forecast System Version 2 (CFSv2) 6-hourly Products. Research Data Archive at the National Center for Atmospheric Research, Computational and Information Systems Laboratory. doi:10.5065/D61C1TXF. Accessed 13 February 2023.

Santos Jr, R., 2014. TIMELINE: Super Typhoon Yolanda (Haiyan). Rappler. Accessed 20 October 2014. Available at: rappler.com/nation/43316-timeline-super-typhoon-yolanda.

Shibayama T., Matsumaru R., Takagi H., de Leon M., Esteban M., Mikami T., Oyama T., and Nakamura R. 2014. "Field Survey and Analysis of Storm Surge Caused by the 2013 Typhoon Haiyan (Yolanda)". [In Japanese]. *J Jpn Soc Civil Eng Ser B3*, 70(2), I_1212-I_1217. doi:10.2208/jscejoe.70.I_1212.

Skamarock W., Klemp J., Dudhia J., Gill D., Barker D., Duda M., Huang X., Wang W., and Powers J. 2008. "A Description of the Advanced Research WRF Version 3". NCAR Technical Note. doi:10.5065/D68S4MVH.

Tajima Y., Yasuda T., Pacheco B., Cruz E., Kawasaki K., Nobuoka H., Miyamoto M., Asano Y., Arikawa T., Ortigas N., Aquino R., Mata W., Valdez J., and Briones F. 2014. "Initial Report of JSCE-PICE Joint Survey on the Storm Surge Disaster Caused by Typhoon Haiyan". *Coastal Engineering Journal*, 56(1), 14500061-12. doi:10.1142/S0578563414500065.

Takabatake T., Mäll M., Esteban M., Nakamura R., Thit Oo Kyaw, Ishii H., Valdez J., Nishida Y., Noya F., and Shibayama T. 2018. "Field Survey of 2018 Typhoon Jebi in Japan: Lessons for Disaster Risk Management". *Geosciences*, 8(11), 412. doi:10.3390/geosciences8110412.

Takagi H., Li S., De Leon M., Esteban M., Mikami T., Matsumaru R., Shibayama T., and Nakamura R. 2016. "Storm surge and evacuation in urban areas during the peak of a storm". *Coastal Engineering*, 108, 1-9. doi:10.1016/j.coastaleng.2015.11.002.

Tasnim K., Ohira K., Shibayama T., Esteban M., and Nakamura R. 2014. "Numerical Simulation of Cyclonic Storm Surges Over the Bay of Bengal Using a Meteorology-Wave-Surge-Tide Coupled Model". In *Proceedings of the 33rd International Conference on Coastal Engineering 2014*, 1(34), 26. doi:10.9753/ice.v34.currents.26.

Tomkratoke S. and Sirisup S. 2020. "Effects of tropical cyclone paths and shelf bathymetry on inducement of severe storm surges in the Gulf of Thailand". *Acta Oceanol. Sin.*, 39(3), 90-102. doi:10.1007/s13131-020-1558-4.

Valdez J. 2014. "Adoption of a Town-wide Forensic Structural Investigation Procedure for Typhoon Effects: A Case Study of Palo, Leyte, Philippines". Undergraduate Thesis, University of the Philippines Diliman, Philippines.

Valdez J. 2019. "An Integrated Model for Analyzing the Strength of Beams and Columns Against the Driving Forces from Past and Future Storm Surge Events: Case Study of San Pedro Bay, Philippines". Master's Thesis, Waseda University, Japan.

Valdez J., Shibayama T., Takabatake T., and Esteban M. 2022. "Simulated flood forces on a building due to the storm surge by Typhoon Haiyan". *Coastal Engineering Journal*. doi: 10.1080/21664250.2022.2099683.

Wang W., Bruyere C., Duda M., Dudhia J., Gill D., Mavulich M., Keene K., Chen M., Lin H., Michalakes J., Rizvi S., Zhang X., Berner J., Ha S., and Fossell K. 2017. WRF-ARW V3; User's Guide. Accessed from: https://www2.mmm.ucar.edu/wrf/users/docs/user_guide_V3/contents.html.

Wang Y., Gao T., Han Z., and Liu Q. 2017. "Impacts of wind-field correction on the numerical simulation of storm-surge inundation during typhoon "Rammasun"". *Estuarine Coastal and Shelf Science*, 196(1), 198-206. doi:10.1016/j.ecss.2017.07.006.

World Bank Group. 2016. "Disaster Risk Profile: Mauritius". Accessed online on 01 September 2022. Available at: gfdrr.org/sites/default/files/mauritius.pdf.

Wessel P. and Smith W. 1996. "A global, self-consistent, hierarchical, high-resolution shoreline database". *J. Geophys. Res.*, 101(B4), 8741-8743. doi:10.1029/96JB00104.

Yokota M., Hashimoto N., Tanaka Y., and Hodama M. 2011. "Dependence property of the distance from the strong wind area to the wave observation station in the inverse estimation of sea surface drag coefficient". [In Japanese]. *J Jpn Soc Civil Eng Ser B*, 67(2). 903-907. doi:10.2208/jscejoe.67.I_903.

Yoon J., Shim J., Park K., and Lee J. 2014. "Numerical experiments of storm winds, surges, and waves on the southern coast of Korea during Typhoon Sanba: the role of revising wind force". *Nat. Hazards Earth Syst. Sci.*, 14(12), 3279-3295. doi:10.5194/nhess-14-3279-2014.

Yoon J. 2018. "Fine-resolution Numerical Simulations to Estimate Storm Surge Height and Inundation Vulnerability Considering Future Climate Change Scenario". *Journal of Coastal Research*, Special Issue No. 85, 916-920, ISSN 0749-0208.

APPENDIX A: LIST OF JOURNAL PAPER PUBLICATIONS

- **Corresponding Author**

Valdez J., Shibayama T., Takabatake T., and Esteban M. 2022. "Simulated flood forces on a building due to the storm surge by Typhoon Haiyan". *Coastal Engineering Journal*, 65(1), 28-38. doi: 10.1080/21664250.2022.2099683.

- **Co-Author**

Esteban M., Valdez J., Tan N., Rica A., Vasquez G., Jamero L., Valenzuela P., Sumalinog B., Ruiz R., Gera W., Chadwick C., Sparatu C., and Shibayama T. 2023. "Field Survey of 2021 Typhoon Rai – Odette - in the Philippines". Journal of Coastal and Riverine Flood Risk, 1. doi: 10.48438/jcrfr.2023.0001.

Ngo P., Garciano L., De Leon M., Lopez, N., Ishii H., Iimura K., Valdez J., and Shibayama T. 2022. "Experimental and Numerical Modelling of a Tide Embankment Section in Tacloban City, Philippines subjected to Storm Surge". *Natural Hazards Review*, 23(4). doi: 10.1061/(ASCE)NH.1527-6996.0000575.

Takabatake T., Han D., Valdez J., Inagaki N., Mäll M., Esteban M., and Shibayama T. 2021. "Three-Dimensional Physical Modelling of Tsunamis Generated by Partially Submerged Landslides". *Journal of Geophysical Research*, 127(1). doi: 10.1029/2021JC017826.

Takabatake T., Mäll M., Esteban M., Nakamura R., Thit Oo Kyaw, Ishii H., Valdez J., Nishida Y., Noya F., and Shibayama T. 2018. "Field Survey of 2018 Typhoon Jebi in Japan: Lessons for Disaster Risk Management". Geosciences, 8(11), 412. doi:10.3390/geosciences8110412.

Tajima Y., Yasuda T., Pacheco B., Cruz E., Kawasaki K., Nobuoka H., Miyamoto M., Asano Y., Arikawa T., Ortigas N., Aquino R., Mata W., Valdez J., and Briones F. 2014. "Initial Report of JSCE-PICE Joint Survey on the Storm Surge Disaster Caused by Typhoon Haiyan". *Coastal Engineering Journal*, 56(1), 14500061-12. doi:10.1142/S0578563414500065.

APPENDIX B: LIST OF INTERNATIONAL CONFERENCES

- **(2023 November) 11th International Conference on Asian and Pacific Coasts (APAC) – Kyoto, Japan (upcoming)**
  Valdez J., Shibayama T., Esteban M., Tasnim K., Nowbuth M., and Spataru C. 2023. "Numerical Modelling of Recent Storm Surge in the Philippines: Case Study of 2021 Typhoon Rai", For oral presentation (abstract accepted), 11th International Conference on Asian and Pacific Coasts 2023, Kyoto, Japan (Presenter).

- **(2023 October) 10th International Conference on Coastal and Port Engineering in Developing Countries (PIANC-COPEDEC) – Manila, Philippines (upcoming)**

  Valdez J. and Shibayama T. 2023. "The role of numerical modelling of typhoons and storm surges in building back better". For oral presentation (abstract accepted), 10th International Conference on Coastal and Port Engineering in Developing Countries, Manila, Philippines. (Presenter).

- **(2022) 37th International Conference on Coastal Engineering (ICCE) – Sydney, Australia**

  Valdez J., Shibayama T., and Esteban M. 2022. "Identification of Potential Storm Surges due to Typhoon Rai Using Numerical Models". Poster Presentation, 2022 International Conference on Coastal Engineering, Sydney, Australia. (Presenter).

  Esteban M., Valdez J., Jamero L., Tan N., Rica A., Valenzuela P., Ruiz R., Sumalinog B., Vasquez G., Chadwick C., and Shibayama T. 2022. "Survey of Storm Surge due to Typhoon Rai in December 2021 in the Philippines". Oral Presentation, 2022 International Conference on Coastal Engineering, Sydney, Australia. (Presenter).

- **(2020) 36th International Conference on Coastal Engineering (ICCE) – Sydney, Australia (Online)**

  Valdez J. and Shibayama T. 2020. "Analysis of a School Building against Typhoon Haiyan Storm Surge Forces". In Lynett P. (Ed), Proceedings of virtual Conference on Coastal Engineering, 2020. doi:10.9753/icce.v36v.waves.12.

APPENDIX C: FUNDING ACKNOWLEDGMENT

Typhoon Haiyan study and publication:

List of research achievements for application of Doctor of Engineering, Waseda University

Full Name： Valdez　Justin Joseph Panlilio　　　　　　seal or signature

Date Submitted(yyyy/mm/dd):　2023/2/3

種類別 (By Type)	題名、　発表・発行掲載誌名、　　発表・発行年月、　　連名者（申請者含む） (theme, journal name, date & year of publication, name of authors inc. yourself)
Journal	O **Valdez J.**, Shibayama T., Takabatake T., and Esteban M. 2022. "Simulated flood forces on a building due to the storm surge by Typhoon Haiyan". Coastal Engineering Journal. doi: 10.1080/21664250.2022.2099683.
Journal	O Esteban M., **Valdez J.**, Tan N., Rica A., Vasquez G., Jamero L., Valenzuela P., Sumalinog B., Ruiz R., Gera W., Chadwick C., Sparatu C., and Shibayama T. "Field Survey of 2021 Typhoon Rai – Odette-in the Philippines". Journal of Coastal and Riverine Flood Risk, 1. doi: 10.48438/jcrfr.2023.0001.
Journal	Ngo P., Garciano L., De Leon M., Lopez, N., Ishii H., Iimura K., **Valdez J.**, and Shibayama T. 2022. "Experimental and Numerical Modelling of a Tide Embankment Section in Tacloban City, Philippines subjected to Storm Surge". Natural Hazards Review, 23(4). doi: 10.1061/(ASCE)NH.1527-6996.0000575.
Journal	Takabatake T., Han D., **Valdez J.**, Inagaki N., Mäll M., Esteban M., and Shibayama T. 2021. "Three-Dimensional Physical Modelling of Tsunamis Generated by Partially Submerged Landslides". Journal of Geophysical Research, 127(1). doi: 10.1029/2021JC017826.
Journal	Takabatake T., Mäll M., Esteban M., Nakamura R., Thit Oo Kyaw, Ishii H., **Valdez J.**, Nishida Y., Noya F., and Shibayama T. 2018. "Field Survey of 2018 Typhoon Jebi in Japan: Lessons for Disaster Risk Management". Geosciences, 8(11), 412. doi:10.3390/geosciences8110412.
Journal	O Tajima Y., Yasuda T., Pacheco B., Cruz E., Kawasaki K., Nobuoka H., Miyamoto M., Asano Y., Arikawa T., Ortigas N., Aquino R., Mata W., **Valdez J.**, and Briones F. 2014. "Initial Report of JSCE-PICE Joint Survey on the Storm Surge Disaster Caused by Typhoon Haiyan". Coastal Engineering Journal, 56(1), 14500061-12. doi:10.1142/S0578563414500065.
Conference	O **Valdez J.** and Shibayama T. 2023. "The role of numerical modelling of typhoons and storm surges in building back better", 10th International Conference on Coastal and Port Engineering in Developing Countries, Manila, Philippines. (Peer reviewed; oral presentation; set on October 9-13, 2023).
Conference	O **Valdez J.**, Shibayama T., and Esteban M. 2022. "Identification of Potential Storm Surges due to Typhoon Rai Using Numerical Models", 2022 International Conference on Coastal Engineering, Sydney, Australia. (Peer reviewed; poster presentation; presenter).
Conference	O Esteban M., **Valdez J.**, Jamero L., Tan N., Rica A., Valenzuela P., Ruiz R., Sumalinog B., Vasquez G., Chadwick C., and Shibayama T. 2022. "Survey of Storm Surge due to Typhoon Rai in December 2021 in the Philippines". Oral Presentation, 2022 International Conference on Coastal Engineering, Sydney, Australia. (Peer reviewed; oral presentation; presenter).
Conference	O **Valdez J.** and Shibayama T. 2020. "Analysis of a School Building against Typhoon Haiyan Storm Surge Forces". In Lynett P. (Ed), Proceedings of virtual Conference on Coastal Engineering, 2020. doi:10.9753/icce.v36v.waves.12. (Peer reviewed; oral presentation; presenter).